TECHNICAL REPORT R-67

PROPELLANT VAPORIZATION AS A DESIGN CRITERION FOR ROCKET-ENGINE COMBUSTION CHAMBERS

By RICHARD J. PRIEM and MARCUS F. HEIDMANN

Lewis Research Center
Cleveland, Ohio

CONTENTS

TECHNICAL REPORT R–67

PROPELLANT VAPORIZATION AS A DESIGN CRITERION FOR ROCKET-ENGINE COMBUSTION CHAMBERS [1]

by Richard J. Priem and Marcus F. Heidmann

SUMMARY

A model and theory for describing the rocket combustion process are presented. The model is based on the assumption that propellant vaporization is the rate-controlling combustion process. Calculations of the vaporization rate and histories show the effects of propellants, spray conditions, engine design parameters, and operating parameters on the vaporization process. The results are correlated with an effective chamber length for ease in using them for design purposes. An analysis is presented of the quantitative effect of incomplete propellant vaporization on combustor performance. With this analysis, experimental and calculated combustor performances are compared for injectors where drop size can be calculated. For other injectors the drop sizes are deduced and are shown as functions of injector type and orifice size. The technique for using the calculated results to design rocket combustors is also described.

INTRODUCTION

The design of a rocket-engine combustor is usually considered an art rather than a science because of the large number of different phenomena that occur during the combustion process. Considering all the phenomena results in a large number of similarity parameters (refs. 1 to 4) that should be used in designing and scaling rocket combustors. Since it is impossible to satisfy all the similarity parameters, experience and intuition are used to determine the emphasis on each parameter. This suggests the need of a better understanding of the combustion process and of a technique for determining the governing factors in combustion efficiency.

This report shows how propellant vaporization (one of the many steps within the combustion process) will influence combustion efficiency if vaporization is the rate-controlling step. Vaporization rates are calculated for a wide range of various combustor parameters to show how each parameter affects combustion efficiency. The equations needed for the calculations are derived from a model that assumes that the vaporization process is the rate-controlling step. This assumption appears justified based on the recent findings of the times or distances required for atomization, mixing, and chemical reactions (refs. 5 to 7). The analysis also assumes one-dimensional steady-state flow with no interaction between drops and no shattering of drops. From these results a generalized correlation is developed to show the effect of chamber length, length of nozzle convergent section, chamber contraction ratio, nozzle shape, chamber pressure, injection velocity, drop size, and initial propellant temperature for five propellants: heptane, ammonia, hydrazine, oxygen, and fluorine. The generalized results enable one to determine the amount of propellant vaporized in the combustor for any values of the preceding parameters.

The relation between propellant vaporized and combustor performance is also derived to show what effect the vaporization process has on performance. With this relation the calculated amounts of propellant vaporized are converted to efficiencies in order to compare experimental and calculated efficiencies. This comparison exhibits good agreement both in absolute values and trends, indicating that propellant vaporization is the

[1] Supersedes NACA Technical Notes 3883, 3985, 4098, and 4219.

rate-controlling step in most rocket combustors.

A detailed explanation of the way the calculated results can be used for design procedure is also included as an aid in interpreting and using the results. In addition, drop-size data required for this use are presented.

SYMBOLS

A area, sq in.
$\mathcal{A}$ chamber contraction ratio, A_c/A_N
a constant for number distribution, $100/(\sqrt{2\pi}\ln\sigma_G)$
B film thickness, in.
b nozzle exponent
C_D coefficient of drag for spheres, dimensionless
c^* characteristic exhaust velocity, ft/sec or in./sec
c_p specific heat at constant pressure, Btu/(lb)(°F)
D molecular diffusion coefficient, sq in./sec
d diameter, in.
d_{30} volume-number mean drop size, $\sqrt[3]{\sum_i n_i d_{S,i}^3 / \sum_i n_i}$, in.
F aerodynamic drag force, lb force
$\mathscr{F}$ fraction of fuel vaporized
$\mathscr{G}$ gravitational constant, 32.2 ft/sec² or 386.4 in./sec²
h heat-transfer coefficient, Btu/(sq in.)(sec)(°F)
j molal rate of diffusion, lb mole/(sq in.)(sec)
K coefficient of mass transfer, lb mass/(lb force)(sec)
$\mathscr{K}$ constant for burning drop, (in.)^n/sec
k thermal conductivity, Btu/(in.)(sec)(°F)
l length, in.
l_{ef} effective length (eq. (102)), in.
l_{gen} generalized length (eq. (103)), in.
M Mach number
$\mathcal{M}$ molecular weight, lb mass/lb mole
m mass of drop, lb
$m_{t,o}$ initial mass of all drops, $\sum_i n_i m_{i,o}$
Nu_h Nusselt number for heat transfer, $2rh/k_{mx}$
Nu_m Nusselt number for mass transfer, $2r_S R\overline{T}\,\mathscr{K}/\mathcal{M}_a D$
$\mathcal{N}$ percent of drops having radii smaller than r
n_i number of drops in group of i-sized drops
O/F oxidant-to-fuel weight-flow ratio, $\dot{w}_O/\dot{w}_F$
$\mathcal{O}$ fraction of oxidant vaporized
P chamber total pressure, lb/sq in.
Pr Prandtl number, $c_{p,mx}\mu_{mx}/k_{mx}$
p partial pressure, lb force/sq in.
p_s chamber static pressure, lb force/sq in.
q_l sensible heat rate of drop, Btu/sec
q_{sh} heat carried back with diffusing vapor in form of superheat, Btu/sec
q_t total heat transfer from gases to vapor film, Btu/sec
q_v heat received at drop surface, Btu/sec
q_λ heat to vaporize diffusing vapor, Btu/sec
R universal gas constant, 18,510 (in.)(lb force)/(°R)(lb mole)
Re Reynolds number, $2rU\rho_{mx}/\mu_{mx}$
$\mathcal{R}$ percent of mass in drops smaller than r
r radial distance from center of drop, in.
r_m mass-median drop radius, in.
r_n number-median drop radius, $r_m\ exp\ [-3(\ln\sigma_G)^2]$, in.
S nozzle shape factor, Nozzle volume/$A_c l_N$
Sc Schmidt number, $\mu_{mx}/D\rho_{mx}$
T temperature at a particular point, °R
$\overline{T}$ mean temperature in boundary, °R
T_b temperature of surrounding gases, °R
T_{cr} critical temperature of propellant, °R
T_l temperature of liquid drop, °R
$T_{l,o}$ initial propellant temperature, °R
$T_{l,o,R}$ reduced initial propellant temperature, $T_{l,o}/T_{cr}$, dimensionless
T_t total gas temperature in nozzle, °R
t time, sec
U velocity difference between gas and drop, in./sec
u velocity of gas, in./sec
u_v gas velocity at position where vaporization is complete, in./sec
v droplet velocity, in./sec
We Weber number, $\rho_{mx}U^2 r_S/\sigma_l$
w vaporization rate, lb/sec
$\dot{w}_F$ liquid-fuel weight flow, lb/sec
$\dot{w}_{F,in}$ liquid-fuel weight flow through injector, lb/sec
$\dot{w}_O$ liquid-oxidant weight flow, lb/sec
x axial position, in.
Z correction factor for heat transfer, $z/(e^z-1)$, dimensionless
z heat-transfer factor, $wc_{p,f}/2\pi k_{mx} r_S Nu_h$, dimensionless

α correction factor for mass transfer, $(p_s/p_{a,s}) \ln [p_s/(p_s - p_{a,s})]$, dimensionless
γ ratio of specific heats
η characteristic-exhaust-velocity efficiency, percent of theoretical
λ latent heat of vaporization, Btu/lb
μ viscosity, lb/(in.)(sec)
ρ density, lb/cu in.
σ_G geometric standard deviation, (r at $\mathcal{R}=84.13$)/(r at $\mathcal{R}=50.00$), dimensionless
σ_l surface tension of liquid, lb/in.
τ average time between drops that pass through given cross section of chamber, sec

Subscripts:

a vaporizing material
b surrounding medium
c cylindrical chamber
cal calculated value
cs cross section of drop
exp experimental
f vaporizing propellant vapor
g gaseous medium
i i^{th}-sized drops
j jet
l liquid propellant
mx vapor mixture
N nozzle throat
O/F oxidant-to-fuel weight-flow ratio, $\dot{w}_O/\dot{w}_F$
$O/\mathcal{F}$ ratio of oxidant weight flow to vaporized fuel, $\dot{w}_O/\mathcal{F}\dot{w}_F$
$\mathcal{O}/F$ ratio of vaporized oxidant to fuel weight flow, $\mathcal{O}\dot{w}_O/\dot{w}_F$
$\mathcal{O}/\mathcal{F}$ ratio of vaporized oxidant to vaporized fuel, $\mathcal{O}\dot{w}_O/\mathcal{F}\dot{w}_F$
o initial
q assumed value
S surface of drop
t total
th theoretical
x at position x in chamber or nozzle
$x+\Delta x$ at position $x+\Delta x$ in chamber
z average value between positions x and $x+\Delta x$
I case I, complete combustion
II case II, incomplete combustion

DESCRIPTION OF MODEL

Propellant injected into a combustion chamber is believed to pass through the following stages: The propellant leaves the injector as a ligament or sheet. These ligaments or sheets then break down into different size droplets with heat transfer from the surrounding hot gases occurring after the ligament has broken up into droplets. As heat transfer takes place, the droplets are heated and at the same time lose part of their mass by vaporization and diffusion. After vaporizing, the propellants are mixed and react to form hot gases. As the droplets vaporize they are also slowed down (or speeded up, depending on the magnitude of the drop velocity and surrounding bulk gas velocity) by aerodynamic drag forces. The bulk gas velocity meanwhile increases because of the increased mass of propellants in the gas phase as combustion products.

In this analysis the vaporization rate of one propellant is calculated from the point at which droplets are formed. This is equivalent to assuming that the distance required to form droplets is negligible or that some additional length is required for the atomization process before vaporization begins. Furthermore, it is assumed that mixing and reaction rates are fast and that reacted products are formed as soon as the propellants are vaporized. This condition is satisfied in a chamber in which the propellants are uniformly introduced over the entire cross-sectional area and in which the concentrations of propellants and the temperature of the products are high (high chamber pressure and close to stoichiometric mixture for high temperature).

With this description, a model can be set up for each droplet as shown schematically in figure 1.

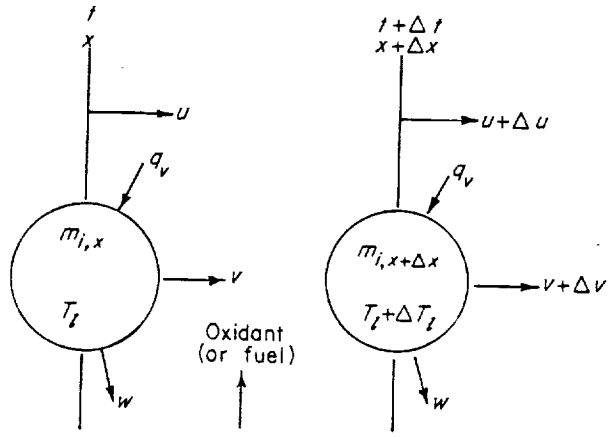

FIGURE 1.—Schematic model of fuel or oxident drops vaporizing in rocket engine.

A liquid droplet is shown at position x in the chamber and a small increment later in time Δt and distance Δx. During this increment, the drop velocity v changes by a small amount Δv. In this increment the gas velocity u changes by Δu. The drop velocity starts at the axial injection velocity and slows down. Similarly, the gas velocity starts at zero and increases as the propellants vaporize and burn. While the drop is moving through the increment, heat is transferred to the liquid surface at a rate q_v (no internal heat generation), and propellant is transferred from the surface at a rate of w. During the increment, the mass and the radius of the drop change from m_x to $m_{x+\Delta x}$ and r_x to $r_{x+\Delta x}$, respectively, while the drop temperature T_l changes by ΔT_l.

With the calculation technique used herein, the process is divided into sufficiently small increments that only small changes occur over that period. It is assumed that steady-state mass-, momentum-, and heat-transfer equations are applicable during this increment. These equations will be explained later.

For analytical purposes it is necessary to assume one-dimensional steady-state flow and that all drops have the same initial velocity and never shatter or coalesce. To determine properties in the bulk gas flow it is necessary to assume that they correspond to conditions produced by stoichiometric combustion. This implies that all the combustion is at the outer edge of the film surrounding the drops (characteristic of a burning drop) and that the amount of unburned propellant in the bulk gases is negligible.

THEORY

MASS TRANSFER

Neglecting thermal diffusion and assuming that diffusion results from a driving force of a concentration gradient in the direction of diffusion, the following equation is obtained for a diffusing system (ref. 8):

$$\frac{dp_a}{dr}=\frac{-RT}{Dp_s}(j_a p_b - j_b p_a) \tag{1}$$

For a vaporizing droplet, the diffusion rate of component b (i.e., oxidant diffusing to the fuel drop) is usually insignificant and is considered to be zero, or

$$j_b=0 \tag{2}$$

When the molal rate of diffusion at the droplet surface is defined as $j_{a,s}$, then, for a spherical droplet and film by the continuity equation,

$$j_{a,s}=\frac{j_a r^2}{r_s^2} \tag{3}$$

Then,

$$\frac{dp_a}{dr}=\frac{-RT}{Dp_s} j_{a,s}\frac{r_s^2}{r^2}p_b \tag{4}$$

If it is assumed that the temperature is equal to a constant value $\overline{T}$ (arithmetic mean) throughout the film and that D is also constant and determined at $\overline{T}$, equation (4) can be integrated between $r=r_s$ and $r=r_s+B$ (where B is the film thickness). For this integration, $p_a(r_s)=p_{a,s}$, $p_a(r_s+B)=0$, and $p_a+p_b=p_s$. There is then obtained for $j_{a,s}$

$$j_{a,s}=\frac{Dp_s}{R\overline{T}}\left(\frac{1}{B}+\frac{1}{r_s}\right)\ln\left(\frac{p_s}{p_s-p_{a,s}}\right) \tag{5}$$

The mass transfer from the surface in pounds per second is then

$$w=j_{a,s}A_s\mathcal{M}_a=\left[\frac{D\mathcal{M}_a}{R\overline{T}}A_s\left(\frac{1}{B}+\frac{1}{r_s}\right)p_{a,s}\right]\left[\frac{p_s}{p_{a,s}}\ln\left(\frac{p_s}{p_s-p_{a,s}}\right)\right] \tag{6}$$

or

$$w=\frac{D\mathcal{M}_a}{R\overline{T}}A_s\left(\frac{1}{B}+\frac{1}{r_s}\right)\alpha p_{a,s} \tag{7}$$

where

$$\alpha=\frac{p_s}{p_{a,s}}\ln\left(\frac{p_s}{p_s-p_{a,s}}\right) \tag{8}$$

In equation (7), α is normally thought of as a term to convert the equimolal diffusion ($j_a=j_b$) to unidirectional diffusion ($j_b=0$), or

$$(j_{a,s})_{\text{unidirectional}}=(j_{a,s})_{\text{equimolal}}\ \alpha.$$

Because the film thickness B is unknown, it is customary to use the following engineering equation given by reference 9:

$$w=A_s K p_{a,s}\alpha \tag{9}$$

where K is the mass-transfer coefficient, which can be obtained from the empirical correlation of reference 10:

$$Nu_m=\frac{2r_s\dfrac{R}{\mathcal{M}_a}\overline{T}K}{D}=2+0.6(Sc)^{1/3}(Re)^{1/2} \tag{10}$$

Equation (10) is not identical to that given by reference 10, since $R\overline{T}/\mathcal{M}_a$ has been substituted for p_s/ρ_{mx}. For water droplets, used by reference 10, there is little difference between $R\overline{T}/\mathcal{M}_a$ and p_s/ρ_{mx}, and the same correlation would have been obtained using $R\overline{T}/\mathcal{M}_a$. Other investigators (see ref. 9, pp. 72–73) have obtained similar correlations using the $R\overline{T}/\mathcal{M}_a$ term. In determining their correlation, Ranz and Marshall (ref. 10) did not use the α term in equation (9). Justification for its use is that by using it better agreement was obtained in reference 11 between experimental and calculated histories. Also, the vapor pressures encountered by Ranz and Marshall were so low that the α term would have been essentially equal to unity in their experiments.

The Ranz and Marshall correlation was used for the Nusselt number Nu_m, since a heat-transfer and mass-transfer correlation had been determined therein under conditions involving simultaneous heat and mass transfer. Also, the nature of their investigation was similar to that in a rocket combustion chamber, although the maximum temperatures and pressures were not so high.

Combining equations (7), (9), and (10) gives

$$\frac{2r_S}{B}=Nu_m-2 \tag{11}$$

This states that the thickness of the mantle around the drop is infinite when the drop is at a standstill relative to the gas ($Re=0$ and $Nu_m=2$). The higher the relative velocity, the smaller the thickness, approaching zero thickness for infinite velocity. Combining equations (9) and (10) produces the following equation used in the calculations:

$$w=\frac{D\mathcal{M}_a A_S}{R\overline{T}2r_S}\,\alpha Nu_m p_{a,s}=\frac{2\pi D\mathcal{M}_a r_S}{R\overline{T}}\,\alpha Nu_m p_{a,s} \tag{12}$$

where Nu_m and α are defined in equations (10) and (8), respectively. This requires a knowledge of the radius, velocity, temperature, and physical properties of the droplet at every instant.

HEAT TRANSFER

Referring to figure 2, the total heat transfer q_t from the surrounding gases to the film around the drop goes (1) to heat the liquid droplet q_l, (2) to vaporize the diffusing vapor q_λ, and (3) to the diffusing vapor in the form of superheat q_{sh}.

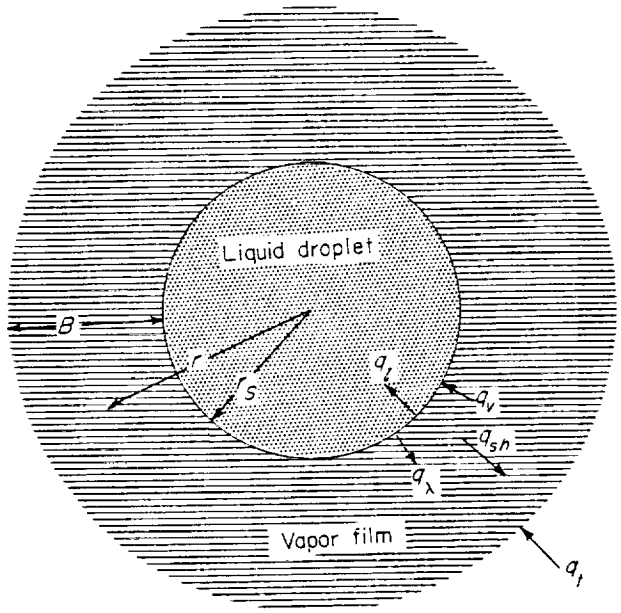

FIGURE 2.—Schematic diagram of heat transfer to vapor film and liquid drop.

The heat arriving at the droplet surface equals the sum of q_l and q_λ and is defined as q_v.

If at any instant during vaporization a surface in the gas-air vapor film at a distance r from the center of the droplet is considered,

$$q_v=q_t-q_{sh} \tag{13}$$

then

$$q_v=4\pi r^2 k\frac{dT}{dr}-wc_{p,a}(T-T_l) \tag{14}$$

Assuming that the thermal conductivity and specific heat are constant at some mean value, equation (14) can be integrated between $r=r_S$ and $r=r_S+B$, where $T(r_S)=T_l$ and $T(r_S+B)=T_b$. Then,

$$\ln\left[\frac{q_v+wc_{p,a}(T_b-T_l)}{q_v}\right]=\frac{wc_{p,a}}{4\pi k_{mx}}\frac{B}{r_S(r_S+B)} \tag{15}$$

Defining

$$z=\frac{wc_{p,a}}{4\pi k_{mx}}\frac{B}{r_S(r_S+B)} \tag{16}$$

then

$$q_v=wc_{p,a}\frac{T_b-T_l}{e^z-1} \tag{17}$$

Multiplying and dividing by z and r_S give

$$q_v=k_{mx}\left(\frac{1}{B}+\frac{1}{r_S}\right)A_S(T_b-T_l)\frac{z}{e^z-1} \tag{18}$$

or

$$q_r=k_{mx}\left(\frac{1}{B}+\frac{1}{r_S}\right)A_S(T_b-T_l)Z \tag{19}$$

where

$$Z=\frac{z}{e^z-1} \tag{20}$$

In equation (20), Z represents the ratio of the heat that would be conducted to the surface with pure convective heat transfer and no mass transfer, to the heat transfer with convection and mass transfer. The value of Z is always less than unity, since the mass transfer reduces the heat transferred to the surface of the drop.

The film thickness B again appears in equation (19); therefore, the following engineering equation given by reference 9 is used:

$$q_v=hA_S(T_b-T_l)Z \tag{21}$$

where h is the heat-transfer coefficient, which, like the mass-transfer coefficient, is normally obtained from an empirical correlation. The correlation used was that given by reference 10 (for the same reasons as given for the mass-transfer correlation):

$$Nu_h=\frac{h2r_S}{k_{mx}}=2+0.6\,(Pr)^{1/3}(Re)^{1/2} \tag{22}$$

In determining their correlation, Ranz and Marshall did not use the Z-factor in equation (21). Its use in the present calculations seems valid, since better agreement was obtained in reference 12 between experimental and calculated histories by using it. In addition, there is a close similarity between equations (21) and (19) that indicated it should be included. Finally, in Ranz's experimental work the mass-transfer rate was so low that the Z-factor would have been unity.

Combining equations (19), (21), and (22) gives

$$\frac{2r_S}{B}=Nu_h-2 \tag{23}$$

which is similar to equation (11) for film thickness determined for mass transfer. Combining equations (16), (19), (21), and (22) produces the following equation used in the calculations:

$$q_v=\frac{k_{mx}Nu_hA_S}{2r_S}(T_b-T_l)Z=2\pi k_{mx}Nu_hr_S(T_b-T_l)Z \tag{24}$$

where Nu_h and Z are given by equations (22) and (20), respectively, and

$$z=\frac{wc_{p,a}}{2\pi k_{mx}r_SNu_h} \tag{25}$$

This requires a knowledge of the drop radius, velocity, temperature, mass transfer, and physical properties of the droplet at every instant.

DROPLET TEMPERATURE

The droplet temperature is determined from an energy balance applied at the liquid droplet surface. The heat transferred to the liquid surface q_v goes to two places: (1) heat for vaporizing the mass transferred out of the drop q_λ, and (2) heat for raising the liquid temperature q_l:

$$q_v=q_l+q_\lambda \tag{26}$$

However,

$$q_\lambda=w\lambda \tag{27}$$

Then

$$q_l=q_v-w\lambda \tag{28}$$

The values for q_v and w are given by equations (24) and (12), respectively, and the heat of vaporization λ is determined by the temperature of the liquid droplet.

By assuming that the temperature of the droplet is uniform, which implies infinite thermal conductivity or very fast circulation within the drop, the change in droplet temperature is related to the heat as follows:

$$q_l=mc_{p,l}\frac{dT_l}{dt} \tag{29}$$

or

$$\frac{dT_l}{dt}=\frac{1}{mc_{p,l}}(q_v-w\lambda) \tag{30}$$

Equation (30) states that determining the rate of change of the droplet temperature requires a knowledge of the instantaneous heat-transfer rate, mass-transfer rate, droplet temperature, and droplet size. If the heat-transfer rate q_v is larger than the rate at which heat is carried away by the vaporizing liquid $w\lambda$, the droplet temperature increases. If the heat-transfer rate is lower than the heat carried away by the vapor, the droplet temperature decreases. At some point the heat-transfer rate equals the heat carried away by the vapor, and the droplet temperature remains con-

stant. This corresponds to a "wet-bulb" temperature.

MOMENTUM TRANSFER

Momentum is transferred between the liquid drop and the gases by aerodynamic drag. This force will either slow down the drop or speed it up so that the velocity of the drop approaches that of the surrounding gases.

The aerodynamic drag force exerted by a moving fluid on an immersed body may be calculated from the following equation (ref. 13):

$$F=C_D \frac{A_{cs}\rho_{mx}}{g}\frac{U^2}{2} \tag{31}$$

For a spherical droplet

$$F=\frac{-m}{g}\frac{dv}{dt}=C_D \frac{A_{cs}\rho_{mx}}{g}\frac{U^2}{2} \tag{32}$$

or

$$\frac{dv}{dt}=-\frac{3}{8} C_D \frac{\rho_{mx}}{\rho_l}\frac{U^2}{r_s} \tag{33}$$

The drag coefficient obtained by reference 14 was used as it was determined for evaporating sprays:

$$C_D=27(Re)^{-0.84} \tag{34}$$

To calculate the acceleration of the droplet at any instant again requires a knowledge of the instantaneous drop radius, velocity, and physical properties.

GAS VELOCITY IN CYLINDRICAL CHAMBER

For a constant cross-sectional area of the chamber, the gas velocity can be obtained by applying a mass balance to the system, or

Increase mass of gases=Decrease mass of liquid

$$\rho_g A_c\, du_x=-(d\dot{w}_{F,x}+d\dot{w}_{O,x}) \tag{35}$$

The ratio of oxidant- to fuel-flow rate is

$$\frac{\dot{w}_O}{\dot{w}_F}=\frac{O}{F} \tag{36}$$

and, therefore, for equal vaporization rates of the two propellants,

$$d\dot{w}_{F,x}+d\dot{w}_{O,x}=\left(1+\frac{O}{F}\right) d\dot{w}_{F,x} \tag{37}$$

Combining equations (35) and (37) gives

$$du_x=\frac{-\left(1+\frac{O}{F}\right)}{\rho_g A_c} d\dot{w}_{F,x} \tag{38}$$

Assuming a constant gas density ρ_g and integrating between the boundary conditions of $u_x=0$ where $\dot{w}_{F,x}=\dot{w}_{F,in}$ and $u_x=u_x$ where $\dot{w}_{F,x}=\dot{w}_{F,x}$ result in

$$u_x=\frac{\left(1+\frac{O}{F}\right)}{\rho_g A_c}(\dot{w}_{F,in}-\dot{w}_{F,x}) \tag{39}$$

Similarly, when $u_x=u_v$, $\dot{w}_{F,x}=0$; then

$$u_v=\frac{\left(1+\frac{O}{F}\right)}{\rho_g A_c}\dot{w}_{F,in} \tag{40}$$

and

$$\frac{u_x}{u_v}=\left(1-\frac{\dot{w}_{F,x}}{\dot{w}_{F,in}}\right) \tag{41}$$

The mass-flow rate can be expressed in terms of the sum of the masses of the liquid drops by

$$\dot{w}_{F,x}=\sum_i \frac{n_i}{\tau} m_{i,x} \tag{42}$$

The boundary condition $\dot{w}_{F,x}=\dot{w}_{F,in}$ is applied where $m_{i,x}=m_{i,o}$, so that equation (42) becomes

$$\dot{w}_{F,in}=\sum_i \frac{n_i}{\tau} m_{i,o} \tag{43}$$

A combination of equations (41) to (43) gives the following equation used in the calculations:

$$\frac{u_x}{u_v}=1-\frac{\sum_i n_i m_{i,x}}{\sum_i n_i m_{i,o}}=1-\frac{\sum_i n_i m_{i,x}}{m_t} \tag{44}$$

Calculation of gas velocity from equation (44) requires a knowledge of drop size or vaporization rate.

NOZZLE AERODYNAMICS

The problem of incomplete vaporization in the cylindrical chamber is now considered. The equations for heat transfer and momentum transfer given in the previous section all require a knowledge of the gas velocity and pressure at the position under consideration. Therefore, in order to calculate vaporization rates in the convergent nozzle attached to the cylindrical chamber, the

gas velocity and pressure must be defined in terms of the position in the nozzle. There are numerous equations for determining area in terms of velocity or pressure, but the relation between velocity and pressure usually is given by tables (e.g., ref. 15). For calculation purposes, an empirical equation was used to relate velocity and pressure to position or area. The empirical equations were obtained by curve-fitting to the values described in reference 15 for a perfect gas.

The empirical nozzle equation for pressure in terms of diameter that is used in the calculations is

$$\frac{p_{s,x}}{P}=\frac{1-1.060411\,(d_x/d_N)}{0.930665-1.036163\,(d_x/d_N)} \tag{45}$$

The equation for velocity is

$$\frac{u_x}{u_N}=\frac{1}{-4.28561+4.440105\,(d_x/d_N)+0.855491\,(d_x/d_N)^2} \tag{46}$$

Pressures and velocities obtained with equations (45) and (46) are compared with data from tables of reference 15 (for inviscid adiabatic flow) in figures 3 and 4, respectively.

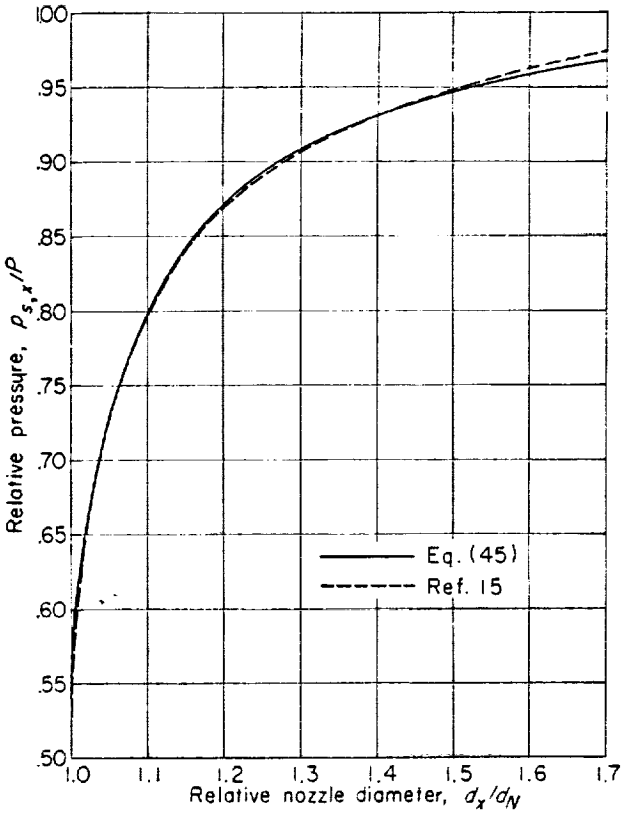

FIGURE 3.—Comparison of pressure obtained by equation (45) with pressures of reference 15.

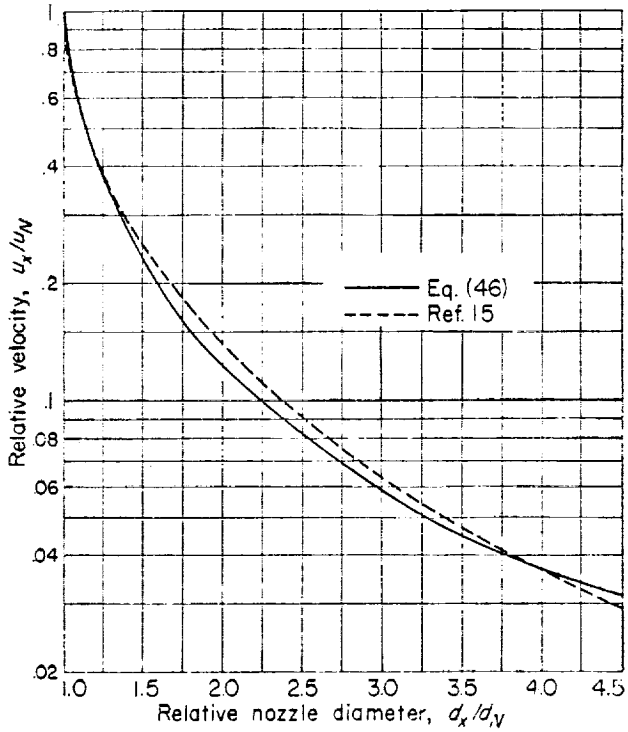

FIGURE 4.—Comparison of velocities obtained by equation (46) with velocities of reference 15.

To relate diameter to position, nozzles having contours described by the following equation were used:

$$\frac{d_x}{d_N}=\frac{d_c}{d_N}-\left(\frac{d_c}{d_N}-1\right)\left(\frac{x}{l_N}\right)^b \tag{47}$$

Nozzle exponents b of 2, 1, and ½ were used, which resulted in nozzle shapes as shown in figure 5 for a ratio of chamber to throat diameter d_c/d_N of 2.

Since the nozzle of a rocket attaches directly to the end of the cylindrical chamber, the diameter, gas velocity, and pressure at the end of the cylindrical chamber must be identical to those at the beginning of the nozzle. This then interrelates velocity, pressure, and diameter of the chamber, gas velocity where vaporization is complete u_v, and percent mass vaporized at the cylindrical-chamber exit by equations (44) and (45) to (47). For calculation purposes, the gas velocity where vaporization is complete u_v and

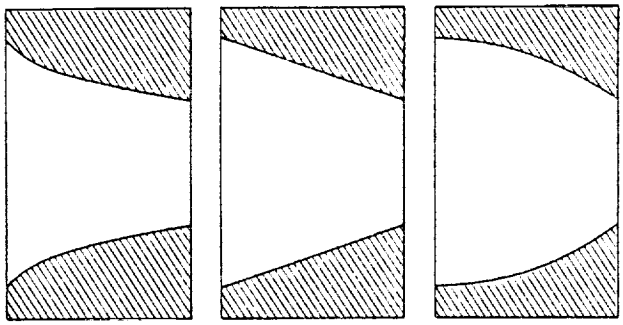

(a) Exponent $b=\frac{1}{2}$. (b) Exponent $b=1$. (c) Exponent $b=2$.

FIGURE 5.—Nozzle shapes for contraction ratio of 4.

percent mass vaporized at the exit of the cylindrical chamber were specified. With u_v specified and initial and vaporized mass known, the chamber diameter or area A_c is determined from equation (40). Thus, specifying u_v and percent vaporized at the chamber exit completely describes the combustor for which the calculations were performed.

RELATION BETWEEN PERCENTAGE OF PROPELLANT VAPORIZED AND ENGINE PERFORMANCE

For incomplete combustion, the rocket exhaust contains a mixture of oxidant drops, fuel drops, and gaseous combustion products. The gaseous combustion products are assumed to be at thermodynamic equilibrium concentrations. If the volume and kinetic energy of the liquid drops are neglected, the characteristic velocity c^* that can be theoretically realized may be computed from the thermodynamic properties of the combustion products and related to combustion-chamber parameters by applying the basic definition from reference 16 (p. 74):

$$(c^*_{th})_{\mathcal{O}/\mathcal{F}}=\frac{PA_N g}{\mathcal{O}\dot{w}_O+\mathcal{F}\dot{w}_F} \tag{48}$$

The experimental c^* in terms of measured engine parameters is expressed

$$(c^*_{exp})_{O/F}=\frac{PA_N g}{\dot{w}_O+\dot{w}_F} \tag{49}$$

Combining equations (48) and (49) gives

$$(c^*_{exp})_{O/F}=(c^*_{th})_{\mathcal{O}/\mathcal{F}}\left(\frac{\mathcal{O}\dot{w}_O+\mathcal{F}\dot{w}_F}{\dot{w}_O+\dot{w}_F}\right) \tag{50}$$

The c^* efficiency η is usually taken to be

$$\eta=\frac{(c^*_{exp})_{O/F}}{(c^*_{th})_{O/F}} \tag{51}$$

Combining equations (50) and (51) gives

$$\eta=\frac{(c^*_{th})_{\mathcal{O}/\mathcal{F}}}{(c^*_{th})_{O/F}}\left(\frac{\mathcal{O}\dot{w}_O+\mathcal{F}\dot{w}_F}{\dot{w}_O+\dot{w}_F}\right) \tag{52}$$

Equation (52) relates c^* efficiencies to the percentages of fuel and oxidant vaporized and may be used for the interpretation of experimental data.

For some combustors, either the oxidant or the fuel is completely vaporized before reaching the exhaust nozzle (e.g., one gaseous propellant or finely atomized propellant). For these conditions, equation (52) reduces to the following equations. With the fuel completely vaporized, the c^* efficiency is related to the fraction of oxidant vaporized by

$$\eta=\frac{(c^*_{th})_{\mathcal{O}/_F}}{(c^*_{th})_{O/F}}\frac{\frac{\mathcal{O}\dot{w}_O}{\dot{w}_F}+1}{\frac{\dot{w}_O}{\dot{w}_F}+1} \tag{53}$$

With the oxidant completely vaporized, the c^* efficiency is related to the fraction of fuel vaporized by

$$\eta=\frac{(c^*_{th})_{o/\mathcal{F}}}{(c^*_{th})_{O/F}}\frac{\frac{\dot{w}_O}{\dot{w}_F}+\mathcal{F}}{\frac{\dot{w}_O}{\dot{w}_F}+1} \tag{54}$$

Computations for engine performance, therefore, require a knowledge of the variation in theoretical c^* over an extended range of mixture ratios and the fraction of fuel and oxidant vaporized.

FINAL GAS VELOCITY FOR INCOMPLETE COMBUSTION

In the calculations for the complete vaporization of propellants in the cylindrical chamber, the final gas velocity when all the propellants are burned is used to describe the gas-velocity environment of the droplet throughout its history. With incomplete combustion, this point is never achieved in the combustor. However, final gas velocity can be related to the throat velocity and percentage of the propellants vaporized in the actual chamber by assuming isentropic expansion and no combustion or vaporization in the nozzle as follows:

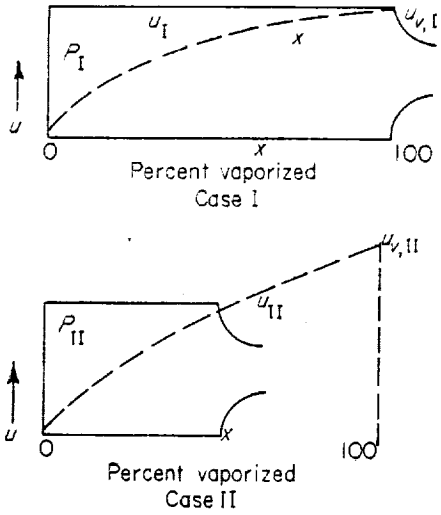

Case I in the diagram illustrates a combustor vaporizing all the propellants, thus obtaining the theoretical c^* value $(c^*_{th})_{O/F}$. The dashed lines are curves representing the gas velocity at various stations. The combustor of case II has the same propellant weight flow and chamber geometry as case I, except that it is shorter and vaporizes only part of the propellants and achieves a lower c^* value, $(c^*_{exp})_{O/F}$. The resultant inefficiency of the case II engine gives it a lower chamber pressure P, so that

$$\frac{P_{II}}{P_I}=\frac{(c^*_{exp})_{O/F}}{(c^*_{th})_{O/F}}=\frac{c^*}{c^*_{th}}=\eta \tag{55}$$

In the two cases, position x of case I and position x of case II have the same amount of propellant vaporized; therefore, the T/M values are the same at these two positions. Thus, the densities will only be functions of the pressure, or

$$\frac{\rho_{x,I}}{\rho_{x,II}}=\frac{P_I}{P_{II}}=\frac{1}{\eta} \tag{56}$$

Applying the continuity equation at position x and realizing that the weight flows of the gases are equal,

$$\frac{u_{x,II}}{u_{x,I}}=\frac{\rho_{x,I}}{\rho_{x,II}}=\frac{1}{\eta} \tag{57}$$

To obtain the gas velocity with complete vaporization for case II, the fact that the ratio of velocities in case I to the velocities in case II (at points where the same fraction of propellant is vaporized) is constant is used. Then,

$$\frac{u_{e,II}}{u_{e,I}}=\frac{u_{x,II}}{u_{x,I}}=\frac{1}{\eta} \tag{58}$$

The efficiency is related to percentage of propellants vaporized by equation (52), so that

$$u_{e,II}=u_{e,I}\frac{(c^*_{th})_{O/F}}{(c^*_{th})_{\mathscr{O}/\mathscr{F}}}\frac{(\dot{w}_O+\dot{w}_F)}{(\mathscr{O}\dot{w}_O+\mathscr{F}\dot{w}_F)} \tag{59}$$

Since $u_{e,I}$ is the velocity at complete vaporization for the 100-percent-efficient combustor, it can be determined from the aerodynamics of the nozzle and the velocity of the gases at the throat. The velocity relation is

$$\frac{u_{e,I}}{u_N}=\frac{u_x}{u_N}=M \tag{60}$$

where u_x/u_N is described in terms of the diameter ratio in equation (46), or, if M is preferred, it is given in reference 15 as a function of the area ratio.

The velocity in the throat can be related to c^* as follows (ref. 16, p. 74):

$$c^*=\frac{\sqrt{g\gamma RT_t/\mathcal{M}}}{\gamma\left(\frac{2}{\gamma+1}\right)^{\frac{\gamma+1}{2(\gamma-1)}}} \tag{61}$$

The velocity of sound, which is also the velocity at the nozzle throat, is (ref. 16, p. 60)

$$u_N=\sqrt{\frac{2g\gamma RT_t/\mathcal{M}}{\gamma+1}} \tag{62}$$

Therefore,

$$u_N=c^*\gamma\left(\frac{2}{\gamma+1}\right)^{\frac{\gamma}{\gamma-1}} \tag{63}$$

Combining equations (59), (60), and (63),

$$u_{e,II}=Mc^*\gamma\left(\frac{2}{\gamma+1}\right)^{\frac{\gamma}{\gamma-1}}\frac{(c^*_{th})_{O/F}}{(c^*_{th})_{\mathscr{O}/\mathscr{F}}}\left(\frac{\dot{w}_O+\dot{w}_F}{\mathscr{O}\dot{w}_O+\mathscr{F}\dot{w}_F}\right) \tag{64}$$

Equation (64) thus relates the final gas velocity for an inefficient combustor $u_{e,II}$ to the fraction of propellants vaporized in the cylindrical chamber and the area or diameter ratio.

AVERAGE PHYSICAL PROPERTIES

The previous equations for mass transfer, heat transfer, and so forth, require the use of the thermal conductivity, viscosity, density, and specific heat of the vapor mixture surrounding the droplet. An exact evaluation of these properties would render the equations almost impossible to integrate; and, furthermore, the precision with which some of the properties are known for the pure components does not justify the work required in determining each property accurately. The properties were therefore calculated at the arithmetic average temperature in the film $\overline{T}$ and for a vapor concentration equal to half the concentration existing at the droplet surface. As a good approximation, the molal concentration of each constituent was taken equal to its partial pressure. The average properties for each drop at a given position were then obtained by averaging each constituent according to its concentration as given in reference 8:

$$\overline{T}=\frac{T_b+T_l}{2} \tag{65}$$

$$k_{mx}=\left(1-\frac{p_{a,s}}{2p_s}\right)k_b+\frac{p_{a,s}}{2p_s}k_a \tag{66}$$

$$\mu_{mx}=\left(1-\frac{p_{a,s}}{2p_s}\right)\mu_b+\frac{p_{a,s}}{2p_s}\mu_a \tag{67}$$

$$\mathcal{M}_{mx}=\left(1-\frac{p_{a,s}}{2p_s}\right)\mathcal{M}_b+\frac{p_{a,s}}{2p_s}\mathcal{M}_a \tag{68}$$

$$c_{p,mx}=\left(1-\frac{p_{a,s}}{2p_s}\right)\frac{\mathcal{M}_b}{\mathcal{M}_{mx}}c_{p,b}+\frac{p_{a,s}}{2p_s}\frac{\mathcal{M}_a}{\mathcal{M}_{mx}}c_{p,a} \tag{69}$$

$$\rho_{mx}=\frac{p_s\mathcal{M}_{mx}}{R\overline{T}} \tag{70}$$

In these relations, subscript a refers to the vaporizing material and subscript b to the surrounding gaseous material. The pure component properties were determined from the equations given in the appendix. To determine the physical properties, it is essential that the temperatures of the liquid drop and the surrounding gases be known at all times.

DROP-SIZE DISTRIBUTIONS

A number of mathematical expressions of size distribution have been proposed and used for liquid sprays. No criterion has been established for choosing the preferred distribution function. For convenience, therefore, the logarithmico-normal distribution function was used in this investigation, and the mathematical expressions for this distribution as given in reference 17 are presented herein.

The distribution of number of drops as a function of size is defined by

$$\frac{dN}{dr}=\frac{a}{r_s}\exp\left\{-\frac{1}{2}\left[\frac{\ln\left(\frac{r_s}{r_n}\right)}{\ln\sigma_G}\right]^2\right\} \tag{71}$$

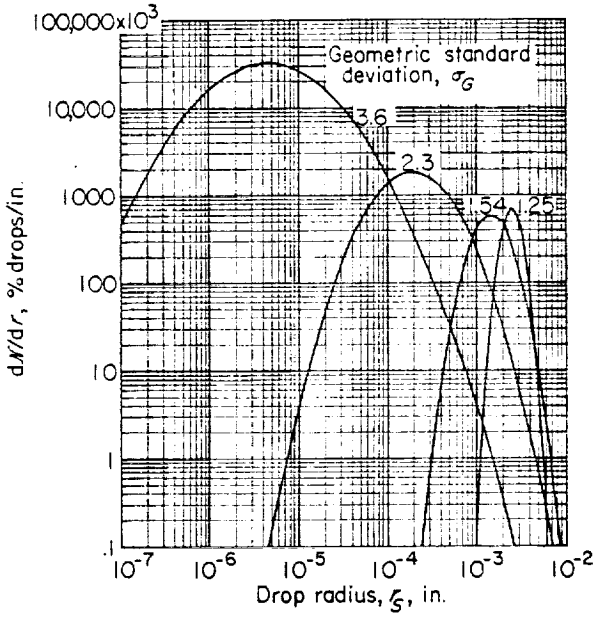

FIGURE 6.—Drop-size distribution. Mass-median drop radius, 0.003 inch (75 microns).

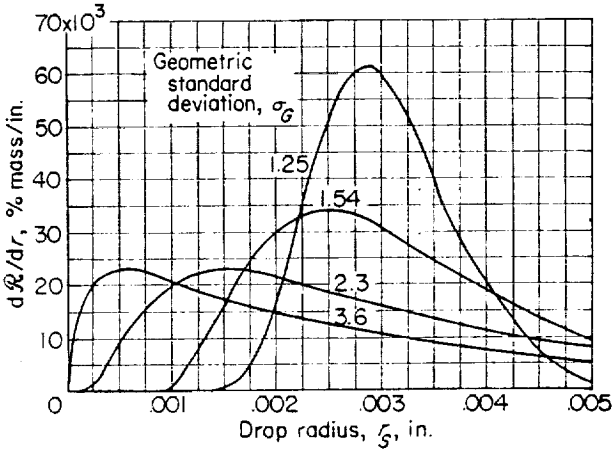

FIGURE 7.—Drop-mass distribution. Mass-median drop radius, 0.003 inch (75 microns).

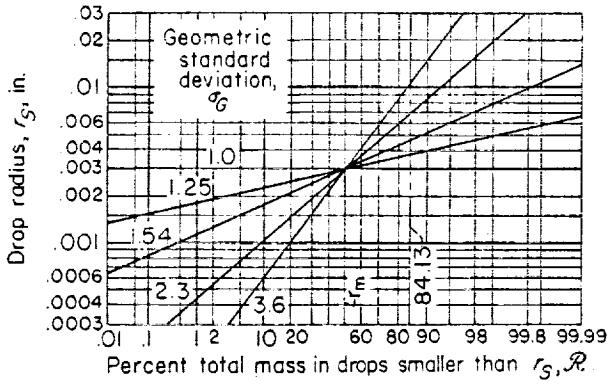

FIGURE 8.—Accumulated drop-mass distribution. Mass-median drop radius, 0.003 inch (75 microns). $\mathcal{R}=\frac{1}{2} \pm[\Gamma \log (r_S/r_m)^{1/2}]/2\Gamma_{1/2}$.

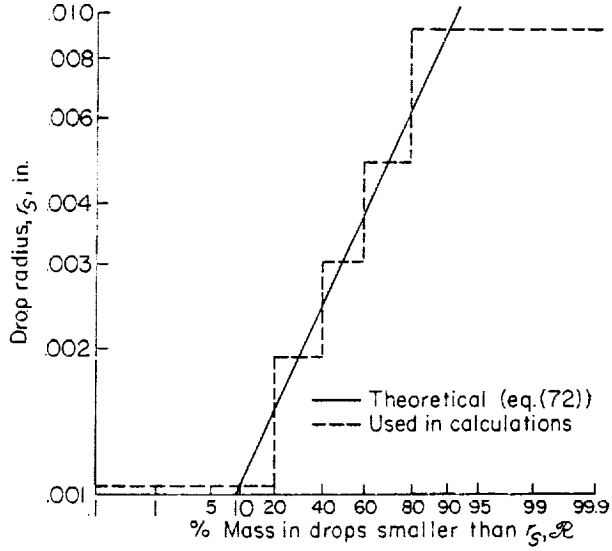

FIGURE 9.—Drop size-mass distribution for geometric standard deviation of 2.3.

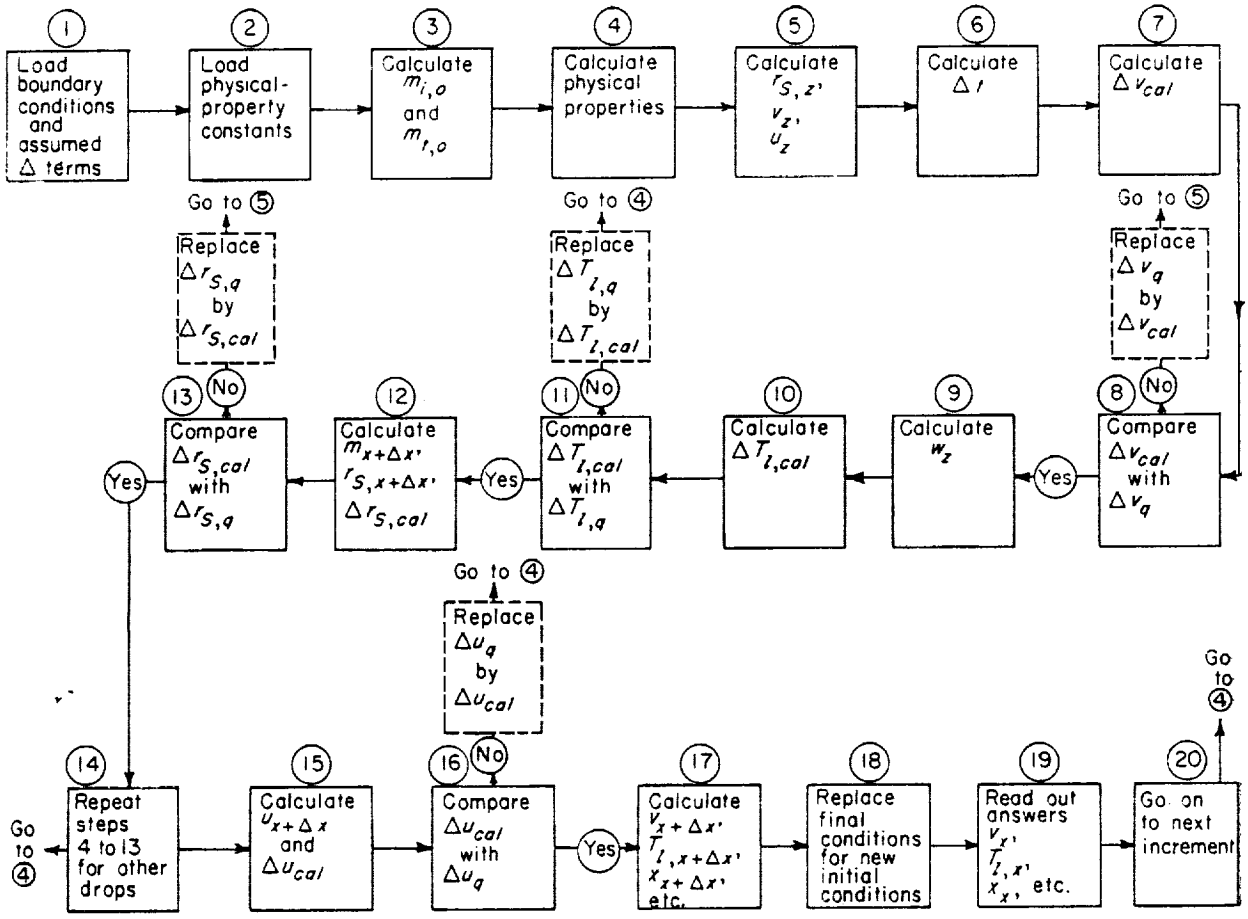

FIGURE 10.—Simplified flow diagram for machine calculations.

while the distribution of mass of drops as a function of size is described by

$$\frac{d\mathcal{R}}{dr}=\frac{a}{r_S}\,exp\left\{-\frac{1}{2}\left[\frac{\ln\left(\frac{r_S}{r_m}\right)}{\ln\sigma_G}\right]^2\right\} \quad (72)$$

Curves for these distributions for various geometric standard deviations σ_G and for a constant mass-median drop radius r_m of 0.003 inch (75 microns) are shown in figures 6 and 7. The accumulated mass-distribution plot of figure 8 indicates the variation obtained with the selected values of the standard deviation. A standard deviation of 2.3 represents a spray in which 68.23 percent of the mass is contained in drops ranging in radius between $r_S=r_m/\sigma_G=32.6$ microns and $r_S=\sigma_G r_m=172.5$ microns.

Because of the difficulty of calculating drop histories for a complete distribution of drop sizes, five different groups of drop sizes were arbitrarily selected to represent the spray for calculation purposes. These sizes were chosen from the log-probability distribution (fig. 8) as those radii for which $\mathcal{R}$ (the percent mass in drops smaller than the given radius) is equal to 10, 30, 50, 70, and 90 percent. The number of drops in each group was then chosen so that each group had 20 percent of the total mass. Plots of the distribution obtained by this method and from equation (72) are shown in figure 9 for a geometric standard deviation σ_G of 2.3.

CALCULATION PROCEDURE

METHOD

The procedure used in calculating the droplet histories is illustrated by the flow diagram of figure 10. The calculation is broken up into small equal increments of chamber length. For the iteration procedure it is necessary to assume values for the changes in drop velocity, temperature, radius, and gas velocity that occur in each increment. For the first step in the calculation these changes were arbitrarily assumed by the machine operator. For other steps the machine used the calculated changes of the previous step as the assumed value. Using the assumed value, the actual changes were calculated and compared with the assumed changes. If calculated and assumed values were within ± 10 percent of each other, the calculated values were assumed to be correct. A limit lower than 10 percent did not appear justified in view of accuracy in the properties or theory. Moreover, a lower limit produced a negligible change in the calculated results. If the assumed and calculated values were outside the ± 10-percent limit, the value that was calculated was used as a new assumed value and the calculation was repeated.

543235—60——3

FLOW DIAGRAM

Step 1.—Load into the machine the following boundary conditions: Final gas velocity u_z, initial size of each drop $r_{l,o}$, number of drops in each size n_i, initial temperature of each drop $T_{l,o,i}$, initial velocity of each drop $v_{l,o}$, and initial gas velocity u_o (which is zero). Also load into the machine assumed values for $\Delta r_{S,i,q}$, $\Delta T_{l,i,q}$, $\Delta v_{l,q}$, and Δu_q for the first step and the size of the increment of length for calculation Δx.

Step 2.—Load all the constants required to calculate physical properties for the propellant being calculated. These appear in the equations given in the appendix.

Step 3.—Calculate the original mass of each drop size $m_{i,o}$ and the total mass:

$$m_{t,o}=\sum_i n_i m_{i,o} \quad (73)$$

where

$$m_{i,o}=\rho_l(4/3)\pi(r_{i,o})^3 \quad (74)$$

The operations in steps 4 to 13 will be for a particular drop i between positions x and $x+\Delta x$.

Step 4.—Calculate the following physical properties for the interval Δx with equations (65) to (70): ρ_l, λ, $c_{p,l}$, $c_{p,a}$, $c_{p,mx}$, $\mathcal{M}_{mx}$, μ_{mx}, and k_{mx} at the mean temperatures determined by

$$T_{l,z}=T_{l,x}+\tfrac{1}{2}\Delta T_{l,q} \quad (75)$$

$$\overline{T}_z=\frac{T_{l,z}+T_b}{2} \quad (76)$$

Step 5.—Calculate mean conditions:

$$r_{S,z}=r_{S,x}+\tfrac{1}{2}\Delta r_{S,q} \quad (77)$$

$$v_z=v_x+\tfrac{1}{2}\Delta v_q \quad (78)$$

$$u_z=u_x+\tfrac{1}{2}\Delta u_q \quad (79)$$

Step 6.—Calculate the time Δt for the drop to travel the increment Δx:

$$\Delta t=\frac{\Delta x}{v_z} \tag{80}$$

Step 7.—Calculate change in drop velocity Δv_{cal} by the equation

$$\Delta v_{cal}=-\tfrac{3}{8}\,C_{D,z}\,\frac{\rho_{mx}}{\rho_l}\,\frac{(u_z-v_z)^2\,\Delta t}{r_{S,z}} \tag{81}$$

where

$$C_{D,z}=27(Re)_z^{-0.84} \tag{82}$$

$$(Re)_z=\frac{2r_{S,z}|u_z-v_z|\rho_{mx}}{\mu_{mx}} \tag{83}$$

Step 8.—Compare Δv_{cal} with Δv_q. If $\left|1-\frac{\Delta v_q}{\Delta v_{cal}}\right|>0.1$, use the value just calculated Δv_{cal} as the new Δv_q and repeat steps 5 to 8.

Step 9.—Calculate vaporization rate:

$$w_z=\frac{D\mathcal{M}_a A_S}{R\overline{T}2r_{S,z}}\,Nu_m p_a\alpha=\frac{2\pi D\mathcal{M}_a r_{S,z}}{R\overline{T}_z}\,Nu_m p_a\alpha \tag{84}$$

where

$$Nu_m=2+0.6(Sc)_z^{1/3}(Re)_z^{1/2} \tag{85}$$

$$(Sc)_z=\frac{\mu_{mx}}{D\rho_{mx}} \tag{86}$$

$$\alpha=\frac{p_s}{p_{a,s}}\ln\frac{p_s}{p_s-p_a} \tag{87}$$

Step 10.—Calculate change in drop temperature:

$$\Delta T_{l,cal}=\frac{1}{mc_{p,l}}(q_{v,z}-w_z\lambda)\Delta t$$

$$=\frac{3}{4\pi r_{S,z}^3\rho_l c_{p,l}}(q_{v,z}-w_z\lambda)\Delta t \tag{88}$$

where

$$q_{v,z}=\frac{A_S k_{mx} Nu_h}{2r_{S,z}}(T_b-T_{l,z})Z$$

$$=2\pi k_{mx} Nu_{h,z} r_{S,z}(T_b-T_{l,z})Z \tag{89}$$

and

$$Nu_{h,z}=2+0.6\,(Pr)_z^{1/3}(Re)_z^{1/2} \tag{90}$$

$$(Pr)_z=\frac{c_{p,mx}\mu_{mx}}{k_{mx}} \tag{91}$$

$$Z=\frac{z}{e^z-1} \tag{20}$$

$$z=\frac{wc_{p,a}}{2\pi k_{mx} r_S Nu_{h,z}} \tag{92}$$

Step 11.—Compare $\Delta T_{l,cal}$ with $\Delta T_{l,q}$. If $\left|1-\frac{\Delta T_{l,q}}{\Delta T_{l,cal}}\right|>0.1$, use the value just calculated $\Delta T_{l,cal}$ as the new $\Delta T_{l,q}$ and repeat steps 4 to 11.

Step 12.—Calculate $m_{x+\Delta x}$, $r_{S,x+\Delta x}$, and $\Delta r_{S,cal}$:

$$m_{x+\Delta x}=m_x-w_z\Delta t \tag{93}$$

$$r_{S,x+\Delta x}=\sqrt[3]{\frac{3m_{x+\Delta x}}{4\pi\rho_l}} \tag{94}$$

$$\Delta r_{S,cal}=r_{S,x+\Delta x}-r_{S,x} \tag{95}$$

Step 13.—Compare $\Delta r_{S,cal}$ with $\Delta r_{S,q}$. If $\left|1-\frac{\Delta r_{S,q}}{\Delta r_{S,cal}}\right|>0.1$, use the value just calculated $\Delta r_{S,cal}$ as the new $\Delta r_{S,q}$ and repeat steps 5 to 13.

Step 14.—Repeat steps 4 to 13 for all drop sizes.

Step 15.—Calculate gas velocity and change of gas velocity:

$$u_{x+\Delta x}=u_x\left(1-\frac{\sum_i n_i m_{i,x+\Delta x}}{m_t}\right) \tag{96}$$

$$\Delta u_{cal}=u_{x+\Delta x}-u_x \tag{97}$$

Step 16.—Compare Δu_{cal} with Δu_q. If $\left|1-\frac{\Delta u_q}{\Delta u_{cal}}\right|>0.1$, use the value just calculated Δu_{cal} as the new Δu_q and repeat steps 4 to 16.

Step 17.—Calculate the following for all drops:

$$v_{x+\Delta x}=v_x+\Delta v_{cal} \tag{98}$$

$$T_{l,x+\Delta x}=T_{l,x}+\Delta T_{l,cal} \tag{99}$$

$$x_{x+\Delta x}=x_x+\Delta x \tag{100}$$

Step 18.—Prepare for calculations in the next increment by setting values for beginning of next increment equal to those at the end of last increment:

$x_{x+\Delta x}$ becomes x_x

$T_{l,t,x+\Delta x}$ becomes $T_{l,t,x}$

$r_{S,t,x+\Delta x}$ becomes $r_{S,t,x}$

$v_{t,x+\Delta x}$ becomes $v_{t,x}$

$m_{t,x+\Delta x}$ becomes $m_{t,x}$

$u_{x+\Delta x}$ becomes u_x

Step 19.—Read out answers for x_x, u_x, $\sum n_i m_{i,x}/m_l$, and for each drop $T_{l,x}$, $r_{S,x}$, v_x, and m_x/m_o.

Step 20.—Perform calculations for the next increment in position by repeating steps 4 to 20.

TYPICAL RESULTS

With the equations and techniques presented in the previous section, it is possible to calculate the histories of individual droplets and sprays for any combustion-chamber configuration, operating condition, or propellant combination. Naturally, this requires considerable time and effort. In addition, it is impossible to perform the calculations now for all conditions that might be desired in the future. Therefore, a few examples have been selected from the numerous calculations (as listed in table I) made to date to illustrate what the various histories look like and the effect on these histories of changes in configurations, operating conditions, or propellants. This section shows what happens in the vaporization process and the effect of certain changes. The results presented herein may also suggest to the reader new problem areas.

HISTORIES OF SINGLE DROPS OF HEPTANE IN A CYLINDRICAL CHAMBER

This section illustrates the histories of single *n*-heptane drops when all the drops initially have the same size. The histories therefore are the same for all drops. This is a highly idealized situation, since most injectors produce sprays that have a wide range in the drop size.

The liquid-droplet temperature T_l is shown in figure 11(a) as a function of the axial distance travelled. The calculated temperature rises rapidly to 845° R (corresponding to a vapor pressure of approximately 133 lb/sq in.), which is the wet-bulb temperature ($q_v = w\lambda$ in eq. (30)) for heptane at the conditions specified. The temperature of 845° R agrees with the measured wall temperatures of internal-film coolants. If the correction factor for unidirectional diffusion α and the effect of mass transfer on heat transfer Z in

TABLE I.—RANGE OF CONDITIONS USED FOR CALCULATIONS IN CYLINDRICAL CHAMBER

Initial drop temperature, $T_{l,o}$, °R					Mass-median drop radius, r_m, microns	Geometric standard deviation, σ_G	Initial drop velocity, v_o, in./sec	Final gas velocity, u_x, in./sec	Chamber total pressure, P, lb/sq in.
Heptane	Ammonia	Hydrazine	Oxygen	Fluorine					
400	300	-----	-----	-----	75	2.3	1,200	9,600	300
[a] 500	[a] 400	[a] 500	[a] 140	[a] 140	25	2.3	1,200	9,600	300
					[a] 75	1.0	1,200	9,600	300
						1.54	1,200	9,600	300
						[a] 2.3	600	9,600	300
							[a] 1,200	2,400	300
								[a] 9,600	150
									[a] 300
									600
								19,200	300
							2,400	9,600	300
						3.6	1,200	9,600	300
					225	2.3	1,200	9,600	300
700	500	700	220	220	75	2.3	1,200	9,600	300

[a] Conditions used for calculations presented in fig. 14.

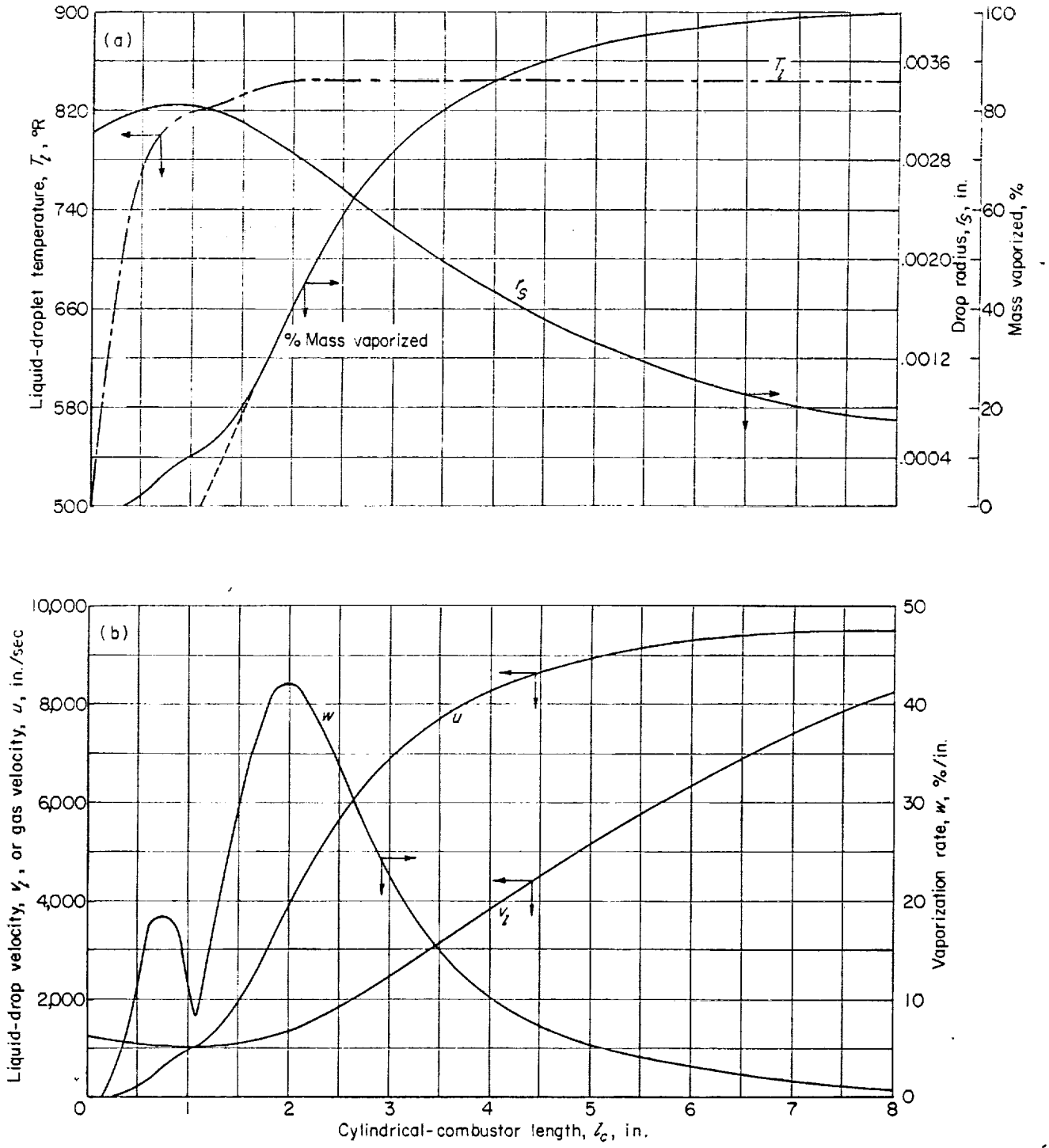

(a) Mass vaporized, drop radius, and liquid-droplet temperature.

(b) Vaporization rate and liquid-drop and gas velocities.

FIGURE 11.—Typical droplet histories. Initial mass-median drop radius, 0.003 inch (75 microns); initial drop velocity, 1200 inches per second; chamber pressure, 300 pounds per square inch absolute; chamber contraction ratio, 3.15; initial drop temperature, 500° R; chamber gas temperature, 5000° R.

equations (12) and (24) were omitted in the calculations, the temperature would be higher (usually taken as the temp. for a vapor pressure of 300 lb/sq in.). It should be noted that approximately 2 inches were required to attain the wet-bulb temperature. In comparison, approximately 8 inches are required to vaporize 99 percent of the drop. Hence, for 25 percent of the distance, this drop was being heated. This point is brought forth to illustrate the significance of assuming that the droplet is initially at the wet-bulb condition to simplify the theoretical calculations.

The percent-mass-vaporized curve (fig. 11(a)) initially has a very small slope because of the low liquid temperature of the drop. As the drop heats, the slope of the percent-mass-vaporized curve increases. At the end of the drop lifetime, the slope again decreases because of the decrease in drop surface area and because the drop is accelerating, thereby decreasing the stay time in a given increment of length. The dashed line indicates what the mass history would look like if the drop were assumed initially to be at the wet-bulb temperature. The dashed line intercepts the x-axis at 1.1 inches, indicating that, on a mass comparison basis, approximately 14 percent of the combustor length required to vaporize 99 percent of the drop had to be added for heating the drop.

The liquid-droplet radius is also shown in figure 11(a). Initially the radius increases because of thermal expansion. After the wet-bulb temperature is reached, the radius curve is proportional to the cube root of 100 minus the percent vaporized. Determining the exponents of the radius curve for

$$r_{S,x}^{n}=r_{S,o}^{n}-\mathscr{K}t \qquad (101)$$

indicated that the exponent n was 1.77 in contrast to the value of 2.0 determined in reference 18 for burning drops in stagnant air.

Gas velocity is plotted as a function of axial distance in figure 11(b). Since gas velocity is proportional to mass vaporized (see eq. (44)), the gas-velocity curve is the same as the mass-vaporized curve and exhibits the same characteristics.

The drop velocity (fig. 11(b)) first decreases because of the drag produced by the low gas velocity. A minimum is reached when the gas velocity equals the drop velocity. After the minimum point the drop velocity increases because of the drag produced by the high gas velocity. There are two significant points of interest in the velocity curves: First, the drop velocity is generally considerably lower than the gas velocity; therefore, simplifying the analysis by assuming that the velocities are equal (as in ref. 19) or a constant ratio (ref. 20) will introduce some errors and will give different results as to the effect of gas velocity and injection velocity on vaporization. The second point of interest is that the velocity difference of 4500 inches per second at 4 inches represents a Weber number We of 150. Under steady-state conditions and long exposure time, drops would shatter at $We>10$. At this time insufficient information is available on drop shattering under transient conditions to determine whether this will occur.

The curve showing the vaporization rate per length of chamber has two peak points and a minimum point (fig. 11(b)). The minimum point occurs when the gas velocity and drop velocity are equal, producing a Reynolds number of zero and a low vaporization rate, as given by equation (12). The vaporization rate is initially low because the vapor pressure (at the low initial temp.) is small, resulting in a low driving force for mass transfer (see eq. (12)). At the end of the chamber, the rate is also low, mainly because of the small surface area of the drop.

HISTORIES OF A HEPTANE SPRAY IN A CYLINDRICAL CHAMBER

This section shows the histories of various individual drops of a heptane spray vaporizing in the cylindrical portion of the combustion chamber. The spray was characterized by having a mass-median drop radius of 0.003 inch (75 microns) and a standard deviation of 2.3 (see eq. (72)). For this spray distribution, the drop sizes and the relative number of drops in each size are as follows:

	Drop size, $r_{s,o}$, microns	Number of drops
$r_{s,1}$	25	1332
$r_{s,2}$	50	207
$r_{s,3}$	75	54
$r_{s,4}$	120	13
$r_{s,5}$	225	2
Total		1608

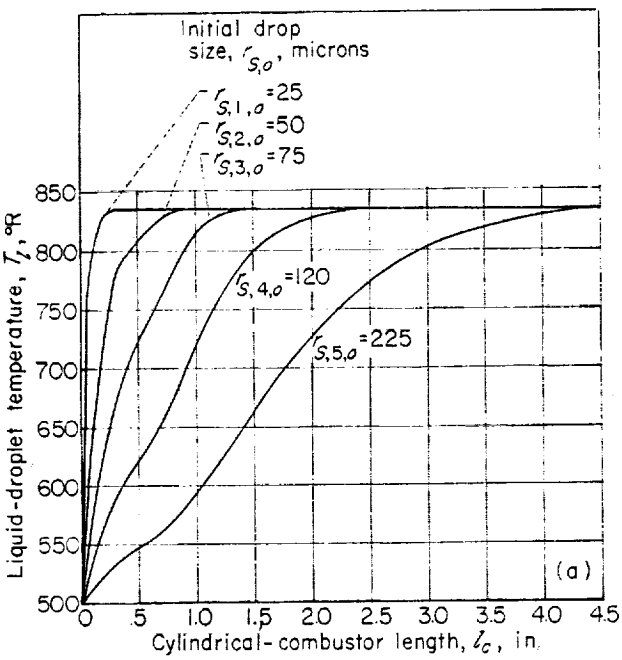

(a) Temperatures of individual drops.

The liquid-droplet temperatures are shown as a function of the axial distance in figure 12(a). The droplets all attain the same wet-bulb temperature as shown in the previous section for the single droplet. (This temperature will vary with the chamber pressure; i.e., decreasing with lower pressures.) The distance and time required to attain the wet-bulb temperature increase with drop size. All the drops use approximately 20 percent of the distance required to vaporize 99 percent of the drops to reach within 1° R of the wet-bulb temperature.

The percent mass vaporized for the individual drops and for the total mass of the spray is shown in figure 12(b). Each drop would follow paths and characteristics similar to those shown in figure 11(a) for single drops when plotted on linear scales. Because of the large variation in length to vaporize the various-sized drops, a log scale for length is used in figure 12(b). To achieve better resolution in both the high and low

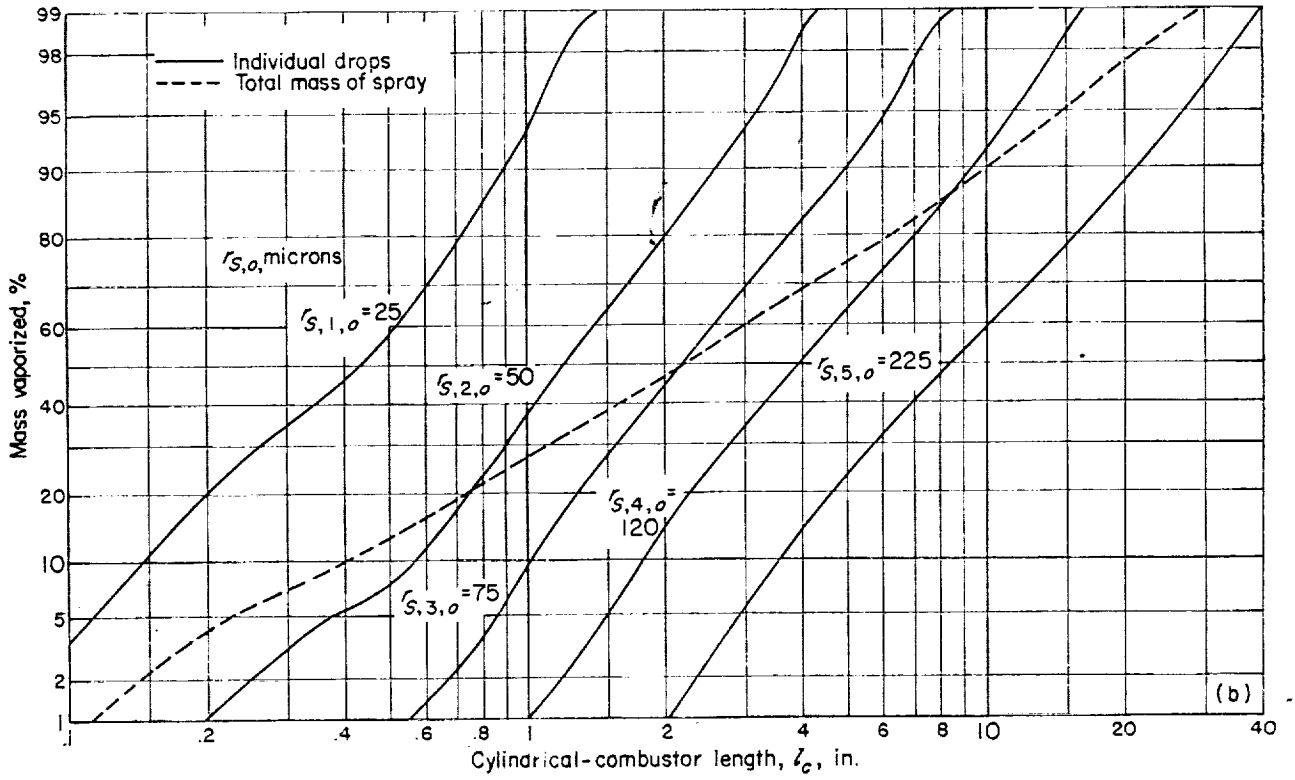

(b) Mass vaporized of individual drops and total mass of spray.

FIGURE 12.—Typical droplet histories for sprays. Initial mass-median drop radius, 0.003 inch (75 microns); geometric standard deviation of spray, 2.3; initial drop velocity, 1200 inches per second; chamber pressure, 300 pounds per square inch absolute; chamber contraction ratio, 3.15; initial drop temperature, 500° R; chamber gas temperature, 5000° R.

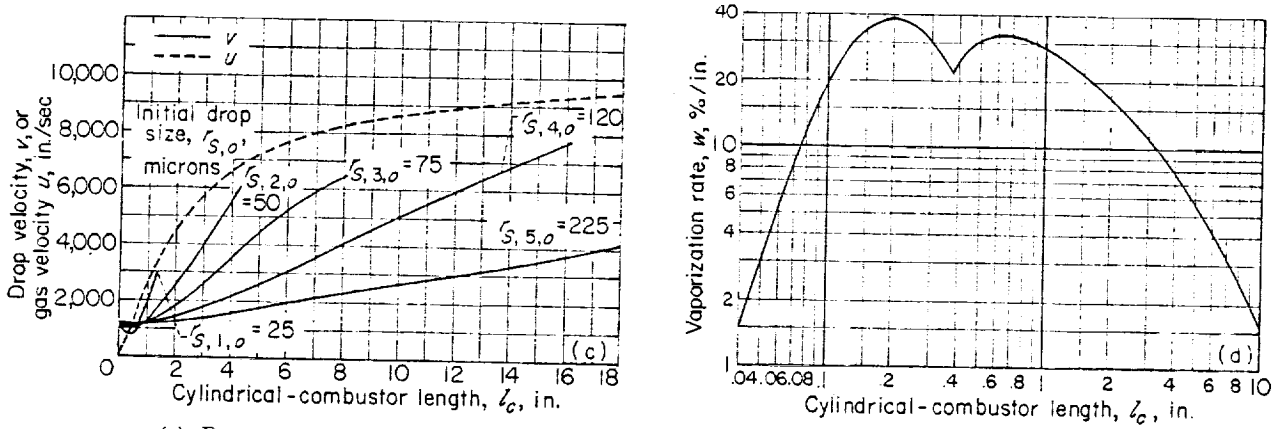

(c) Drop velocities and gas velocity.

(d) Vaporization rate.

FIGURE 12.—Concluded. Typical droplet histories for sprays. Initial mass-median drop radius, 0.003 inch (75 microns); geometric standard deviation of spray, 2.3; initial drop velocity, 1200 inches per second; chamber pressure, 300 pounds per square inch absolute; chamber contraction ratio, 3.15; initial drop temperature, 500° R; chamber gas temperature, 5000° R.

percent mass vaporized, a probability scale was used for this parameter. The small drops (25-micron rad.) vaporize 99 percent of the mass in $\frac{1}{26}$ of the distance required for the large drops (225-micron rad.). The total-mass curve is not as steep as any of the individual curves and crosses the curves of the three intermediate drop-size groups. The total-mass curve initially follows an individual drop size of approximately 35 microns, whereas at the high-percent-vaporized region it is close to a drop size of 120 microns because the two drops in the 225-micron drop-size group are only partially vaporized. Thus, only two drops out of a total of 1608 drops are limiting the total mass vaporized. This then indicates the importance of a few large drops in limiting the performance of an engine and the desirability of eliminating these drops if possible.

The gas and individual drop velocities are shown in figure 12(c). Initially the gas velocity increases rapidly; and, after 1 inch of chamber length, the slope begins to decrease because the small drops are substantially vaporized and the surface area of the larger drops is decreasing. The droplet velocities exhibit the same characteristics as described in the previous section; however, the small drops attain a higher velocity much faster than the larger drops. This drop-velocity difference produces a mixing effect between drops to support the assumption of good mixing. At the same time it also increases the possibility of drop collisions and coalescence between different-sized drops. The importance of this phenomenon cannot be evaluated at this time and suggests another fruitful field of investigation.

The velocity curves for the various drops show that the relation between drop velocity and gas velocity varies with the size of the drops. Small drops follow the gas-velocity curve, while the large drops in a spray remain almost at the injection velocity. The Weber number *We* for the various drops in a spray varies considerably. The small drops attained a Weber number of only 2, while the large drops reach a value around 1000. This further emphasizes the problem of drop shattering, since the large drops are undesirable and appear to be the most likely to shatter.

The total-vaporization-rate curve (fig. 12(d)) for a spray is similar to that for the single drop (fig. 11(b)), the minimum point occurring when the gas velocity reaches the drop velocity, which is approximately the injection velocity of the drops. The maximum vaporization rates for the particular conditions in figure 12(d) are 38 and 32 percent per inch and occur at 0.2 and 0.7 inch. Since 90 percent of the total mass is vaporized in 10 inches, a long chamber would be required to attain complete vaporization even with a high vaporization rate close to the injector.

HISTORIES OF HEPTANE SPRAYS IN A COMBUSTOR WITH A CONVERGENT NOZZLE

This section shows the histories of the three largest drop-size groups of a heptane spray vaporizing in a combustor consisting of a 10-inch

cylindrical chamber and an 8-inch-long convergent conical nozzle. The contraction ratio (ratio of the cross-sectional area of the cylinder to area of the throat) was 3.15. This is believed to represent a typical rocket-engine combustor, although extreme variation from the condition exists. Only the three largest drop-size groups are included, since the smaller drops vaporize in the cylindrical portion of the chamber and therefore their histories are identical to those presented in the previous section. The only additional information in this section illustrates what happens when the convergent nozzle is added to the combustion chamber.

The liquid-droplet-temperature histories (fig. 13) in the cylindrical chamber are identical to those presented in the previous section. In the nozzle portion of the chamber, the droplet temperatures decrease because of the decrease in static pressure and the increase in gas velocity. The rate at which the droplet temperature decreases is a function of the drop size. The smaller the drops, the faster they decrease in temperature as the drops pass through the nozzle.

The percent-mass-vaporized histories (fig. 13) of the individual drops and the total mass in the spray are almost the same for the cylinder and nozzle chamber as for the all-cylindrical chamber. The dash-dot line for the largest drop ($r_{s,5,o}$=225 microns) shows the mass history of this same drop in the all-cylindrical chamber. Initially (between 10 and 15 in.), slightly more mass is vaporized in the all-cylindrical chamber, because the drop temperature is higher, resulting in a higher vapor pressure and driving force for mass transfer. After 15 inches, more mass is vaporized in the chamber with a nozzle, because the velocity difference is much greater.

The gas and individual drop velocities are also shown in figure 13. In the cylinder, the velocities are the same as in the previous section. In the nozzle, the gas velocity increases rapidly, since the speed of sound (46,200 in./sec) must be attained at the nozzle throat. Because of the high gas velocity, the drops accelerate and increase in velocity. Naturally, the acceleration is greatest for the smaller drops, and hence they reach higher velocities. The velocity difference between the gas and droplets is much higher in the nozzle, therefore increasing the Weber number and the possibility of drop shattering. For the

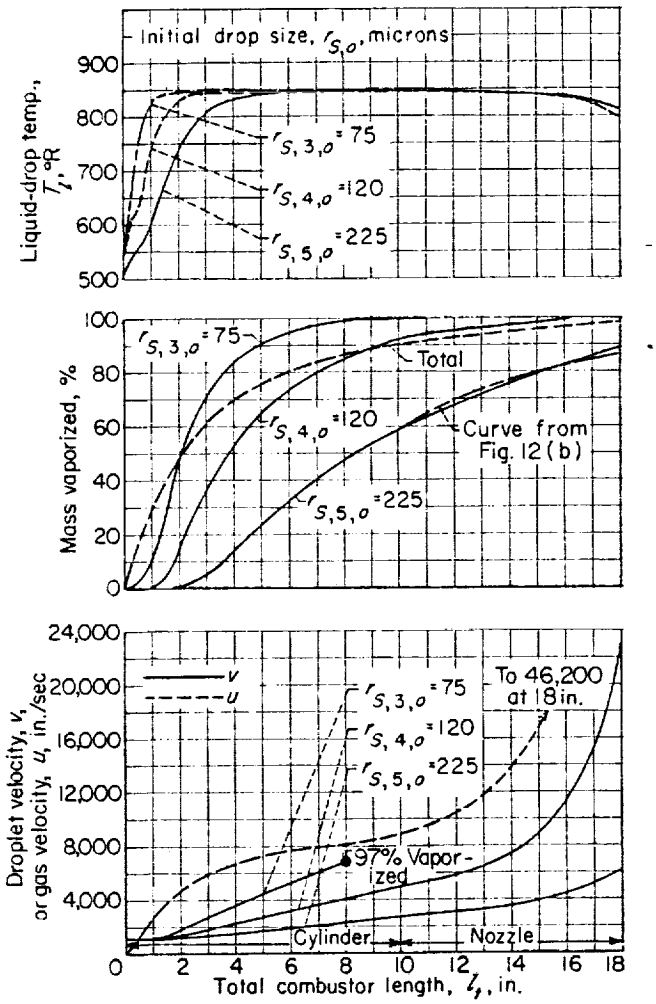

FIGURE 13.—Typical droplet histories in combustor with nozzle. Initial mass-median drop radius, 0.003 inch (75 microns); geometric standard deviation of spray, 2.3; initial drop velocity, 1200 inches per second; chamber pressure, 300 pounds per square inch absolute; chamber contraction ratio, 3.15; initial drop temperature, 500° R; cylindrical-chamber length, 10 inches; nozzle length, 8 inches; nozzle shape, conical; chamber gas temperature, 5000° R.

225-micron drop, the Weber number at the throat is 18,000, which should shatter the drops. This again exemplifies the need for information on drop shattering in steady-flow processes and in accelerating flows that are encountered in a nozzle.

HISTORIES OF VARIOUS PROPELLANT SPRAYS IN A CYLINDRICAL CHAMBER

Previous sections have shown various histories of heptane drops. Changing the propellant will alter these histories. Therefore, this section is

included to illustrate how the propellants influence the drop histories. The heptane curves are the same as presented previously, to facilitate comparisons. For the other propellants all operating and design parameters are the same except initial propellant temperature, which was selected on the basis of typical conditions encountered in rocket engines. Heptane and hydrazine were taken at room temperature, ammonia at its normal boiling point, and fluorine and oxygen at the normal boiling point of liquid nitrogen. The effect of selecting other temperatures is indicated in the section entitled "Effects of Operating and Design Parameters on Mass Histories." For brevity, only the histories of the small drops (25 microns), median drops (75 microns), and large drops (225 microns) in the spray are presented for each propellant.

The calculated temperatures (fig. 14(a)) all rise to a wet-bulb temperature. The wet-bulb temperature and corresponding vapor pressure are tabulated in the following table for the various propellants. Also tabulated is the average ratio of the distance required to reach within 1° R of the wet-bulb temperature to the distance required to vaporize 99 percent of the drop:

Propellant	Wet-bulb temp., °R	Vapor pressure at wet bulb, lb/sq in.	Length to wet bulb / Length to vaporize
Heptane	845	133	1/5
Hydrazine	859	165	1/12
Ammonia	554	205	1/16
Oxygen	234	275	1/10
Fluorine	220	255	1/10

The percent mass vaporized of the individual drops and of the total mass of the spray is shown in figures 14(b) and (c). The listing of the propellants in order of increasing time to vaporize 90 percent of the mass is (1) oxygen and fluorine, (2) heptane, (3) ammonia, and (4) hydrazine. The shapes of all the curves are similar with the exception of the curves for heptane, which cross the ammonia curves.

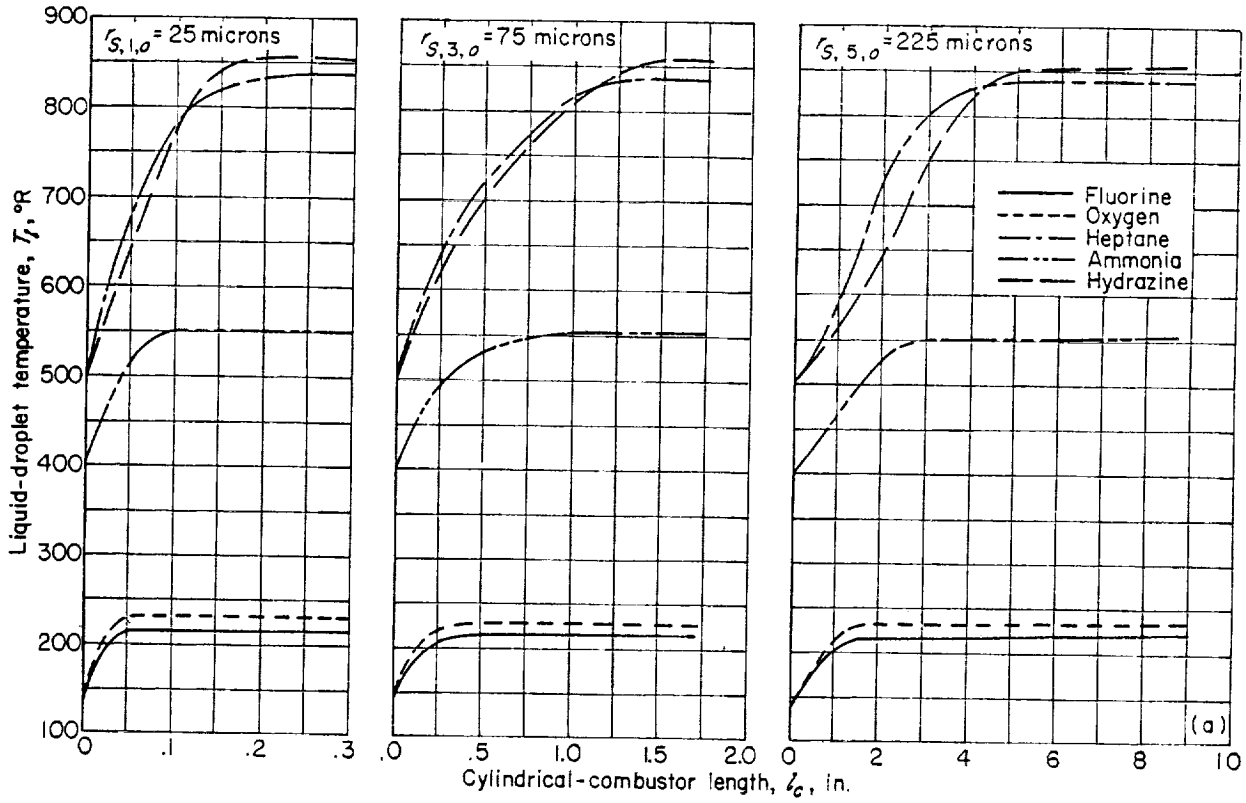

(a) Droplet temperature histories.

FIGURE 14.—Typical droplet histories for various propellants (see table I for conditions).

543235—60——4

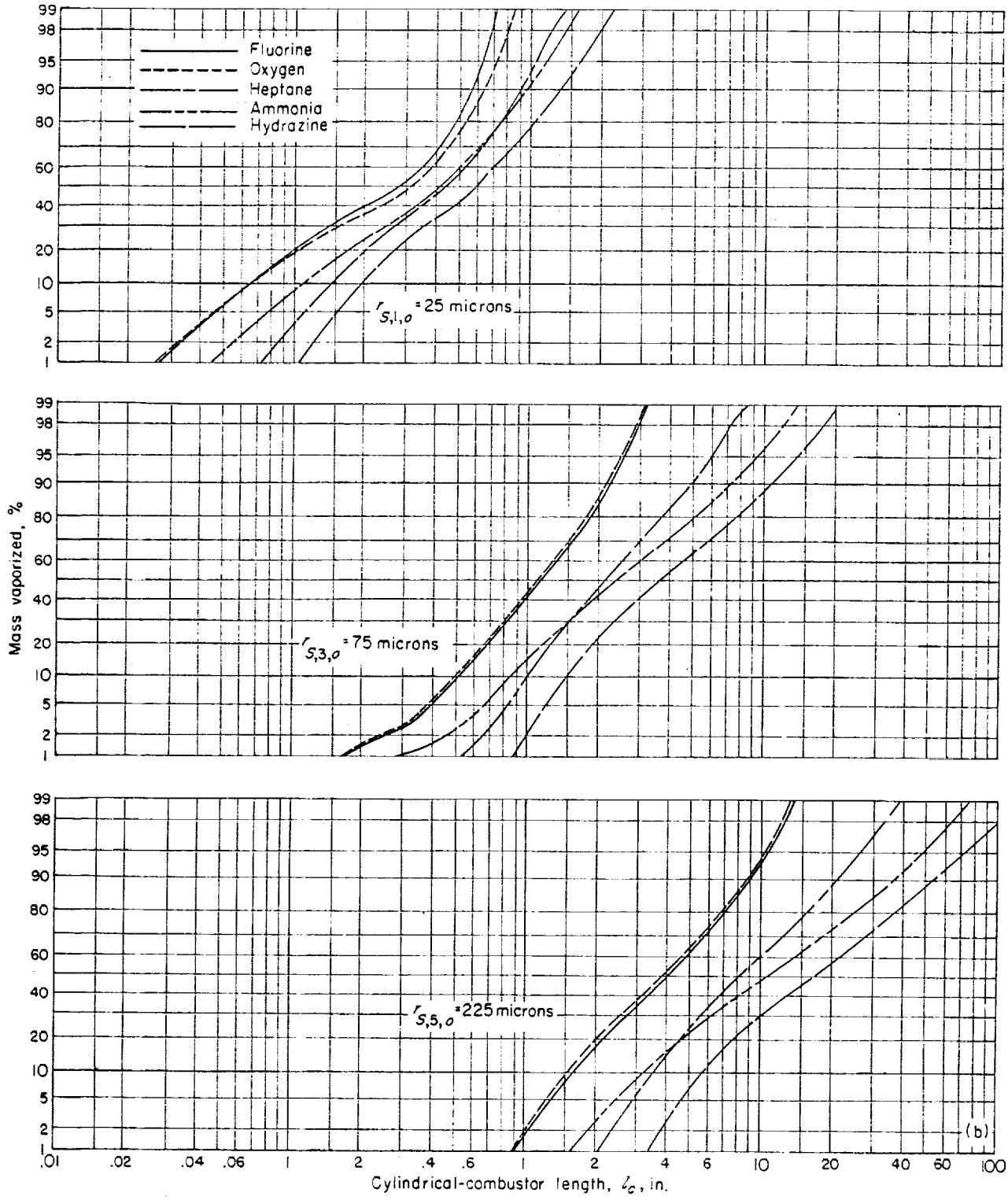

(b) Mass histories for droplets.

FIGURE 14.—Continued. Typical droplet histories for various propellants (see table I for conditions).

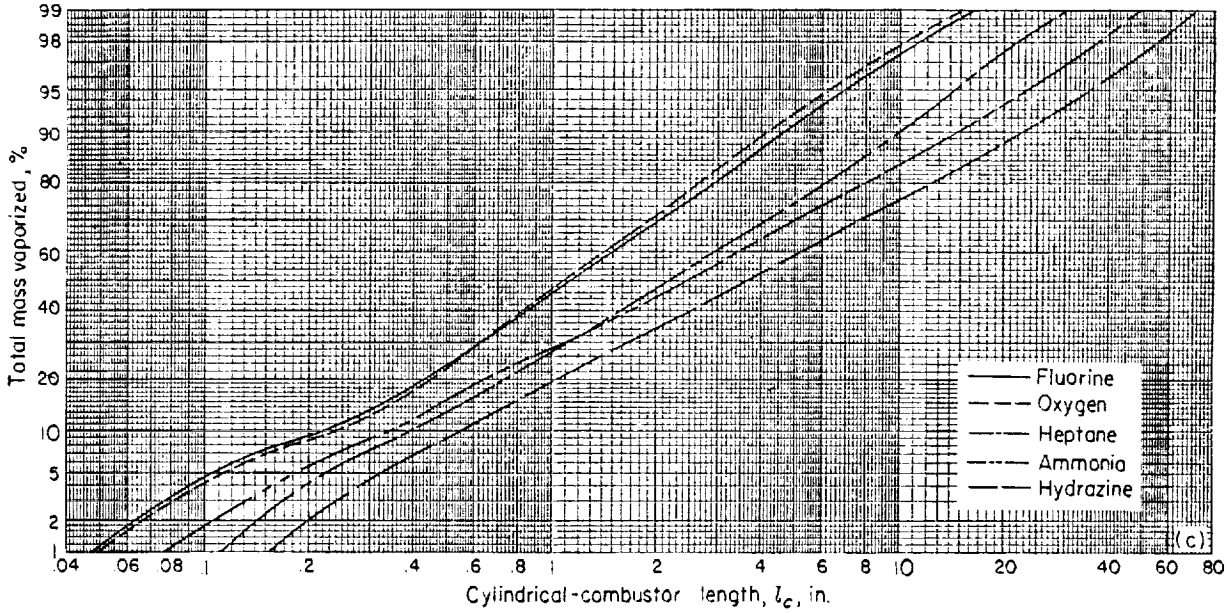

(c) Total mass history for sprays.

The curves of total vaporization rate per unit length (fig. 14(d)) are similar to those presented previously. For each propellant there are two peak points and a minimum. The highest peak vaporization rate is obtained with fluorine. Second highest peak is with oxygen, third with ammonia, fourth with heptane, and the lowest with hydrazine. The peak values occur at different positions in the chamber with the various propellants. The peak occurs closest to the injector face with oxygen and fluorine. The peak is the farthest from the injector with heptane and hydrazine. Ammonia falls between the two extremes.

Gas- and droplet-velocity histories (figs. 14(e) and (f)) for the various propellants all exhibit the same characteristics. A considerable velocity difference between the gas and drops exists for all propellants. For all propellants the maximum Weber number for the large drops is around 1000.

EFFECTS OF OPERATING AND DESIGN PARAMETERS ON MASS HISTORIES

In order to illustrate the effect of changing the conditions from those used in the preceding sections, mass histories of the median drop size (r_m or $r_{S,3,o}$), total mass vaporized, and vaporization rates are presented for several excursions from the conditions presented previously for

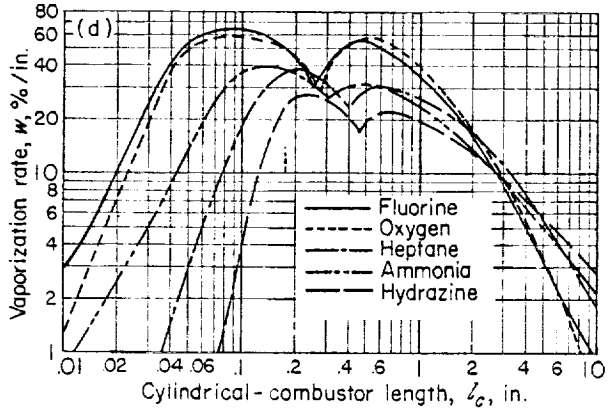

(d) Total vaporization rates.

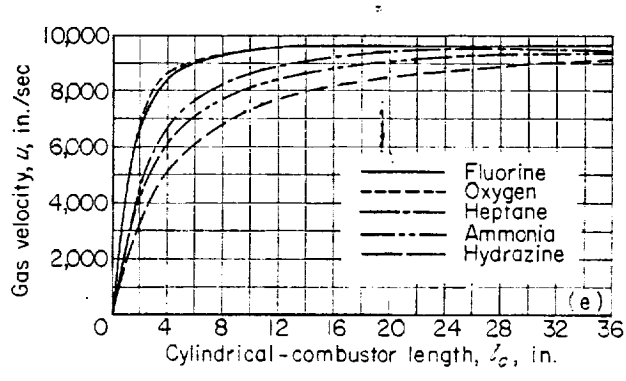

(e) Gas-velocity histories.

FIGURE 14.—Continued. Typical droplet histories for various propellants (see table I for conditions).

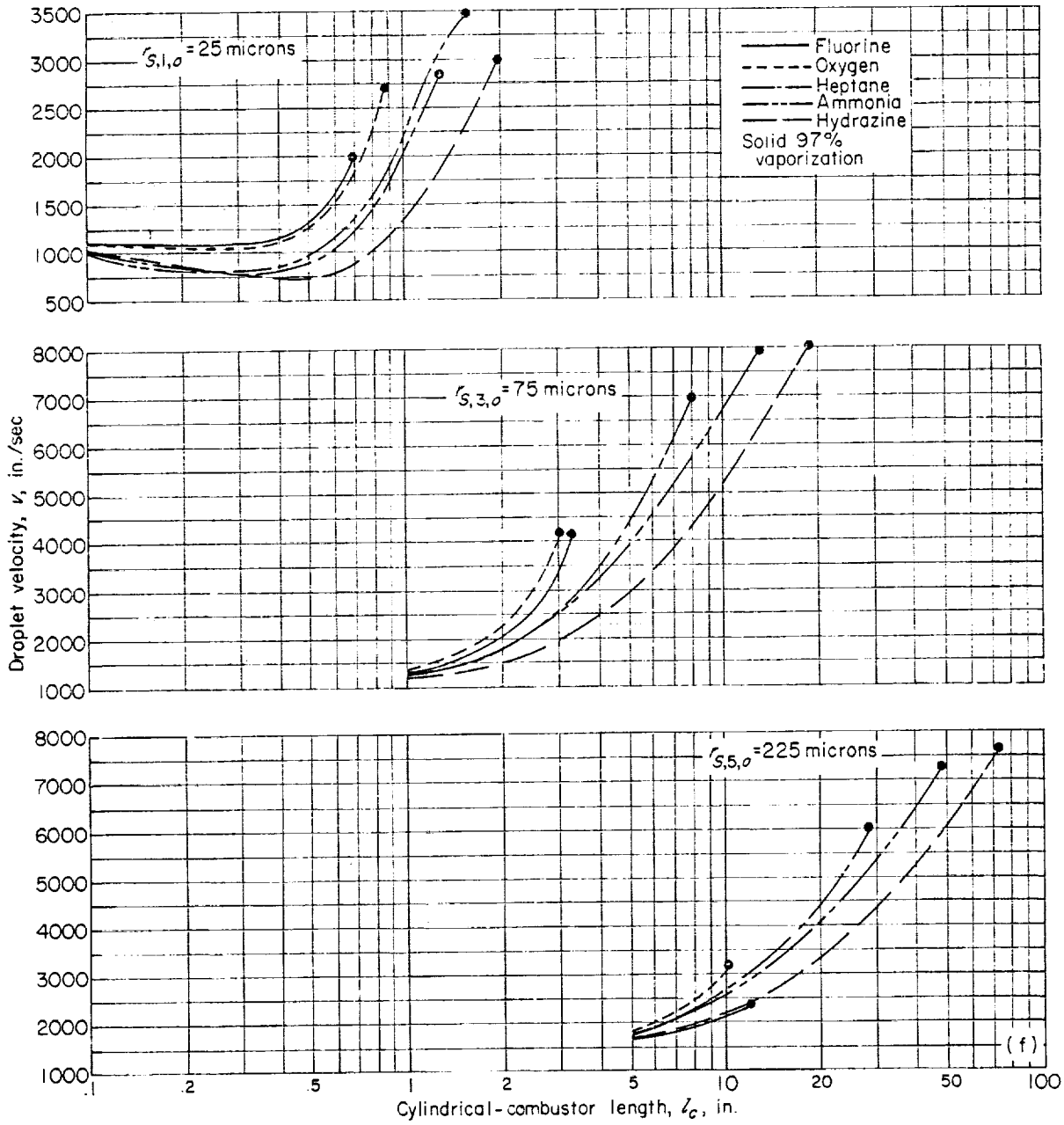

(f) Droplet-velocity histories.

FIGURE 14.—Concluded. Typical droplet histories for various propellants (see table I for conditions).

heptane sprays. Since the variations in histories are quite large for some of the parameter changes, the histories are presented on a log plot of length for convenience. The various conditions for which calculations were performed are given in table I.

The largest effect caused by any parameter change was obtained with a variation in mass-median drop size r_m. The effect of changing the initial mass-median drop size from 0.001- to 0.009-inch (25- to 225-micron) radius is shown in figure 15. As expected, the curves indicate that the smaller drops vaporize in a shorter distance. The mass-vaporized and vaporization-rate curves have about the same shape for all sizes. The results show that the length required to vaporize a given fraction of the total mass of the spray

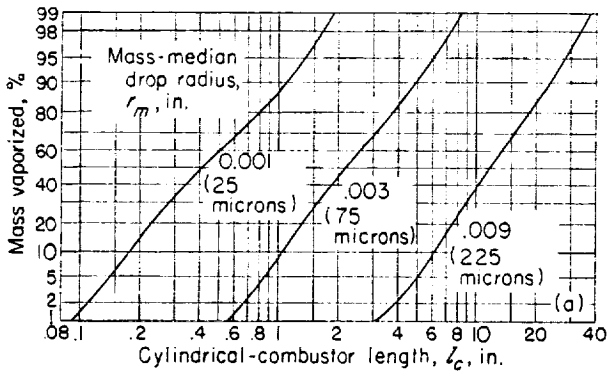

(a) Mass history of median drop.

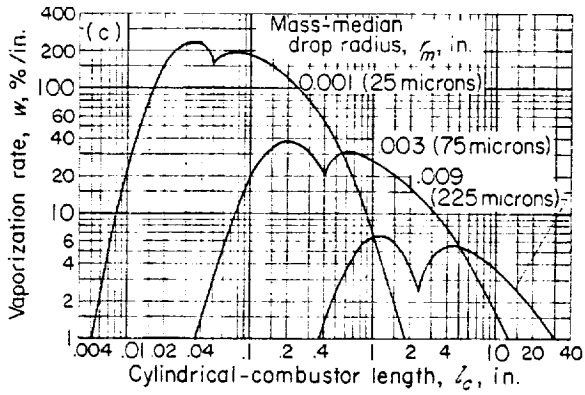

(c) Vaporization rate.

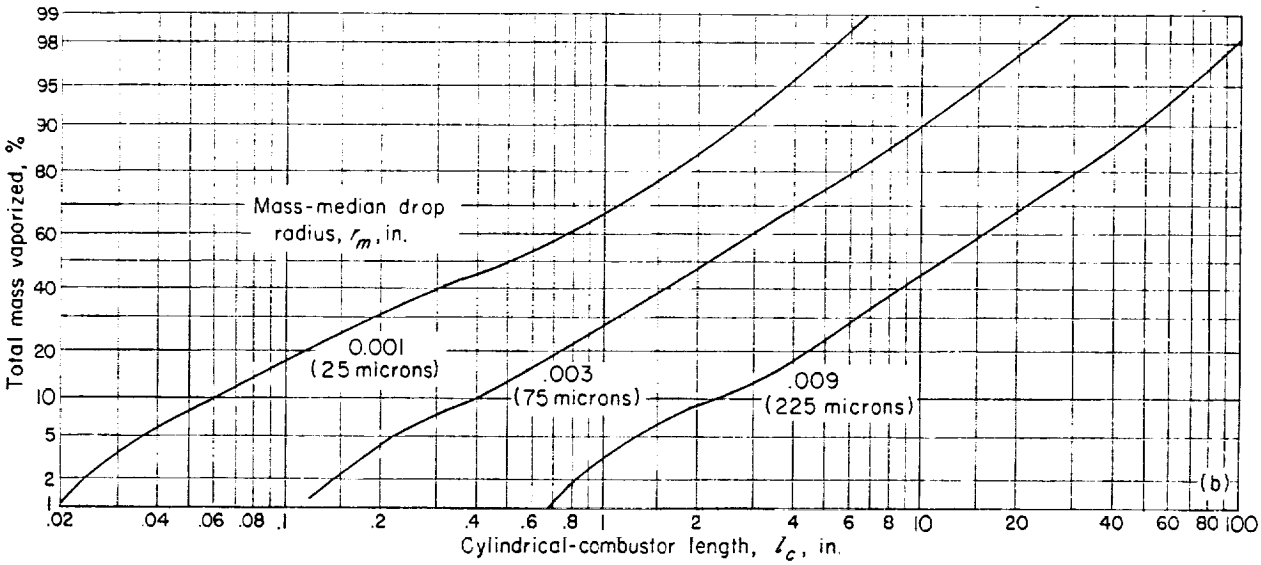

(b) Total mass history.

FIGURE 15.—Effect of mass-median drop size on heptane spray histories. Geometric standard deviation of spray, 2.3; initial drop velocity, 1200 inches per second; chamber pressure, 300 pounds per square inch absolute; chamber contraction ratio, 3.15; initial drop temperature, 500° R; chamber gas temperature. 5000° R.

is proportional to the 1.45 power of the mass-median drop size. The maximum vaporization rate is inversely proportional to the 1.45 power of the mass-median drop size.

The effect of a change in the geometric standard deviation (change in distribution of drop sizes) is shown in figure 16. The effect of changing the standard deviation on the median-drop-size history is rather negligible, as shown in figure 16(a). Since these curves are for the same drop size, one would not expect much variation. The occurrence of some variation is due to the change in gas velocity, which is proportional to the curve of total mass vaporized. Figures 16(b) and (c) show that, in the low precent-mass-vaporized region, the percent of the spray vaporized and the vaporization rate near the injector increase because of the large number of small drops in

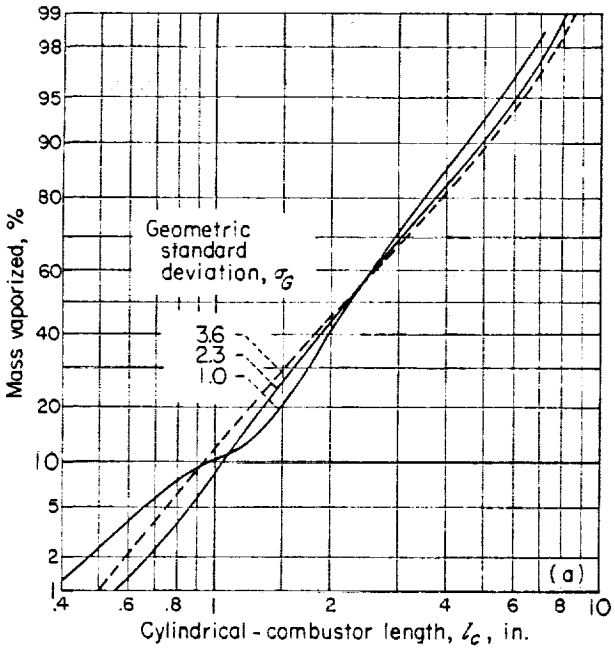

(a) Mass history of median drop.

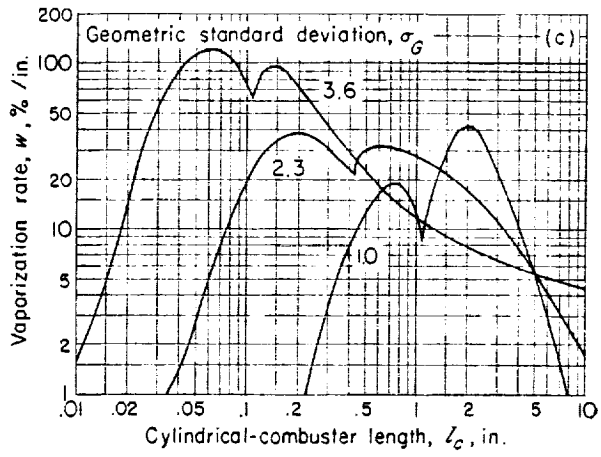

(c) Vaporization rate.

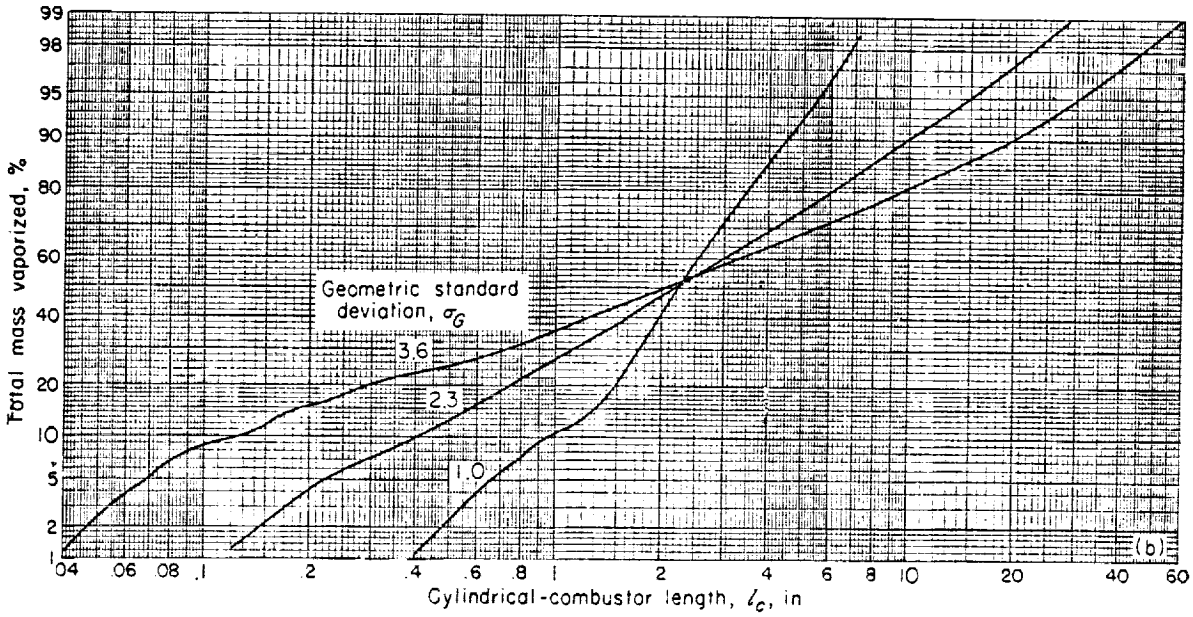

(b) Total mass history.

FIGURE 16.—Effect of geometric standard deviation on heptane spray histories. Initial mass-median drop radius, 0.003 inch (75 microns); initial drop velocity, 1200 inches per second; chamber pressure, 300 pounds per square inch absolute; chamber contraction ratio, 3.15; initial drop temperature, 500° R; chamber gas temperature, 5000° R.

a distribution with a large deviation, as shown in figures 6 and 7. The curves for the various deviations all cross in the 50- to 60-percent-mass-vaporized region. In the high percent-mass-vaporized region, the spray with a larger standard deviation requires a longer chamber to vaporize a given percentage of the mass, since it requires more time and distance to vaporize the larger drops, as explained previously. A spray with a deviation of 3.6 requires a chamber eight times as long as one with a deviation of 1.0 (single drop size) to vaporize 99 percent of the fuel.

Changes produced by varying the intitial drop velocity are shown in figure 17. The slopes of the total and individual-drop mass-vaporized curves vary somewhat with initial velocity, but to a reasonable degree of accuracy remain the same with initial velocity. The length required to vaporize a given percentage of total mass of the spray is proportional to the 0.75 power of initial velocity. If entrainment of drops in the gas or a constant ratio between drop and gas velocity had been assumed, there would be no effect on the mass-vaporized curves of a change in initial drop velocity. The rate curve shows that the maximum vaporization rate is obtained with a low initial velocity. The vaporization-rate curves also show that the minimum point, which occurs when the

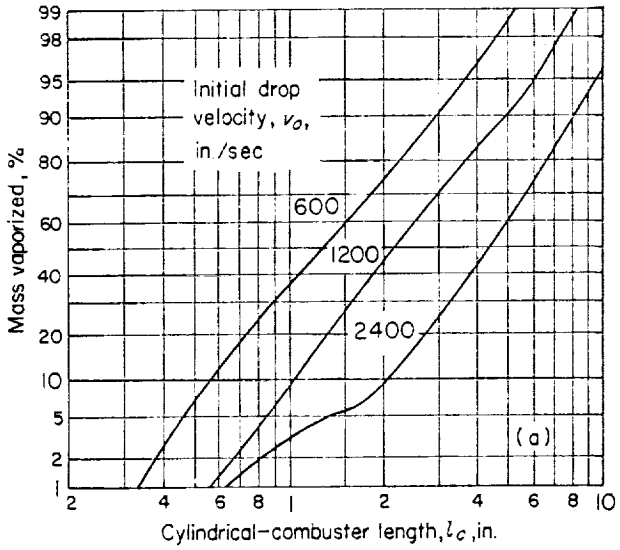

(a) Mass history of median drop.

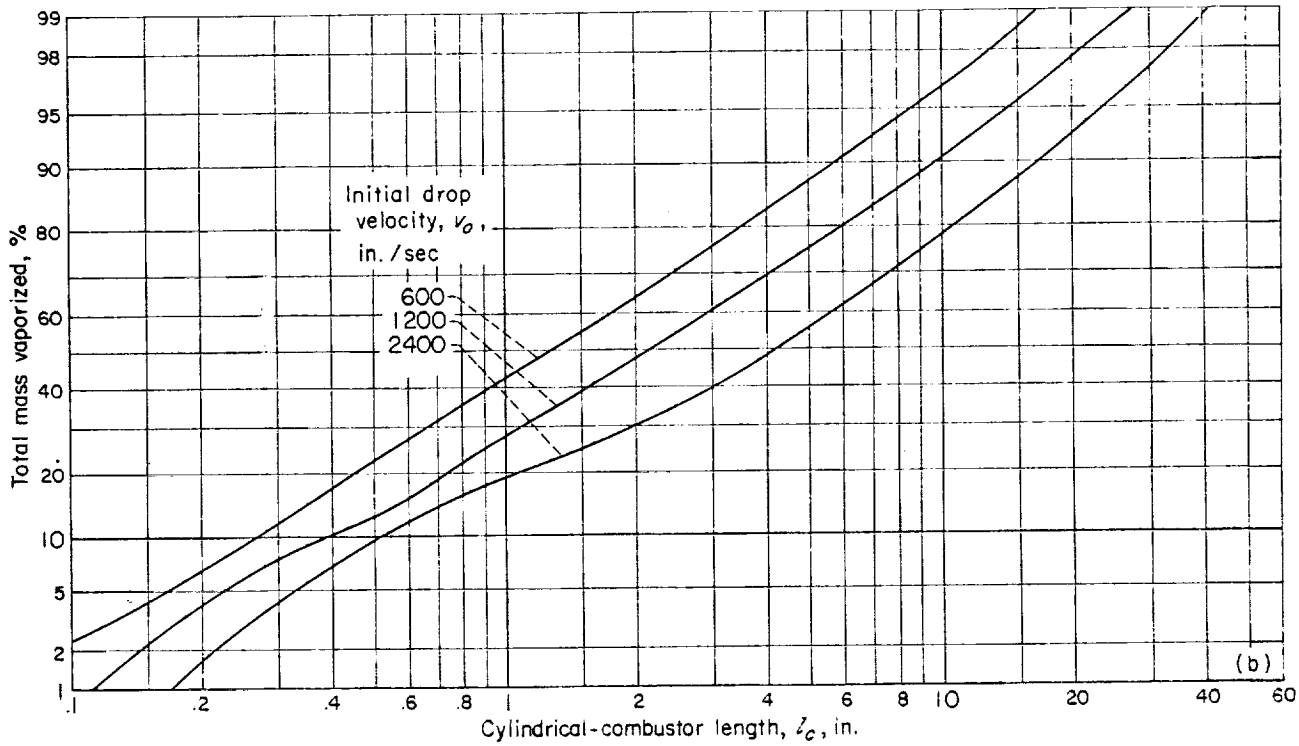

(b) Total mass history.

FIGURE 17.—Effect of initial drop velocity on heptane spray histories. Initial mass-median drop radius, 0.003 inch (75 microns); geometric standard deviation of spray, 2.3; chamber pressure, 300 pounds per square inch absolute; chamber contraction ratio, 3.15; initial drop temperature, 500° R; chamber gas temperature, 5000° R.

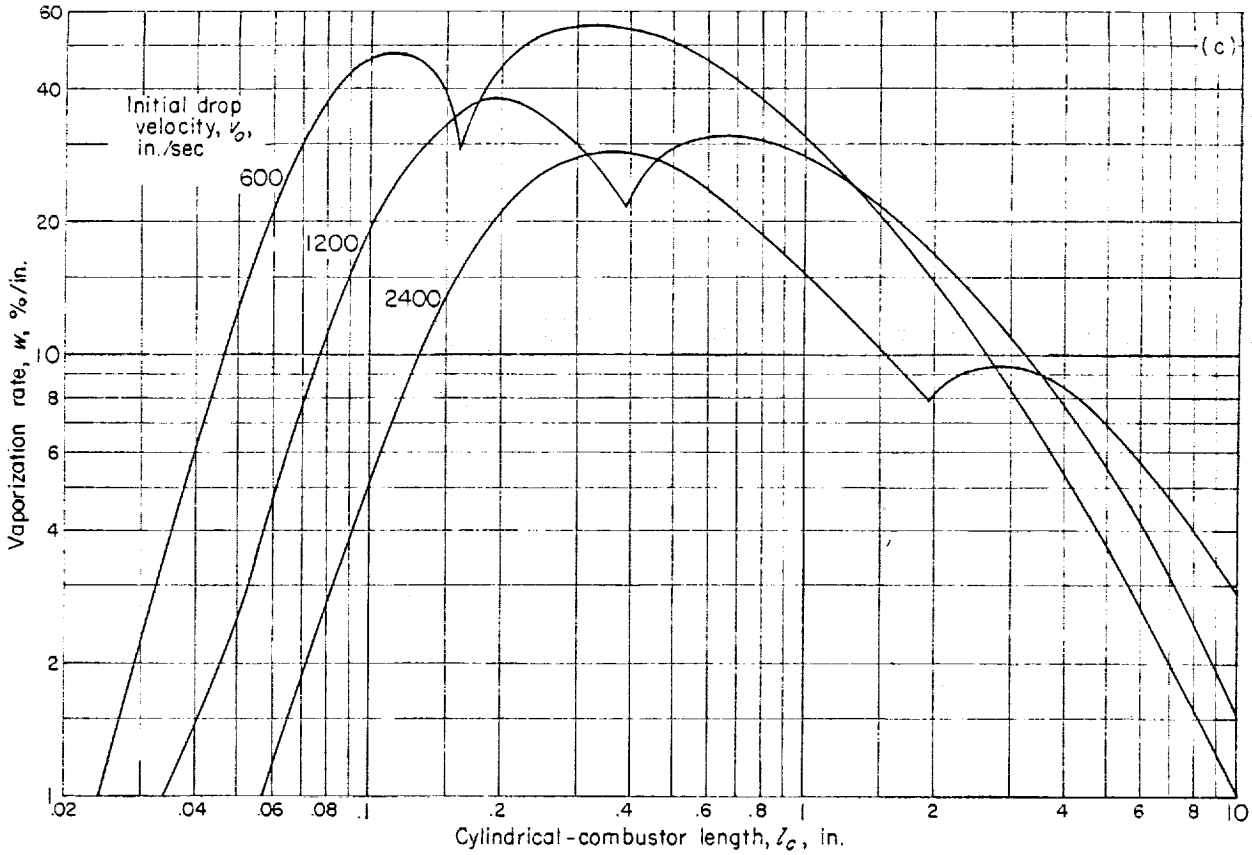

(c) Vaporization rate.

FIGURE 17.—Concluded. Effect of initial drop velocity on heptane spray histories. Initial mass-median drop radius, 0.003 inch (75 microns); geometric standard deviation of spray, 2.3; chamber pressure, 300 pounds per square inch absolute; chamber contraction ratio, 3.15; initial drop temperature, 500° R; chamber gas temperature, 5000° R.

droplet velocity is the same as the gas velocity, varied with initial velocity. The vaporization-rate curves or percent-mass-vaporized curves show that the higher the initial velocity, the more mass that is vaporized before the minimum point is reached.

Variations obtained by changes in the chamber pressure are shown in figure 18. The higher the chamber pressure, the higher the vaporization rate and amount vaporized in a given length. The length of chamber required to attain a given high percentage of mass vaporized is inversely proportional to the 0.66 power of chamber pressure. This effect of chamber pressure would not occur in an analysis which assumed that the vaporization process followed equation (101), since there is no pressure dependence in it. The pressure dependence is introduced in the theory via the drop equation (33) and the vaporization equation (8) through the pressure term $p_s - p_{a,s}$ and density ρ_{mx}.

Contraction ratio is the ratio of the cylindrical-chamber cross-sectional area to the nozzle throat area. Small contraction ratios yield high gas velocities, while large contraction ratios yield low gas velocities. Changes produced in droplet histories by variation in the contraction ratio of the combustor are shown in figure 19. The slopes of the total and individual-drop mass-vaporized curves (figs. 19(a) and (b)) vary somewhat with contraction ratio, but, like the effect of initial velocity, remain constant to a reasonable degree of accuracy. In the short lengths the slopes are different, which produces a crossover point in the curves. The curves show that the smaller the contraction ratio, the greater the amount of propellant vaporized in a long chamber. For very large contraction ratios where the gas velocity is always lower than the injection velocity, the trend of figure 19 will reverse as residence time becomes the phenomenon governing the conversion rate. This reversal should occur at a contraction ratio

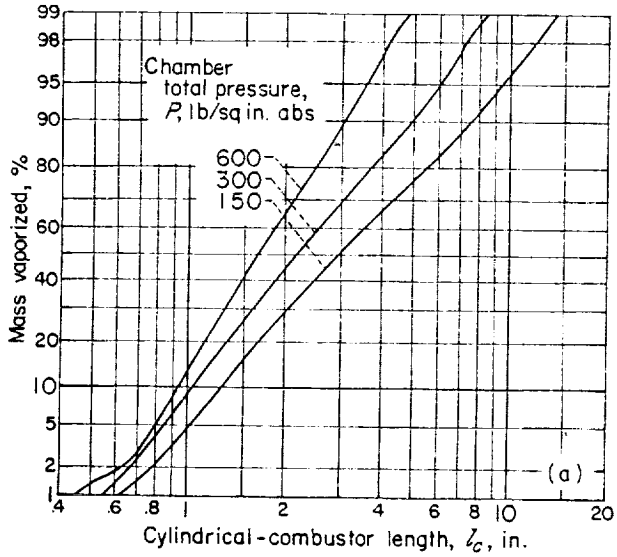

(a) Mass history of median drop.

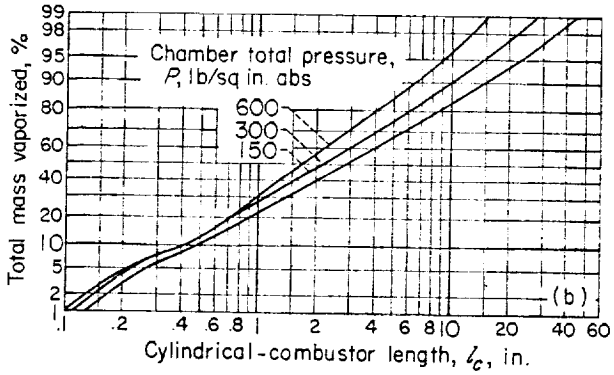

(b) Total mass history.

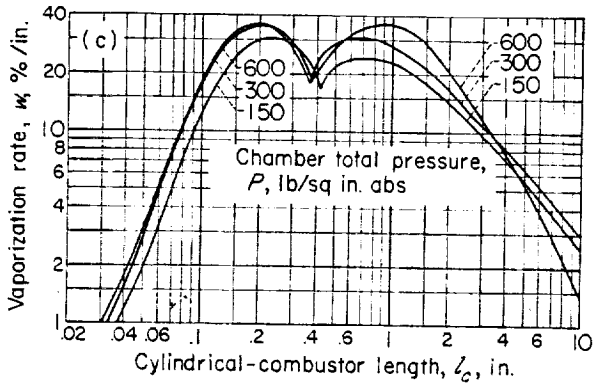

(c) Vaporization rate.

FIGURE 18.—Effect of chamber pressure on heptane spray histories. Initial mass-median drop radius, 0.003 inch (75 microns); geometric standard deviation of spray, 2.3; initial drop velocity, 1200 inches per second; chamber contraction ratio, 3.15; initial drop temperature, 500° R; chamber gas temperature, 5000° R.

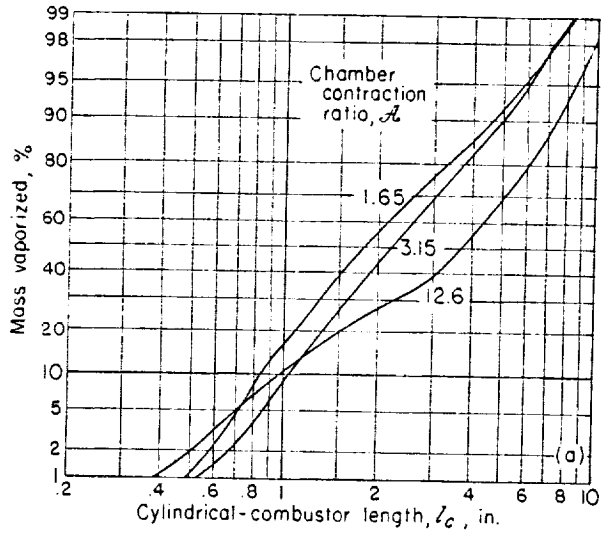

(a) Mass history of median drop.

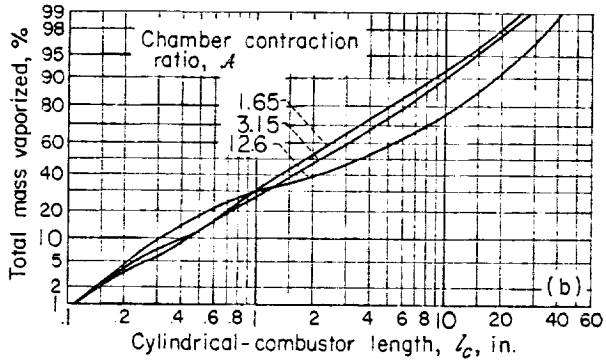

(b) Total mass history.

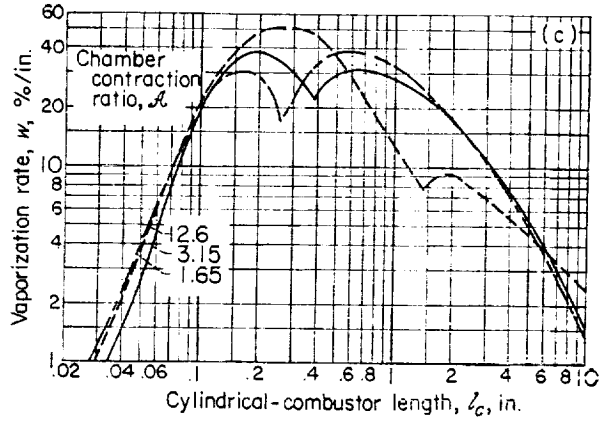

(c) Vaporization rate.

FIGURE 19.—Effect of chamber contraction ratio on heptane spray histories. Initial mass-median drop radius, 0.003 inch (75 microns); geometric standard deviation of spray, 2.3; initial drop velocity, 1200 inches per second; chamber pressure, 300 pounds per square inch absolute; initial drop temperature, 500° R; chamber gas temperature, 5000° R.

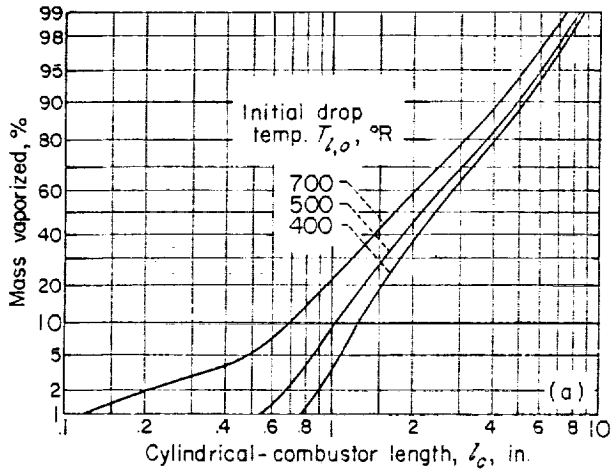

(a) Mass history of median drop.

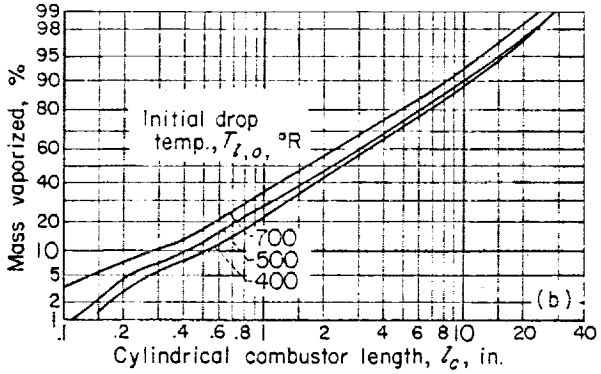

(b) Total mass history.

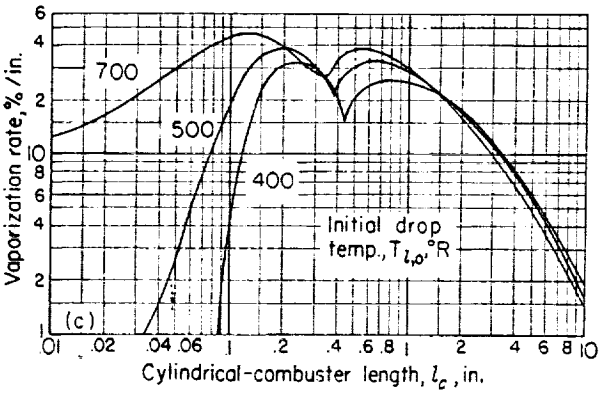

(c) Vaporization rate.

FIGURE 20.—Effect of initial drop temperature on heptane spray histories. Initial mass-median drop radius, 0.003 inch (75 microns); geometric standard deviation of spray, 2.3; initial drop velocity, 1200 inches per second; chamber pressure, 300 pounds per square inch absolute; chamber contraction ratio, 3.15; chamber gas temperature, 5000° R.

of about 20.

The effect of increased vaporization with decreasing contraction ratio shown in the present analysis is opposite to that predicted for a stirred reactor or vaporization calculations as determined in references 19 and 20. In references 19 and 20 the drop velocity is directly proportional to the gas velocity, and the vaporization or burning rate is independent of velocity difference. For a stirred reactor the amount of material reacted is proportional to the stay time of the gases. Since large contraction ratios provide longer residence

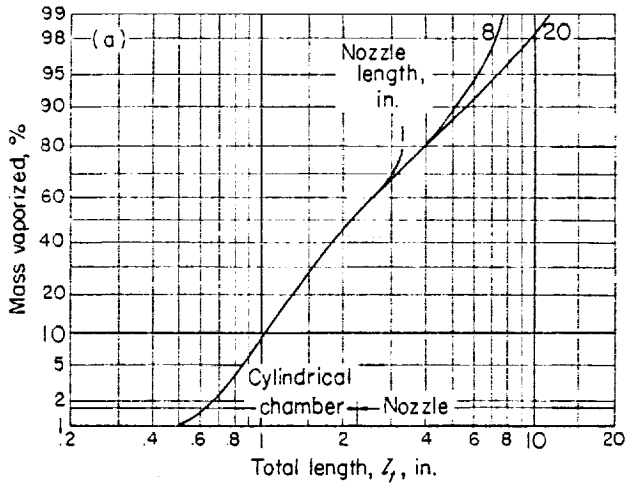

(a) Mass history of median drop.

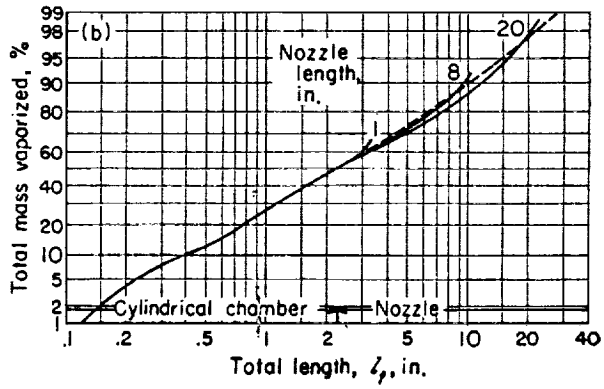

(b) Total mass history.

FIGURE 21.—Effect of nozzle length on heptane spray histories. Initial mass-median drop radius, 0.003 inch (75 microns); geometric standard deviation of spray, 2.3; initial drop velocity, 1200 inches per second; chamber pressure, 300 pounds per square inch absolute; chamber contraction ratio, 3.15; initial drop temperature, 500° R; nozzle exponent, 1.0; chamber gas temperature, 5000° R; chamber length, 2.25 inches.

times of the gases, a large contraction ratio is more favorable for conversion of gaseous propellants to products.

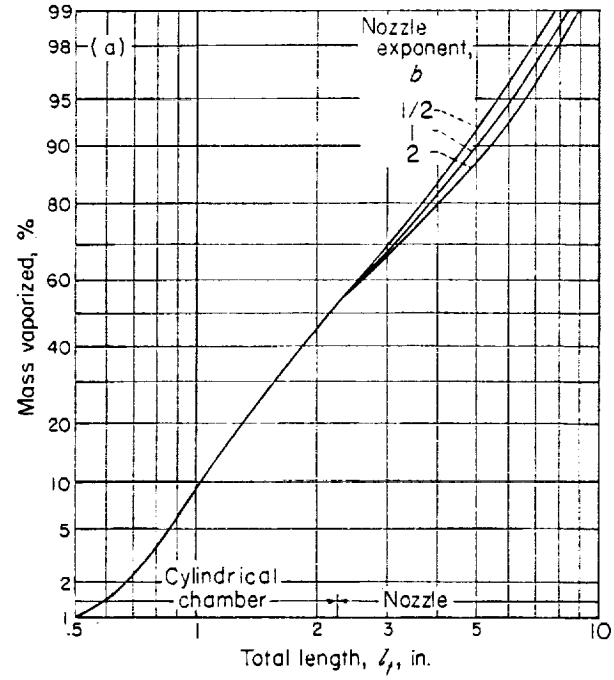

(a) Mass history of median drop.

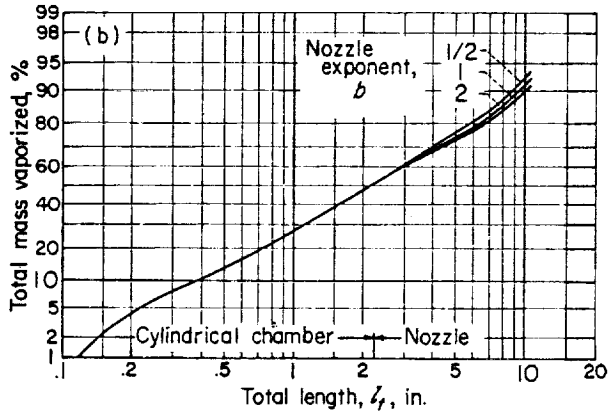

(b) Total mass history.

FIGURE 22.—Effect of nozzle exponent on heptane spray histories. Initial mass-median drop radius, 0.003 inch (75 microns); geometric standard deviation of spray, 2.3; initial drop velocity, 1200 inches per second; chamber pressure, 300 pounds per square inch absolute; chamber contraction ratio, 3.15; initial drop temperature, 500° R; nozzle length, 8 inches; chamber gas temperature, 5000° R; chamber length, 2.25 inches.

Figures 19(a) and (b) show that the length required to vaporize a given high percentage of mass, using the model present herein, is proportional to the 0.44 power of contraction ratio. Figure 19(c) shows that the minimum point in the vaporization-rate curve varies with contraction ratio. The higher the contraction ratio, the more mass vaporized before the minimum point is reached.

Histories for three initial drop temperatures are shown in figure 20. All the curves show that a higher initial liquid temperature is moderately beneficial, as the drop spends less time reaching the wet-bulb temperature. The biggest effect is in the very low percent-mass-vaporized region. This effect of initial temperature would not be observed in an analysis that neglects the heating period.

The results of changing the length and shape of the convergent-nozzle section of a combustor are illustrated in figures 21 and 22. The cylindrical chamber for these calculations was 2¼ inches long and vaporized approximately 50 percent of the total mass in the cylindrical chamber. The curves show that the nozzle shape has a small effect on the vaporization histories of the individual drops (illustrated by the curves for the median drop size) and total mass (fig. 21). The largest amount of mass vaporized is obtained in a given length with a nozzle having a horn shape ($b=½$, see fig. 5), and the lowest with a bell shape ($b=2$) (fig. 22). Increasing the length of the nozzle increases the amount of mass vaporized. The total-mass-vaporized curves are different for the different nozzle lengths; however, they all follow the trends shown for the long cylindrical chamber (represented by the dashed line in fig. 21(b)).

To determine whether the gas temperature used in the calculations affected the mass histories, calculations were performed for gas temperatures of 4000°, 5000°, and 7000° R. Except for the time when the drops were heating, the histories were almost identical. For this reason, the 5000° R gas temperature used in most of the calculations does not materially affect the applicability of the results.

The selection of the five drop sizes chosen to represent the normal distribution in the calculations was arbitrary. Therefore, a comparison was

made by performing identical calculations with five different drop sizes representing the same distribution. Initial drop sizes in the five groups used for the comparison are given as case B in the following table:

	Case A		Case B	
	Initial radius, in.	Percent total mass	Initial radius, in.	Percent total mass
$r_{s,1}$	0. 00102	20	0. 000676	8
$r_{s,2}$	. 00192	20	. 00147	24
$r_{s,3}$	. 003	20	. 003	36
$r_{s,4}$	. 0048	20	. 00613	24
$r_{s,5}$	. 00901	20	. 0133	8

There was little difference between the two cases; therefore, it is felt that the five sizes used in most of the calculations were representative of an actual spray. If more groups had been used to represent the actual spray, the results would have been slightly different; however, this minor difference would not appear to justify a more complicated calculation procedure.

EFFECT OF INCOMPLETE VAPORIZATION ON ENGINE PERFORMANCE

Equations (51) to (54) relate c^* efficiencies to the percentage of fuel and oxidant vaporized and burned. This section will illustrate graphically the relation between c^* and percentage of propellant vaporized and burned and the effects of changes in mixture ratio and propellants on this relation.

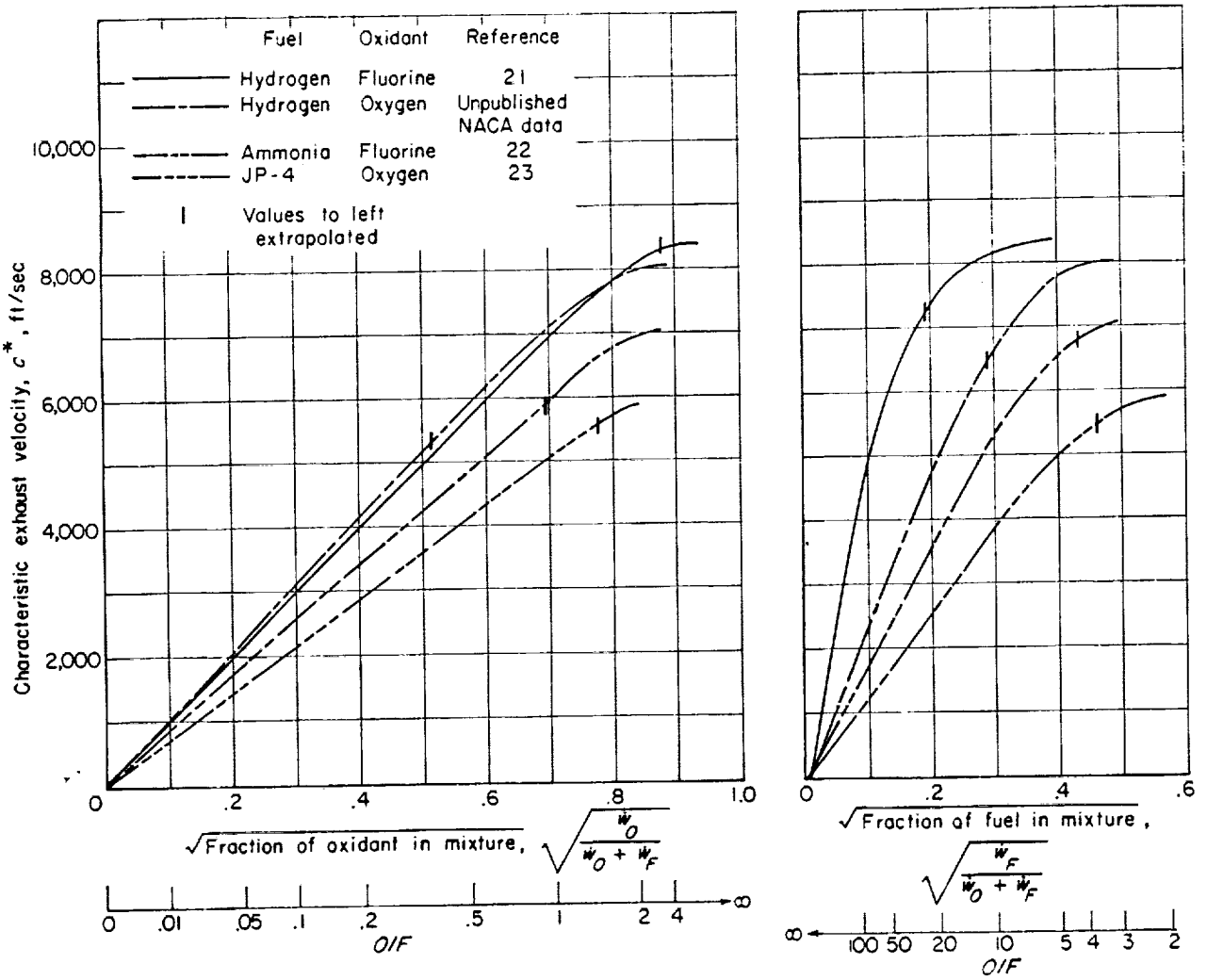

FIGURE 23.—Variation of theoretical characteristic exhaust velocity with mixture ratio for several propellant combinations at combustion-chamber pressure of 300 pounds per square inch absolute and equilibrium expansion.

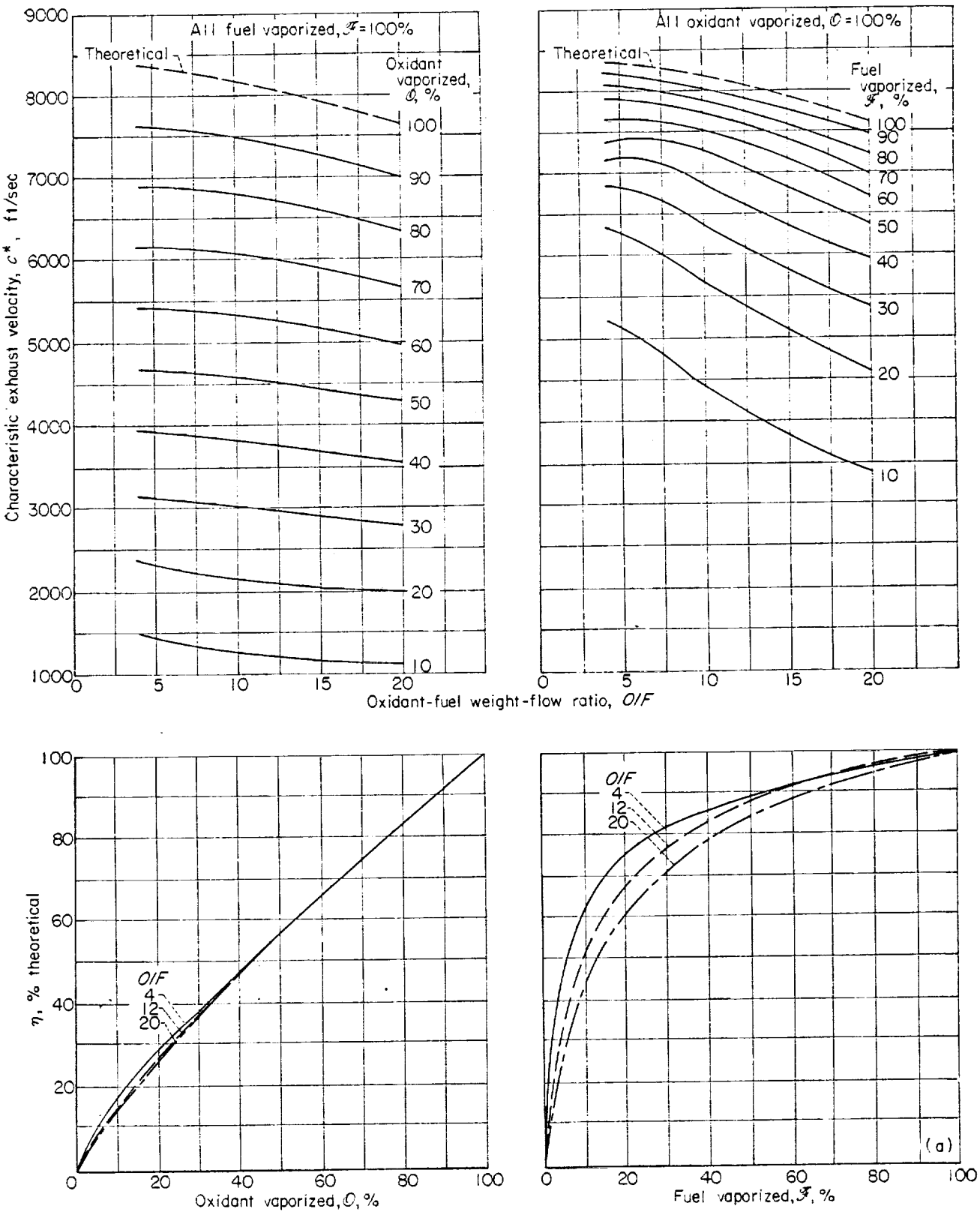

FIGURE 24.—Effect of incomplete vaporization on c^* and η. (a) Hydrogen and fluorine.

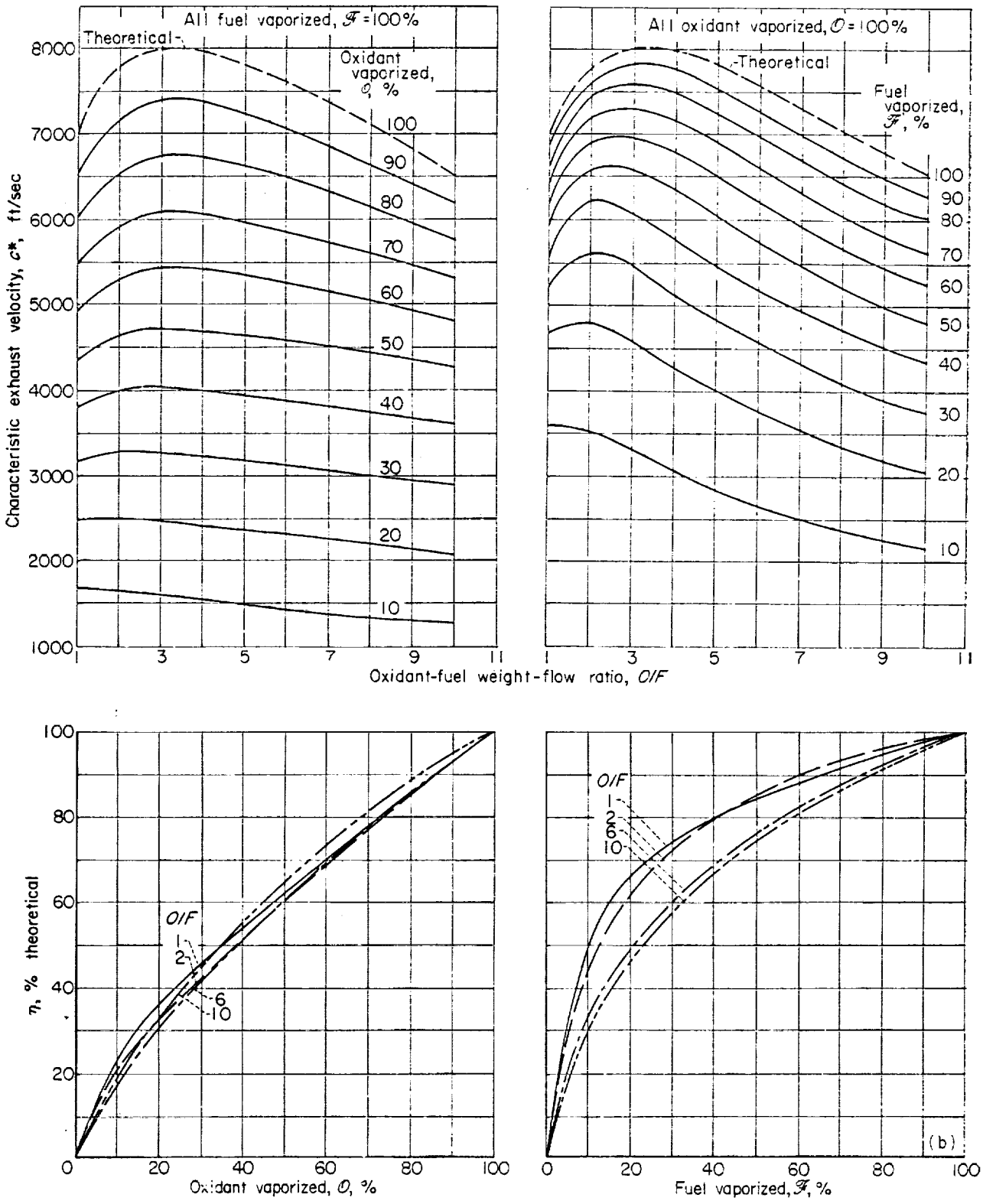

(b) Hydrogen and oxygen.

FIGURE 24.—Continued. Effect of incomplete vaporization on c^* and η.

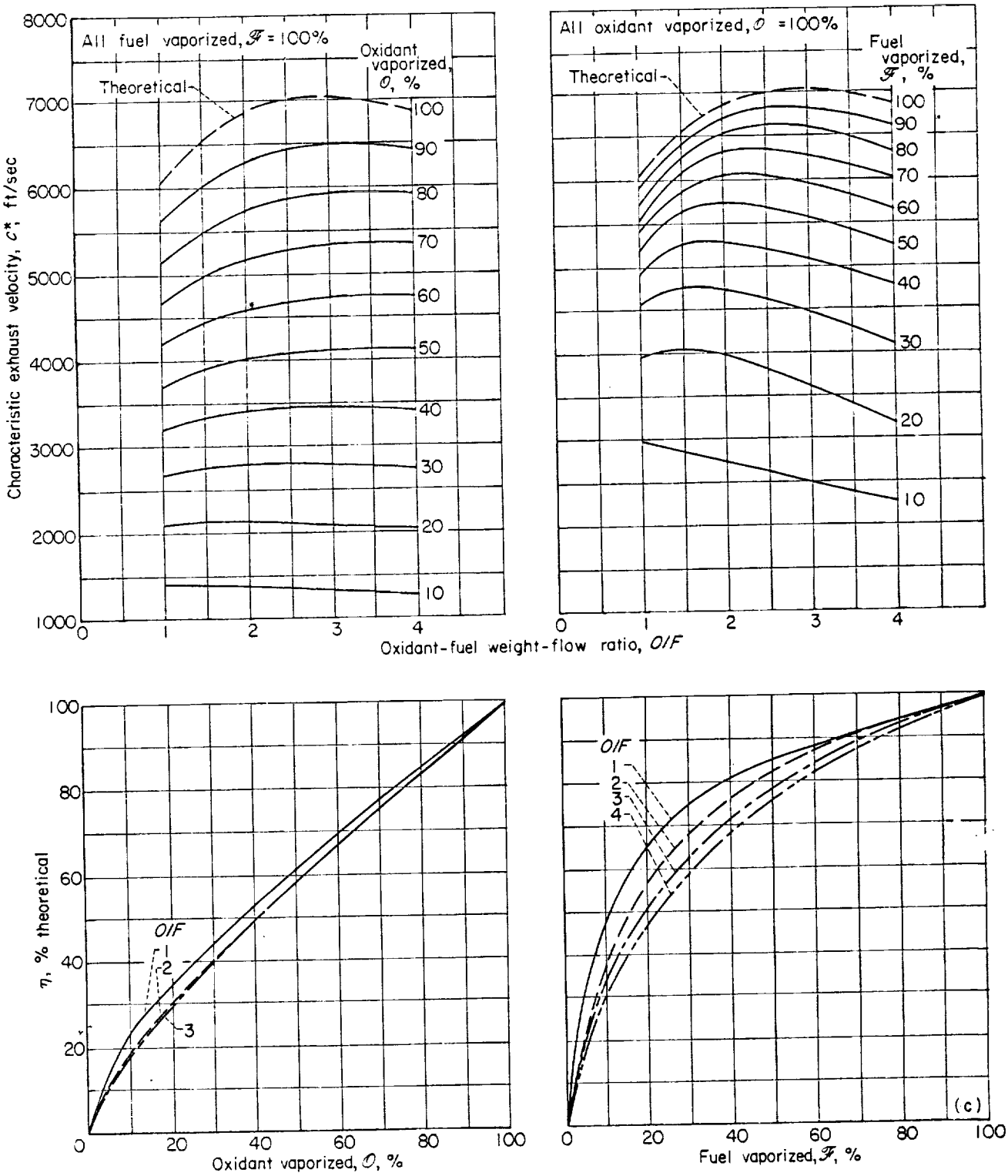

(c) Ammonia and fluorine.

FIGURE 24.—Continued. Effect of incomplete vaporization on c^* and η.

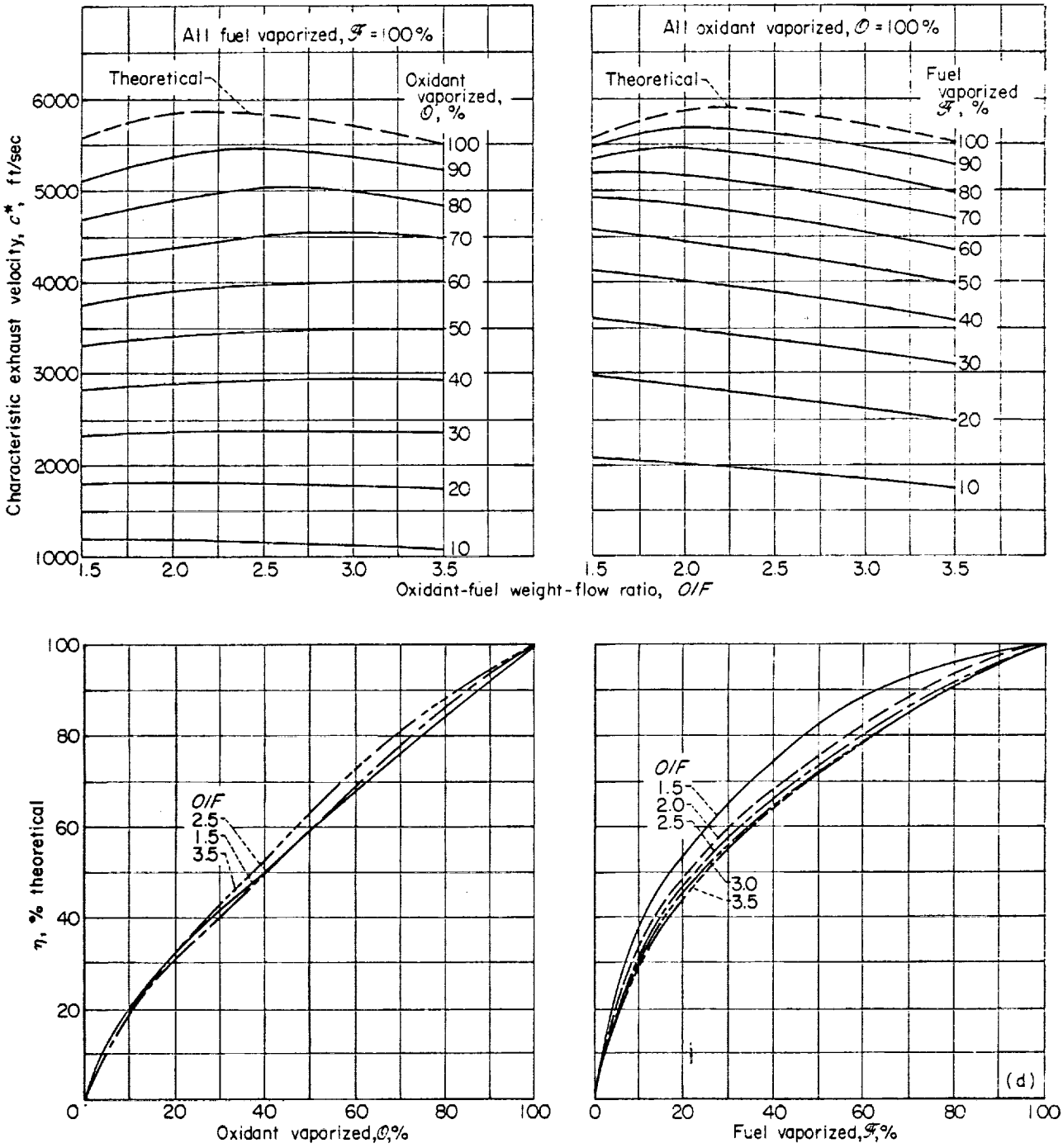

(d) JP–4 and oxygen.

FIGURE 24.—Concluded. Effect of incomplete vaporization on c^* and η.

Relating c^* to propellant vaporized and burned by equation (52) requires a knowledge of the variations in theoretical c^* over an extended range of mixture ratios. These variations for several propellant combinations are shown in figure 23. Theoretical values reported in references 21 to 23 were extrapolated over the region shown. The extrapolations were based on the assumptions that (1) for low percentages of oxidant or fuel, the combustion temperature varies directly as the percentage of fuel or oxidant in the burned mixture, and (2) c^* is proportional to the square root of the combustion temperature.

The variations in c^* efficiency η with percentages of fuel and oxidant vaporized are shown in figure 24 for the hydrogen-fluorine, hydrogen-oxygen, ammonia-fluorine, and JP4-oxygen propellant combinations. For all propellant combinations, a higher c^* efficiency is obtained with a given percentage of fuel vaporized and burned than with an equal percentage of oxidant. For example, with half the fuel vaporized, η is between 70 and 90 percent; whereas, with half the oxidant vaporized, η is about 60 percent. This difference is attributable to several factors, including the shape of the theoretical c^* curve, the fact that peak theoretical c^* occurs in the fuel-rich region, and the fact that the oxidant weight flow accounts for a large part of the total propellant flow.

Figure 24 may be used to interpret experimental c^* performance in terms of the percentage of fuel or oxidant vaporized if the other propellant can be assumed to be completely vaporized. For example, for the ammonia-fluorine propellant combination, η of 85 percent at an oxidant-fuel ratio of 3.0 may indicate that only 60 percent of the ammonia (and all the fluorine) or 80 percent of the fluorine (and all the ammonia) has vaporized. The following table presents a similar comparison for other propellant combinations:

Propellant	η, %	O/F	$\mathcal{F}$, %	$\mathcal{O}$, %
Hydrogen-fluorine	85	4.0	37	82
Hydrogen-oxygen	85	2.0	51	80
Ammonia-fluorine	85	3.0	60	80
JP4-oxygen	85	2.5	70	79

The results may be further interpreted to show the percentages of propellants that must actually be burned to obtain a given c^* efficiency level. For example, with hydrogen and fluorine, only 37 percent of the hydrogen need evaporate and be completely consumed by the fluorine in order to obtain η of 85 percent at an oxidant-fuel weight-flow ratio of 4.0.

Typical experimental variation of η with chamber length (data from ref. 24) is shown in figure 25 for a single-element injector with JP–4 and oxygen. The c^* efficiency data are also evaluated in terms of the percent oxidant vaporized and the percent fuel vaporized, assuming in each case that the other propellant is completely vaporized. An explicit evaluation of the percentage of propellant vaporized cannot be made if incomplete vaporization of both oxidant and fuel is assumed; probably neither the oxygen nor the hydrocarbon vaporized completely in the experiments reported in reference 24. Each value of η, however, defines a specific relation between the percentages of oxidant and fuel vaporized, since there are several sets of $\mathcal{O}$ and $\mathcal{F}$ values that give the same η in equation (52). These relations are shown in figure 26 for oxygen with JP–4 and may be applied to the experimental data shown in figure 25.

The shape of the η curve in figure 25 is typical for most injectors and propellant combinations. It will be used as a hypothetical reference curve

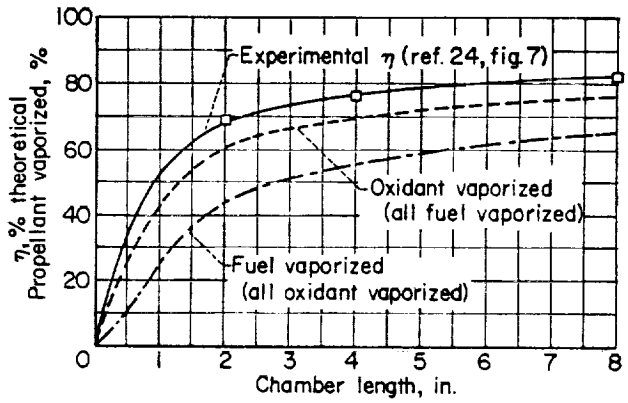

FIGURE 25.—Evaluation of typical performance data for percentages of fuel and oxidant vaporized. Propellants, oxygen and JP–4; oxidant-fuel weight-flow ratio, 2.2.

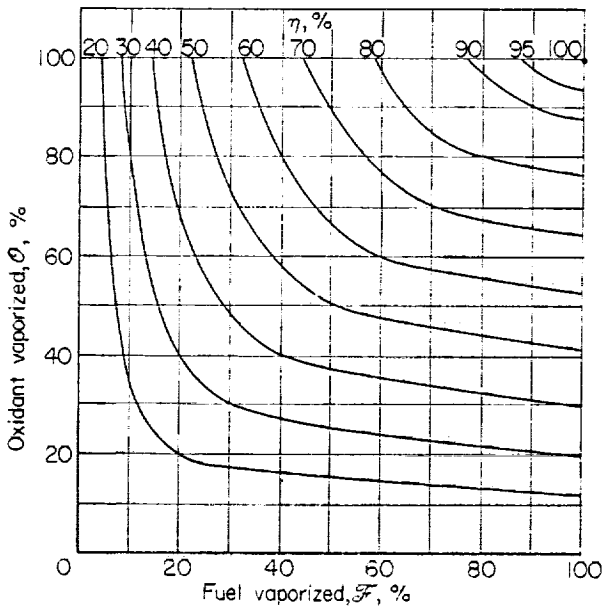

FIGURE 26.—Percentages of vaporized fuel and oxidant required to maintain a given c^* efficiency. Propellants, JP–4 and oxygen; oxidant-fuel weight-flow ratio, 2.2.

to illustrate the importance of vaporization for several different propellant combinations. The variations in the percentages of fuel or oxidant required to vaporize to obtain this efficiency with various propellants are shown in figure 27 at the oxidant-fuel ratio for peak theoretical performance. With oxidant vaporization controlling the reaction, the c^* efficiency is only slightly greater than the

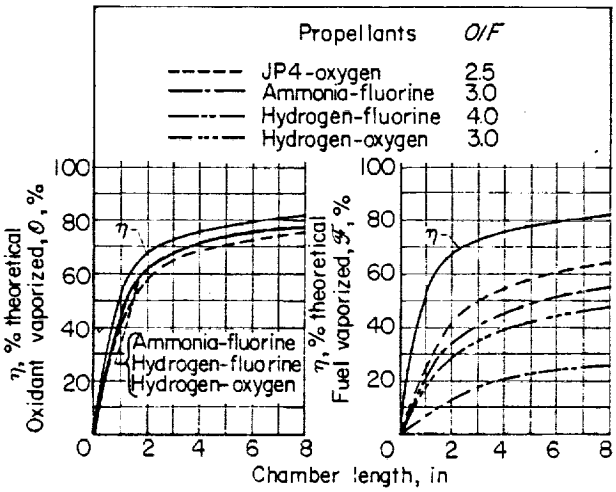

FIGURE 27.—Comparison of calculated percentages of propellant vaporized for several propellant combinations, using a typical experimental variation of c^* with chamber length.

percentage of oxidant vaporized, regardless of the propellant combination. With fuel vaporization controlling, however, the results show that c^* efficiency is significantly higher than the percentage of fuel vaporized and that this difference is greater for hydrogen than for JP–4 or ammonia. The validity of these evaluations depends on whether complete vaporization of one propellant can justifiably be assumed. Injector design features and propellant physical properties are factors that influence this assumption.

CORRELATED RESULTS

Results presented in the previous section show the effect of changing the variables on the vaporization process. This information is helpful when analyzing experimental results from investigations where various parameters were changed or in combustor design when a small change from an existing combustor is desired. For designing a new combustor or for someone new in the rocket combustor field, the material previously presented is of negligible value, since it is difficult to obtain the quantitative information needed to start a combustor design. Therefore, this section is included to give the reader the quantitative information needed to relate combustor design to the vaporization process.

Correlated curves are presented that can be used for any operating or design conditions to obtain the quantitative information relating propellant vaporization to design and operating conditions. Curves of the fraction of fuel vaporized are presented for various propellants and spray conditions as a function of the correlation parameter, effective length:

$$l_{ef}=\left(\frac{l_c}{\mathcal{A}^{0.44}}+\frac{0.83\,l_N}{\mathcal{A}^{0.22}S^{0.33}}\right)\frac{(P/300)^{0.66}}{(1-T_{t.o,R})^{0.4}\left(\frac{r_m}{0.093}\right)^{1.45}\left(\frac{p_o}{1200}\right)^{0.75}} \quad (102)$$

This parameter was obtained by cross-plotting the length required to vaporize 90 percent of the total mass of the spray as a function of the various design and operating conditions and fitting a curve to the points. The correlation parameter is empirical, and the simplest functional forms are assumed for convenience. Other functional forms, determined theoretically or empirically, might reduce the spread in the correlated results.

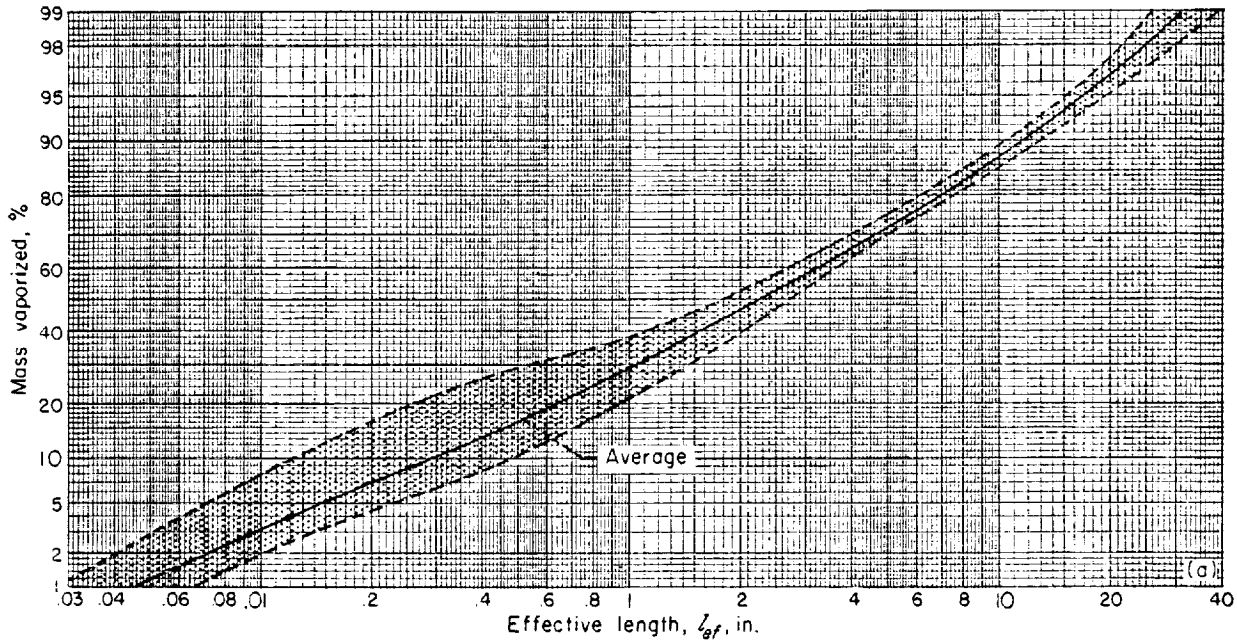

(a) Heptane sprays.

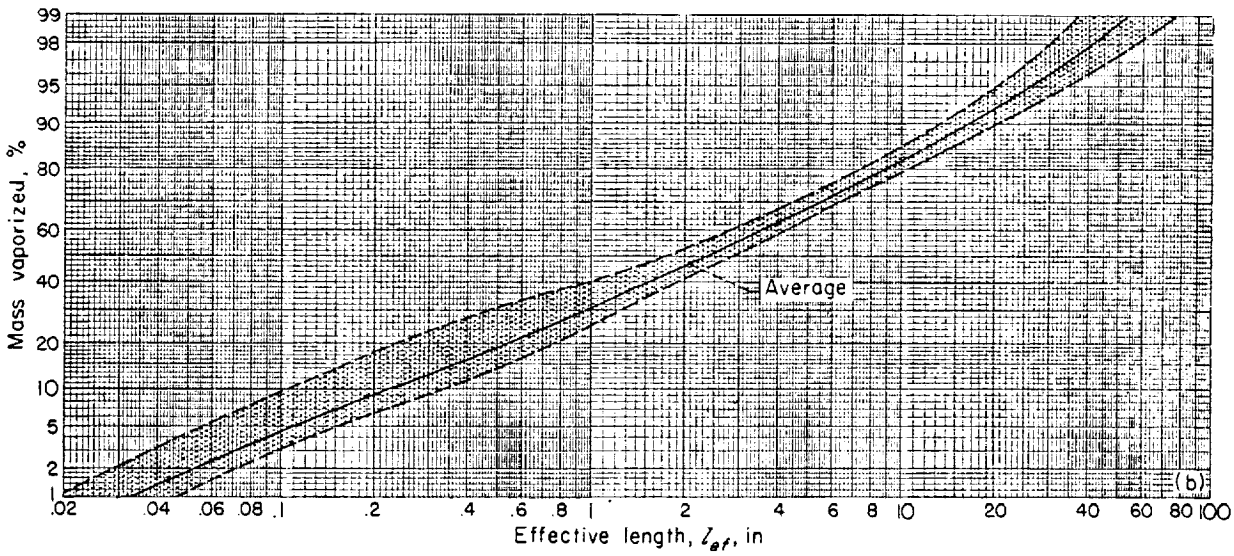

(b) Ammonia sprays.

FIGURE 28.—Correlated results. Geometric standard deviation of spray, 2.3.

VARIOUS PROPELLANTS

Curves for the mass vaporized as a function of effective length for heptane, ammonia, hydrazine, oxygen, and fluorine sprays with a distribution of 2.3 are shown in figures 28(a) to (e). The mass vaporized is plotted on a probability scale to obtain better resolution in the low and high percent-vaporized regions. The effective-length scale is logarithmic.

Correlated results show the same trends as presented in the previous section. The combustor length required to vaporize a given percentage of propellant increases with increasing mass-median drop size r_m, injection velocity v_o, contraction ratio $\mathcal{A}$, and nozzle shape factor S. (Horn shape is better than a bell shape.) The length decreases with increasing chamber pressure P and initial reduced temperature $T_{l,o,R}$.

The spread in the effective length was greatest in the 10- to 20-percent-vaporized region. The variation in the position of the inflection point in

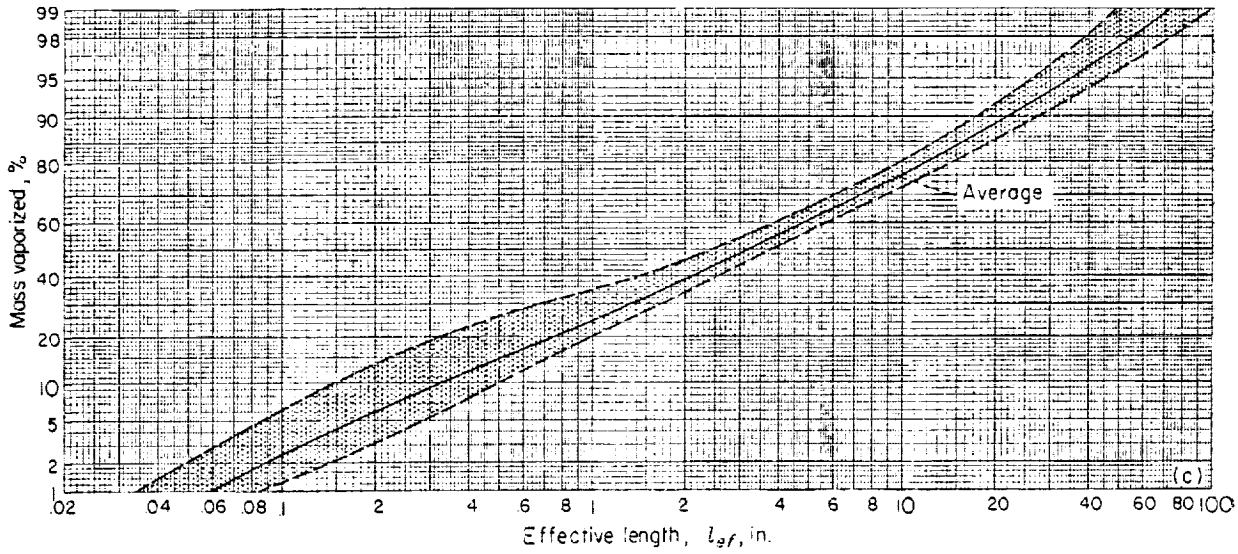

(c) Hydrazine sprays.

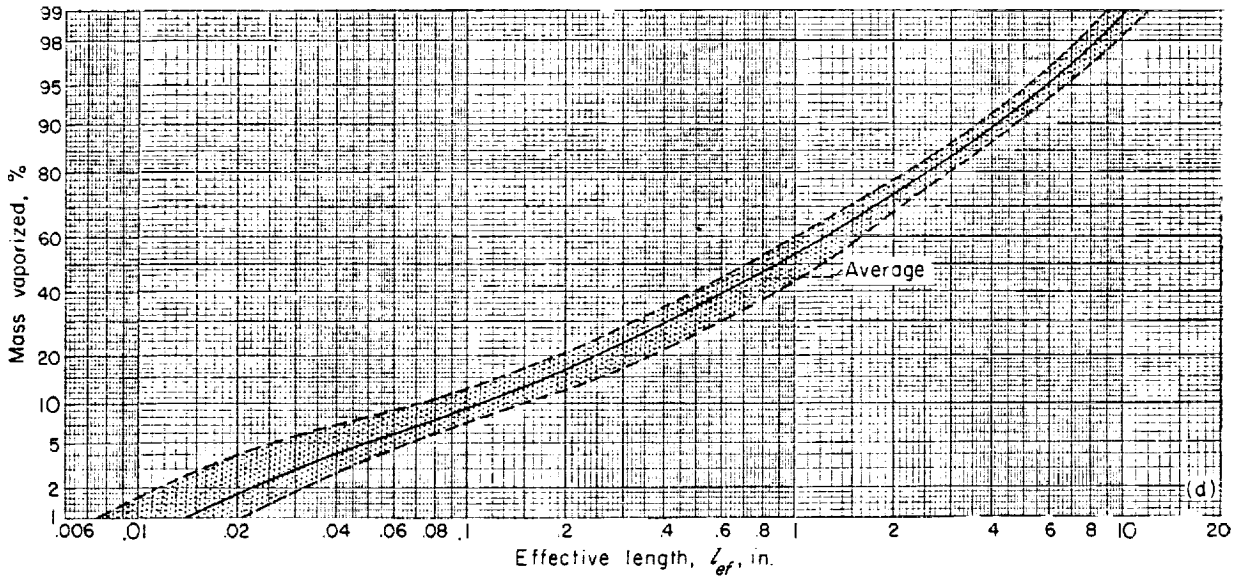

(d) Oxygen sprays.

FIGURE 28.—Continued. Correlated results. Geometric standard deviation of spray, 2.3.

the mass-vaporized curve produced most of the spread. In the high percent-vaporized region, the spread in effective length required to vaporize a given percentage of propellant for various conditions was ±20 percent about the mean curve.

To determine design or operating parameters for propellants other than those represented in figures 28(a) to (e), generalized results are presented in figure 28(f). Here the mass vaporized is plotted against a generalized length:

$$l_{gen}=\left(\frac{l_c}{\mathcal{A}^{0.44}}+\frac{0.83\,l_N}{\mathcal{A}^{0.22}S^{0.33}}\right)\frac{(P/300)^{0.66}}{(1-T_{l,o,R})^{0.4}\left(\frac{r_m}{0.003}\right)^{1.45}\left(\frac{v_n}{1200}\right)^{0.75}\left(\frac{\lambda}{140}\right)^{0.8}\left(\frac{\mathcal{M}_a}{100}\right)^{0.35}} \quad (103)$$

The generalized length differs from the effective length by the heat of vaporization at the normal boiling point λ and the molecular weight of the

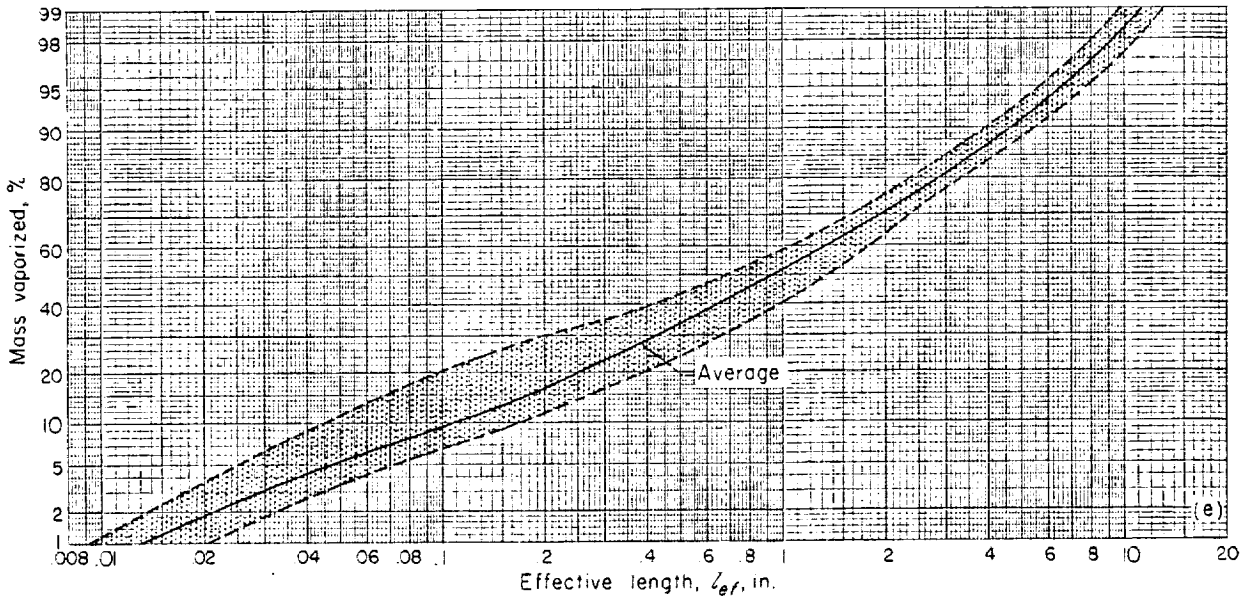

(e) Fluorine sprays.

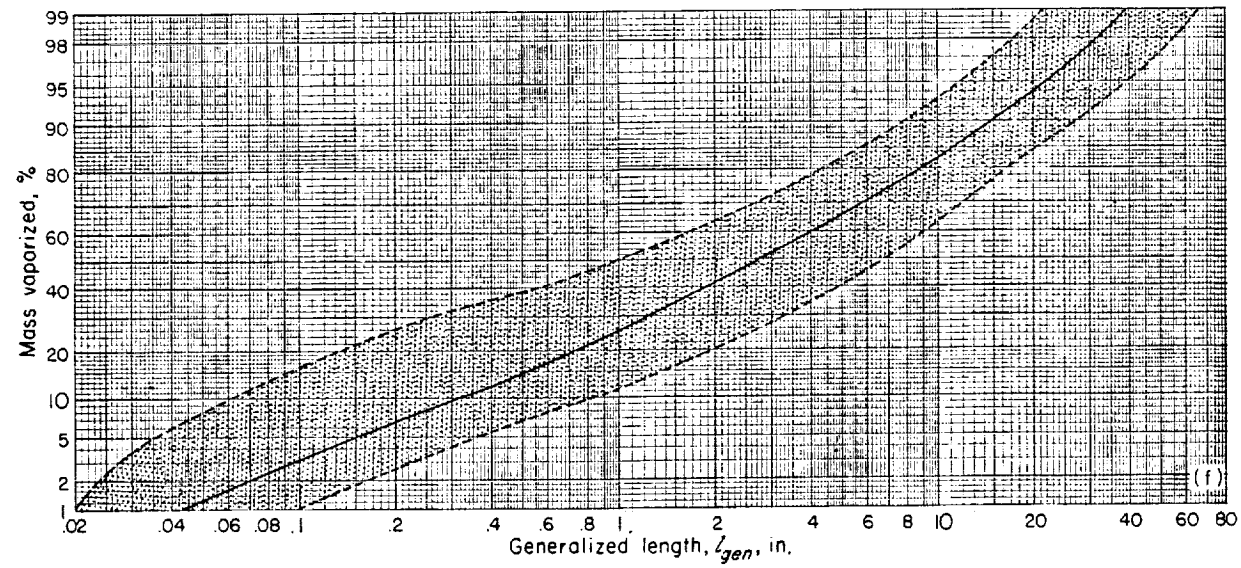

(f) All propellants, operating conditions, and design conditions.

FIGURE 28.—Concluded. Correlated results. Geometric standard deviation of spray, 2.3.

propellant $\mathcal{M}$. The data presented in figure 28(f) result in a spread of ± 35 percent about the mean mass curve. The generalized-length parameter is included to show what would be expected from propellants that have not been calculated by the authors. Its usefulness probably is limited, but it does show that a propellant with a low molecular weight and a low heat of vaporization is desirable to obtain a large fraction of propellant vaporized in a given length. An example of such a propellant is hydrogen, which, if injected as a liquid, will vaporize in much shorter lengths than oxygen or fluorine.

The spray distribution of 2.3 used to obtain figure 28 corresponds to that observed in reference 25 for an impinging-jet injector. It is felt that this distribution adequately describes the sprays produced in most rocket engines. The effect of a different distribution, however, is shown in the next section.

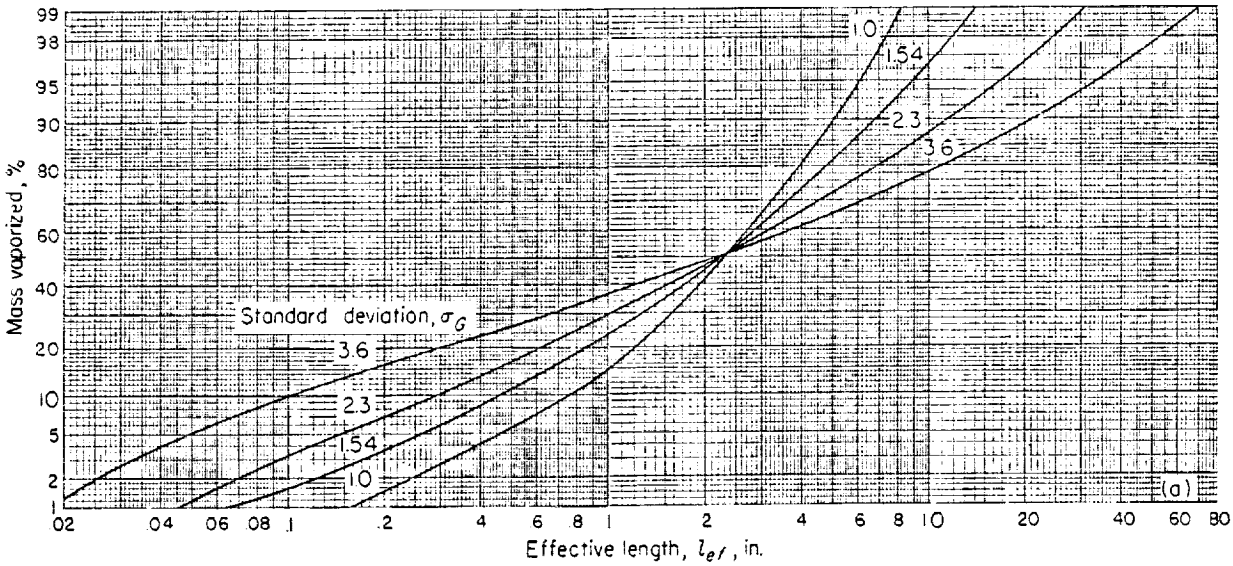

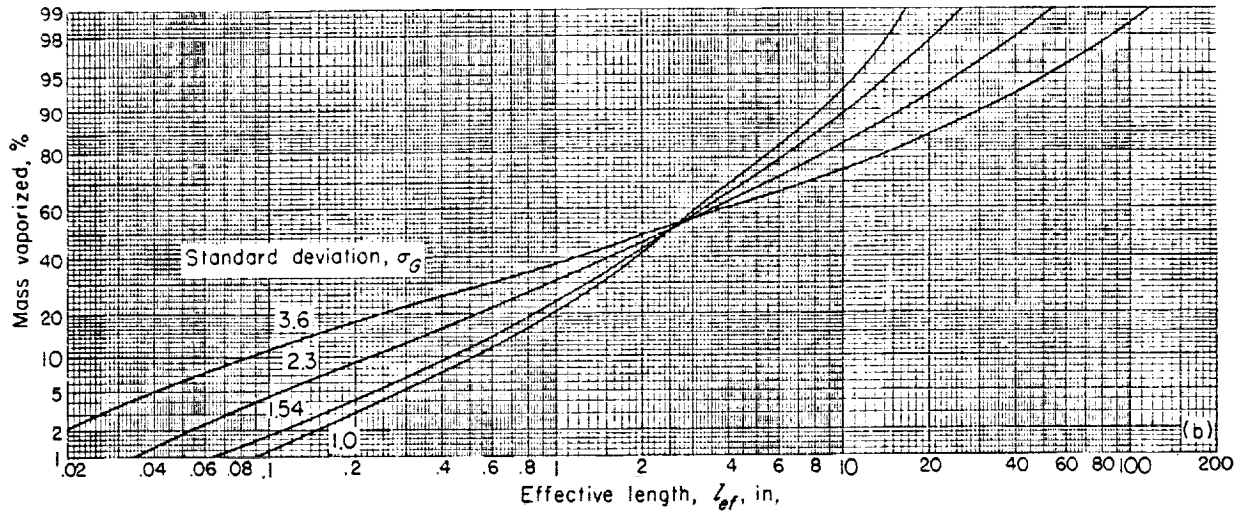

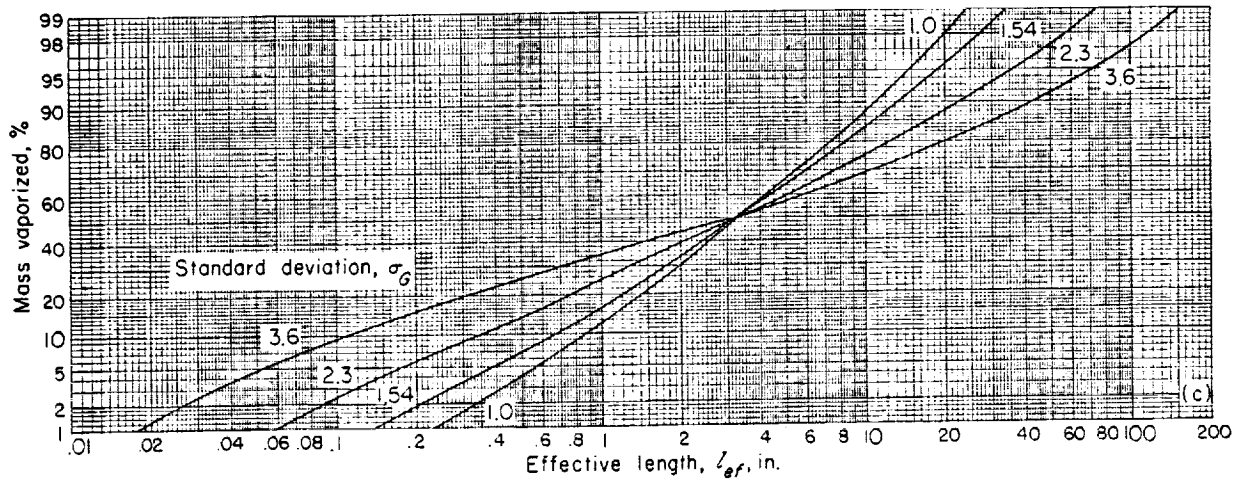

(a) Heptane. (b) Ammonia. (c) Hydrazine.

FIGURE 29.—Correlated results for sprays with various geometric standard deviations.

VARIOUS SPRAY DISTRIBUTIONS

Correlated results for sprays of heptane, ammonia, hydrazine, oxygen, and fluorine with different spray distributions are shown in figure 29. Only the mean curves are shown for each distribution. Increasing the standard deviation results in a curve with a lower slope. All standard-deviation curves pass through the same point at about 50 percent of the mass vaporized. Above the 50-percent-vaporized point, sprays with a large standard deviation require more length to vaporize than sprays with a small deviation. (A standard deviation of 1 represents a spray of uniform drop size; increasing the standard deviation increases the number of drops that are smaller and larger than the median drop size.)

COMPARISON OF EXPERIMENTAL AND CALCULATED PERFORMANCE

In order to determine whether the vaporization model and calculated results represent conditions in an actual rocket combustor, experimental performance results are compared with results calculated from the curves presented in the preceding section.

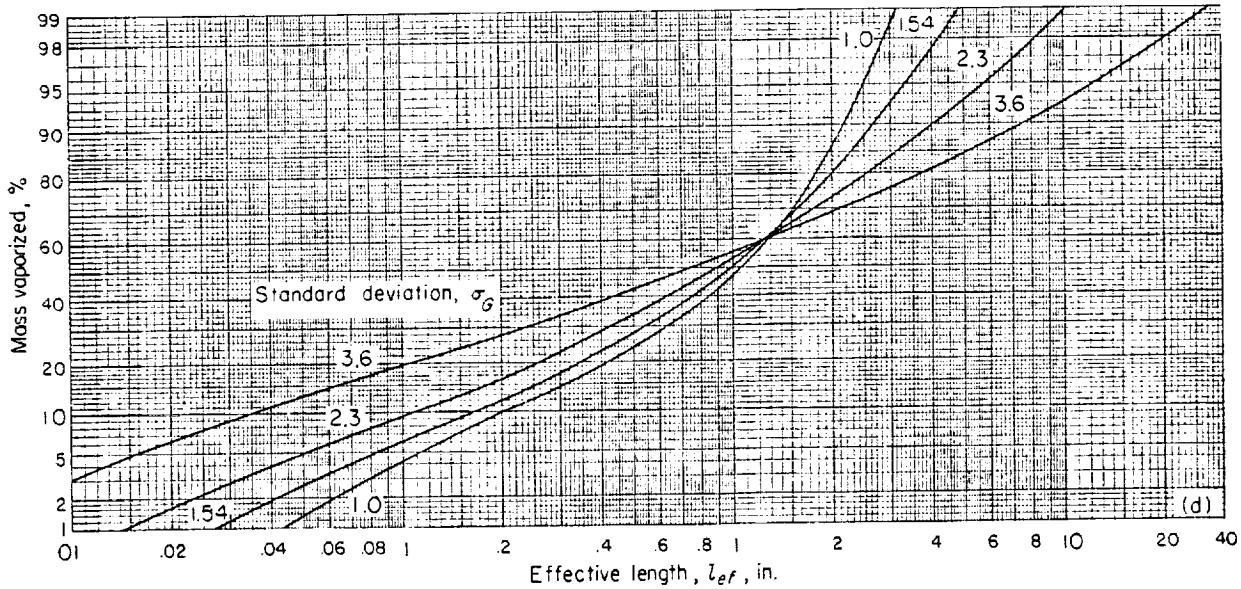

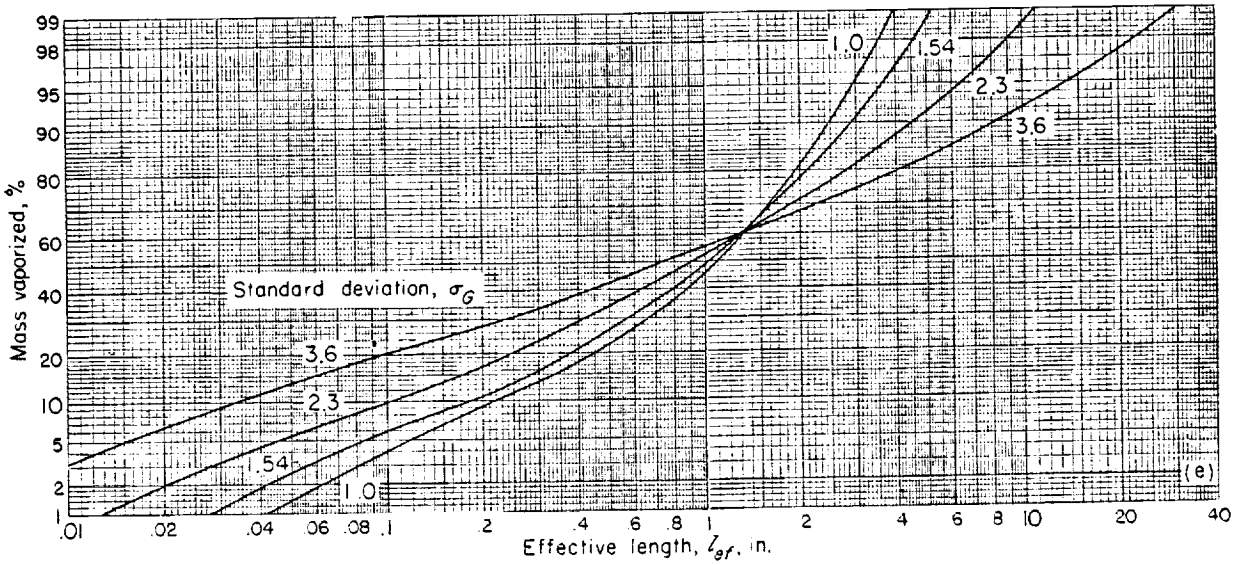

(d) Oxygen. (e) Fluorine.

FIGURE 29.—Concluded. Correlated results for sprays with various geometric standard deviations.

PREDICTED COMBUSTION EFFICIENCY

To calculate or predict engine performance, the experimental values of chamber pressure, injection velocity, initial temperature of each propellant, combustor contraction ratio and length, and nozzle shape factor and length were substituted in the equation for effective length. The mass-median drop size for each test was determined as will be explained in the following section. The effective lengths for each test and propellant were thus obtained. From the appropriate curve of mass vaporized against effective length (fig. 29), the amount of each propellant vaporized was determined. The combustor efficiency was then calculated by equation (52). The calculated or predicted efficiencies calculated by this technique are compared with the actual measured efficiency in figure 30. The experimental efficiencies are those reported in references 24 and 26 to 30 and include different injection techniques, propellant flows, mixture ratios, chamber pressures, chamber lengths, propellants, and injector hole sizes. The calculated and experimental values agree within ± 5 experimental efficiency units, with the exception of hydrazine.

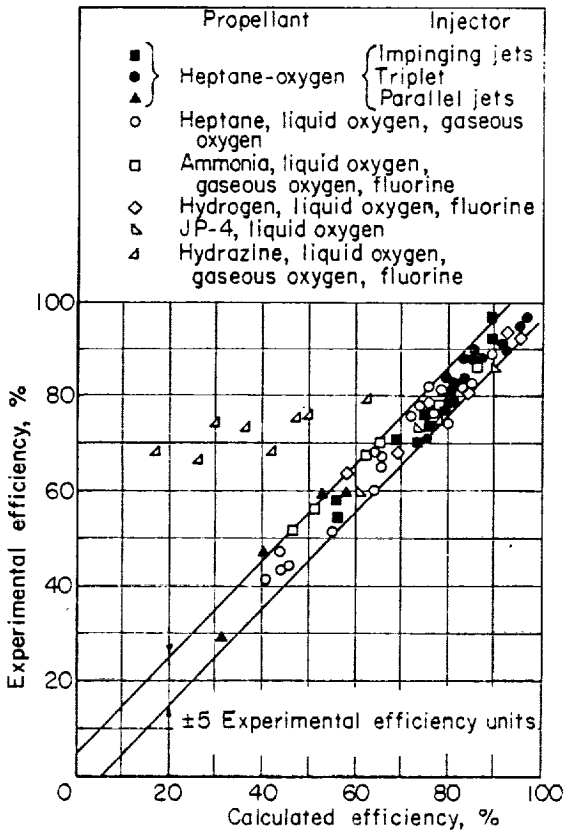

FIGURE 30.—Comparison of experimental and calculated efficiencies.

A possible explanation for the discrepancy with hydrazine may be the fact that hydrazine decomposes at about 1000° R (ref. 31), which is about the temperature the drop reaches as it vaporizes. This decomposition could cause the drops to shatter and thus result in a higher vaporization rate; or it could add heat internally (which was not included in the model), which would also result in a higher vaporization rate.

The spread of ± 5 efficiency units is within the spread of the correlated results; that is, using the maximum and minimum percent vaporized at a given effective length to calculate performance would have resulted in calculated efficiencies at least ± 5 efficiency units different from those obtained by the mean curve. If the percent vaporized had been calculated for the exact conditions at which the combustor was operating instead of using the correlated curve, the agreement between calculated and experimental results would have been better. This excellent agreement between calculated and experimental efficiencies, both in magnitude and variations with changing conditions, certainly indicates that the vaporization model represents the conditions in a rocket combustor with oxygen, fluorine, ammonia, or hydrocarbon fuels as propellants.

DETERMINATION OF MEDIAN DROP SIZE

Drop sizes produced by an impinging-jet injector were determined in cold-flow tests and reported in reference 25. The results therein give the volume-number mean diameter d_{30} as a function of jet diameter, jet velocity, and difference between surrounding gas velocity and jet velocity. Since the calculation of vaporization was made with a mass-median drop size representing the spray, the experimental results obtained in reference 25 were reanalyzed to determine r_m. These results are shown in figure 31, where r_m is plotted against jet diameter d_j for one jet velocity and various velocity differences U. The geometric standard deviation of the sprays (of ref. 25) was 2.2 ± 0.3, indicating that the percent-vaporized curve for sprays with a distribution of 2.3 represents this type of an injector within a reasonable degree of accuracy. Drop sizes in an actual engine cannot be directly determined from figure 31, since the velocity difference in an actual

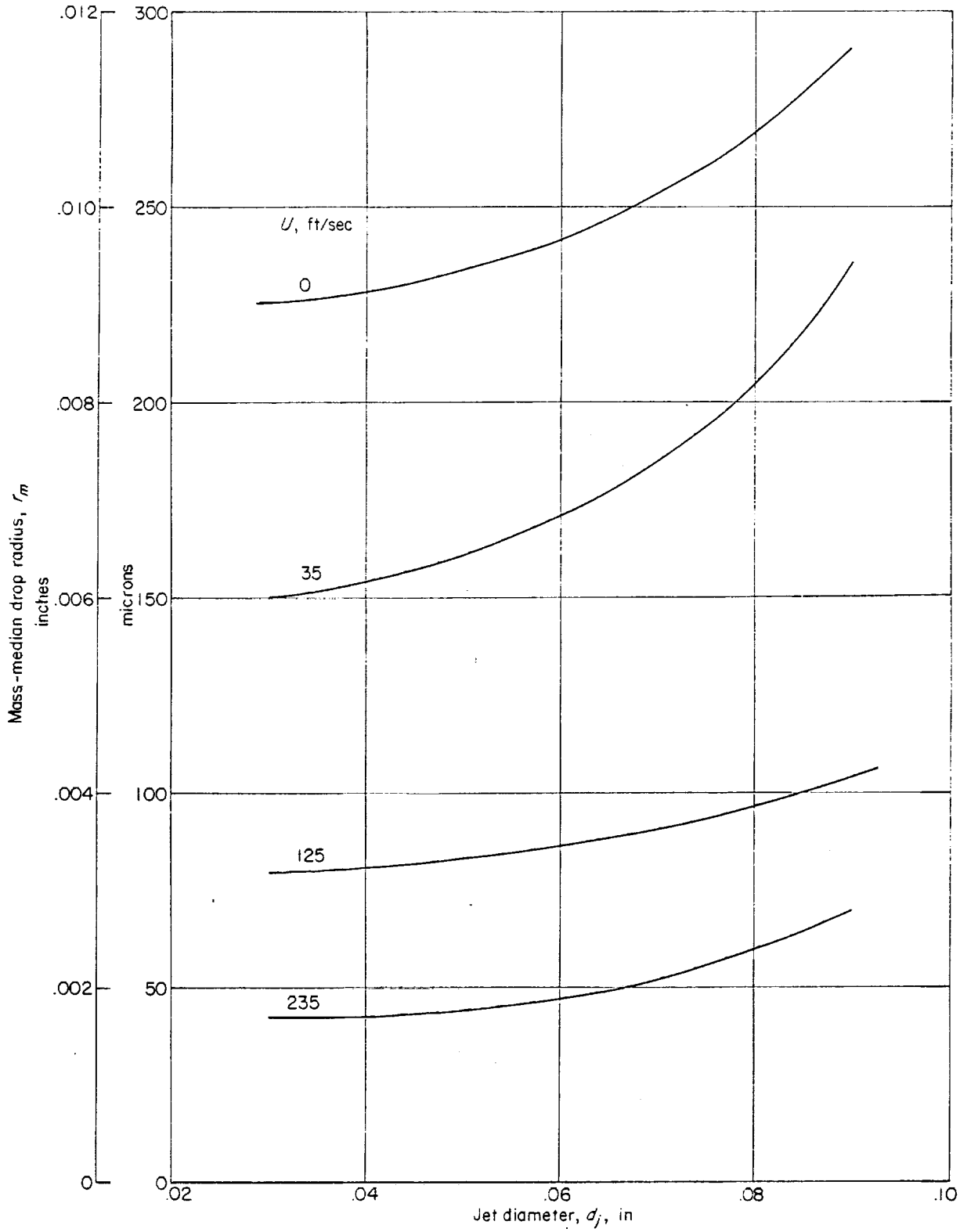

FIGURE 31.—Drop sizes determined from cold-flow measurements. Impinging jets; jet velocity, 65 feet per second.

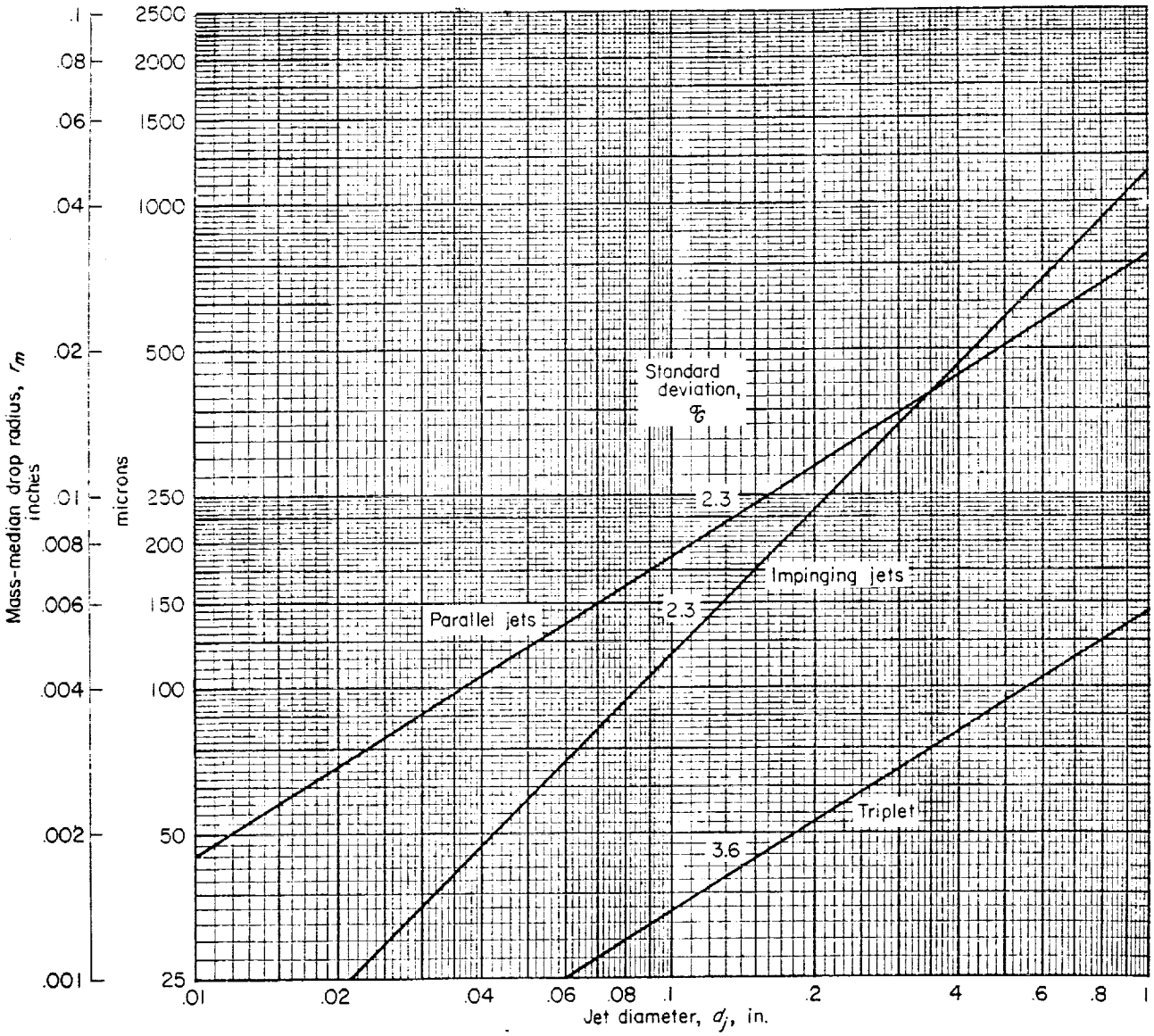

FIGURE 32.—Drop sizes determined from experimental engine performance.

combustor is unknown. As a result, the velocity difference must be either estimated or determined from additional data.

The results presented in references 24 and 29 can be used to determine the drop size, however. The procedure followed is to calculate the mass vaporized of each propellant as a function of length from figure 29 assuming equal drop sizes for both propellants. This relates the percent fuel vaporized to oxidant vaporization. The fuel-to-oxidant relation is used in equation (52) to convert efficiency to percent fuel vaporized. The effective length is then obtained for this percent vaporized from the correlation curves, such as figure 29. The effective-length equation is then solved for the median drop size. The results of such a calculation are shown in figure 32, where drop size is plotted against jet diameter for various injector techniques. The value of σ_G for parallel jets and impinging jets was 2.3, while for the triplet it was 3.6. In all the tests of references 24 and 29 the jet velocity was approximately 65 feet per second, and impingement angles were 90° for the impinging jets and triplet types of injectors. Comparing figures 31 and 32 for the impinging jets indicates that the velocity difference is approx-

imately 150 feet per second. This velocity difference is probably the velocity perturbation produced by small pressure fluctuations, since the same velocity difference is observed with combustors having a wide range of contraction ratios or gas velocities (ref. 32).

To determine drop sizes in the preceding section, figure 31 was used for a velocity difference of 150 feet per second to determine the drop size for various injector velocities, interpolating where necessary. For conditions beyond the range of figure 31 (i.e., large jet diameters and parallel-jet and triplet injectors), the drop size was determined from figure 32.

The effect of propellant properties on drop size can be determined by extrapolating the results obtained in reference 33 for crosscurrent breakup of jets of various liquids. The drop size was found to be a function of surface tension, viscosity, and density, as given by

$$d_{30} \propto r_m \propto \left(\frac{\sigma_l \mu_l}{\rho_l}\right)^{1/4} \tag{104}$$

Therefore, mean size for propellants other than heptane (X) was determined by

$$r_{m,X} = r_{m,C_7H_{16}} \left(\frac{\rho_{C_7H_{16}}}{\rho_X} \frac{\sigma_{l,X}}{\sigma_{l,C_7H_{16}}} \frac{\mu_X}{\mu_{C_7H_{16}}}\right)^{1/4} \tag{105}$$

APPLICATION TO COMBUSTOR DESIGN

Satisfactory steady-state operation of a rocket chamber requires, simultaneously, high combustion efficiency, smooth and stable burning, and adequate cooling of injector, chamber walls, and nozzle. Design features desirable for one factor may not be desirable for another factor, however; for example, fine atomization for high combustion efficiency may promote difficult cooling problems. Also, features such as reignition or throttling may be demanded of the engine. Thus, design compromises are required.

The vaporization theory just developed provides useful relations among combustor dimensions, injector designs, chamber pressure, and injector pressure drop for the steady-state combustion process. The following discussion uses these results in determining a particular combustor design. It should be pointed out that some of the information that is used is still subject to modification; and, wherever the reader feels that additional or new information is more reliable, it should be used instead of that used herein.

SELECTION OF PROPELLANTS AND PERFORMANCE AND OPERATING CONDITIONS

The first step in the design of a combustor is to determine what parameters that enter into the design have been specified by other components or requirements. The necessary parameters are as follows:

(1) Propellants
(2) Combustor efficiency
(3) Chamber pressure
(4) Cylindrical-combustor length
(5) Convergent-nozzle length
(6) Contraction ratio
(7) Initial propellant temperature
(8) Injection velocity or pressure drop
(9) Type of injector
(10) Injector hole size

The propellants and efficiency are usually determined by the impulse required by missile-system analysis. Chamber pressure is frequently specified by an analysis of the pump and engine system for optimum weight and performance. Chamber length, nozzle length, contraction ratio, and initial propellant temperature might be specified by the space allowed for the combustor in the system or the cooling requirements of the engines. The injector pressure drop is often selected by the combustor designer with an eye towards the problems it places on the pumps. Low pressure drops are desirable for the pump but will undoubtedly produce troubles in the form of low-frequency instability. Therefore, a compromise is approximately 100 pounds per square inch, which is also the region in which most of the information on drop size is available. The type of injector and hole size might be determined by the experiment or the limitations of the machine shops available, or both.

In a particular design or application, several of the parameters mentioned will not be specified. The unspecified parameters will vary from application to application. With the unspecified parameters the designer can either find a trial-and-error solution if there is more than one term, or solve directly for one term. In the following example, the injector type and hole size are not specified by other considerations. The specified

parameters in the example are

(1) Propellants, heptane and liquid oxygen
(2) c^* efficiency, 95 percent
(3) Chamber pressure, 300 lb/sq in. abs
(4) Cylindrical-combustor length, 8 in.
(5) Convergent-nozzle length, 12 in.
(6) Contraction ratio, 2.0
(7) Initial fuel temperature, 600° R; initial oxidant temperature, 162° R
(8) Injection velocity, 780 in./sec

DETERMINATION OF DROP SIZE

Specifying the preceding parameters will specify the effective length required to obtain the necessary combustor efficiency. Usual procedure would be to have each propellant vaporize to the same percentage as the desired combustion efficiency. This minimizes off O/F regions and high temperatures and makes the percent vaporized equal to the combustor efficiency given in equation (52).

From plots of the percent vaporized against effective length, the effective length is selected that gives the desired percent vaporized (equal to the combustor efficiency). For heptane, this length is 16.8 inches, and for oxygen, 5.94 inches for a deviation of 2.3. The next step is to solve the effective-length equation for drop size:

$$r_m=0.003\left[\left(\frac{l_c}{\mathcal{A}^{0.44}}+\frac{0.83\,l_N}{\mathcal{A}^{0.22}S^{0.33}}\right)\frac{(P/300)^{0.66}}{(1-T_{l,o,R})^{0.4}\left(\frac{v_o}{1200}\right)^{0.75}l_{ef}}\right]^{1/1.45}$$

For heptane,

$$r_m=0.003\left\{\left[\frac{8}{2^{0.44}}+\frac{(0.83)(12)}{2^{0.22}0.735^{0.33}}\right]\frac{(300/300)^{0.66}}{\left(1-\frac{600}{969}\right)^{0.4}\left(\frac{780}{1200}\right)^{0.75}16.8}\right\}^{1/1.45}$$

$=0.00579$ in.

For liquid oxygen,

$$r_m=0.003\left\{\left[\frac{8}{2^{0.44}}+\frac{(0.83)(12)}{2^{0.22}0.735^{0.33}}\right]\frac{(300/300)^{0.66}}{\left(1-\frac{162}{278}\right)^{0.4}\left(\frac{780}{1200}\right)^{0.75}5.94}\right\}^{1/1.45}$$

$=0.01153$ in.

By this procedure the necessary drop size required for each propellant has been determined.

SELECTION OF INJECTOR

To determine the injector, the authors would advise using figure 32 and equation (105) as the best available data until additional information regarding drop sizes in rocket combustors becomes known. For the heptane drop size of 0.00579 inch, the jet diameter can be read directly from figure 32. Either an impinging jet of 0.13 inch or a triplet-type injector of approximately 0.8 inch would produce a spray of this median drop size. However, the triplet injector has a distribution corresponding to a deviation of 3.6 instead of the value of 2.3 used to obtain the effective length. Also, the triplet produces intense burning close to the injector, resulting in injector burnouts. For these reasons the impinging-jet type of injector would be more desirable, and a hole size of 0.13 inch would be used for the heptane.

To determine hole size for the oxidant from figure 32, the 0.01153-inch mean drop size must be converted to an equivalent size produced with heptane. This is accomplished by equation (105):

$$r_{m,\mathrm{LOX}}=r_{m,\mathrm{C_7H_{16}}}\left(\frac{\rho_{\mathrm{C_7H_{16}}}}{\rho_{\mathrm{LOX}}}\frac{\sigma_{l,\mathrm{LOX}}}{\sigma_{l,\mathrm{C_7H_{16}}}}\frac{\mu_{\mathrm{LOX}}}{\mu_{\mathrm{C_7H_{16}}}}\right)^{1/4}$$

$$0.01153=r_{m,\mathrm{C_7H_{16}}}\left(\frac{0.684}{1.14}\frac{13.2}{16.5}\frac{0.190}{0.310}\right)^{1/4}$$

$$r_{m,\mathrm{C_7H_{16}}}=\frac{0.01153}{(0.294)^{1/4}}=0.01565\text{ in.}$$

To obtain this drop size of 0.01565 inch, parallel jets would be selected with a diameter of 0.33

inch, since the cost of drilling holes for parallel jets is much less than for impinging jets.

The injector would thus consist of pairs of heptane jets from 0.13-inch holes impinging upon each other. The oxidant would be introduced through 0.33-inch holes to form parallel jets.

DISCUSSION AND CONCLUSIONS

Calculations of the mass histories of drops have shown that the vaporization process requires considerable chamber length before complete vaporization is attained. With uniform drops of 75-micron radius, 8 inches are required to reach 99 percent of the mass vaporized for typical combustor conditions; while, for nonuniform sprays, a 225-micron-radius drop requires 40 inches to reach 99 percent of the mass vaporized. Since these are about the size drops produced in rocket engines, it is evident that the propellant vaporization process cannot be overlooked in rocket combustion. Mass histories of vaporizing sprays show that the large drops are responsible for the unvaporized mass in the 90-percent total-mass-vaporized region. For high efficiency the combustor must therefore be designed with sufficient stay time for the large drops to vaporize. The advantage of eliminating these drops if at all possible is also indicated. An analysis that considers the propellant sprays to consist of an average size drop will be in considerable error in predicting the chamber length or stay time required for complete vaporization. A more conservative and probably better approach would be to consider the spray to consist only of the maximum size drops to determine the length or stay time required for complete vaporization.

The analysis has also shown that cryogenic propellants vaporize faster than the usual liquid propellants. This might be considered to be a boiling-point phenomenon as a first impression. In reality, though, the boiling point does not affect the vaporization process in a rocket combustor operating at high temperature and pressure. The higher vaporization rates with the cryogenic propellants are due to the lower heat of vaporization. The heat of vaporization is important, since it controls the pounds of propellant vaporized per Btu of heat arriving at the drop from the surrounding hot gases.

Calculations of the effect of various operating parameters have shown that a low-contraction-ratio chamber and a low injection velocity are desirable. The low contraction ratio is desirable because it produces a higher gas velocity in the combustor, thus providing a higher Reynolds number for the drops with associated higher heat-transfer and mass-transfer rates to the drop. The lower injection velocity is desirable because it provides a longer stay time for the drops, resulting in more mass vaporized before the drops leave the nozzle throat. This conclusion differs from the results obtained by assuming complete entrainment of drops in reference 19.

Comparisons between combustor performance calculated on the basis of propellant vaporization as the rate-controlling step and actual experimental combustor performance with oxygen, fluorine, ammonia, and hydrocarbon fuels as propellants exhibited good agreement. One would therefore infer that the vaporization process is the rate-controlling step in these rocket combustors under normal operating conditions. It is impossible to prove that vaporization is the rate-controlling step, since actual drop sizes have not been measured in a rocket at this time. The drop sizes used in obtaining the agreement mentioned were calculated (assuming vaporization is rate-controlling) from combustor performance tests or were calculated from the data of reference 25 assuming a gas velocity. These are not minor assumptions, and therefore one can only infer that vaporization is rate-controlling. The proof has to wait until the assumptions are proved correct.

It is believed that the material presented herein can be used as an aid in designing or modifying rocket combustors. For the neophyte it is possible to calculate approximate values of various parameters required in the design of a high-efficiency

combustor. For the experienced designer the material presented should suggest certain parameter changes that would be desirable and the extent of these changes to obtain the desired conditions.

The material presented is definitely limited by the assumptions (1) that all the heat for vaporization comes from the hot gases, (2) that no breakup or interactions between drops occur, and (3) that instantaneous mixing and reaction are obtained.

The first assumption is not correct for premixed hypergolic propellants or monopropellants that have liquid-phase reaction. With these conditions the vaporization rate would be increased, depending on the rate of the liquid-phase reaction. In the limit, all the heat for vaporization would be supplied by liquid-phase reaction, and the liquid-phase reaction would be rate-controlling, in which case the performance would be higher than predicted by the vaporization model.

The second assumption is not valid for drops with a large velocity difference between the gas and drops. With a large velocity difference, a critical Weber number ($We=10$) would be exceeded and the drops would shatter. This situation probably exists in the nozzle where some of the large drops are shattered. Shattering would increase the vaporization rate and produce higher performances than predicted by the vaporization model.

The third assumption is not valid when propellants with very low reaction rates are used. Low reaction rates are most likely to happen at very low chamber pressures with a propellant like nitric acid. (Even with these conditions, the reaction rate would probably be faster than the vaporization process, in light of the work of ref. 5.) If the chemical reaction rate is slow, additional time and space will be required to obtain the desired performance. With an injector that does not have a uniform distribution of propellants, the third assumption would also not be valid. Under these conditions there would be variations in the mixture ratio across the chamber. Variations in mixture ratio would result in a lower performance than predicted. The performance of a nonuniform injector can be calculated, however, by dividing the injector into small sections (e.g., 1-in. squares), calculating the performance from each section as though it were a single combustor, and then averaging the performance for all the sections.

The results of this study have suggested additional desirable research relating to rocket combustion and performance. The most important is the study of liquid spray characteristics in hot combustors. Information regarding what controls drop sizes and distribution is definitely meager, and the quantitative information on actual size in combustors is nonexistent. The pictures presented in reference 34 clearly show that liquid drops exist in the combustor, but one cannot obtain drop sizes. Included in the spray characteristics is the problem of drop shattering due to high Weber numbers. The time required for this breakup and the critical number in a combustor are needed.

The results have also indicated a need for more information on the rates for other processes. This includes the rate of liquid-phase reactions in premixed hypergolic propellants and monopropellants as well as decomposition reactions that may occur with nitrogen tetroxide, hydrazine, and so forth. As pointed out previously, with these propellants the rate-controlling step could be the liquid-phase or decomposition reactions, which would have different characteristics from those exhibited by vaporization. Another process deserving more investigation is gas-phase mixing. A technique for accounting for the effect of poor local mixture ratios on performance was just given, but it would be desirable to know the extent of mixing in an actual combustor.

Another aspect of this work that should be investigated is the role of propellant vaporization in combustion instability. The work of reference 35 shows that the vaporization process is accelerated in an oscillating airstream and that the rate exhibits periodic perturbations that could drive a pressure wave. More information is needed, however, to determine whether this perturbation is sufficient to drive the pressure wave.

SUMMARY OF RESULTS

A model and theory for rocket combustion based on the assumption that propellant vaporization is the rate-controlling process have been described. Vaporization rates and histories were calculated for sprays of heptane, ammonia, hydrazine, oxygen, and fluorine for various spray conditions and engine design and operating parameters. These calculations have quantitatively shown the following results:

1. The combustor length required to vaporize a given percentage of propellant increases with larger drop sizes, higher injection velocity, and higher contraction ratio.

2. The combustor length required to vaporize a given percentage of propellant decreases with higher chamber pressure and initial propellant temperature.

3. Combustor length required to vaporize a given percentage of propellant is the shortest with oxygen and increases in order for fluorine, heptane, ammonia, and hydrazine.

An analysis of the quantitative effect of incomplete propellant vaporization on combustor performance has also been presented. The equations relating characteristic exhaust velocity to the percentages of fuel and oxidant vaporized and burned were given. A graphical representation of the relation was presented for the hydrogen-fluorine, hydrogen-oxygen, ammonia-oxygen, and JP4-oxygen propellant combinations. The combustor efficiency is always higher than the percent vaporized of the slow-vaporizing propellant. With all the oxidant vaporized, it is possible to obtain combustor efficiencies of 70 to 90 percent with half the fuel vaporized.

Comparison of experimental and calculated combustor efficiencies showed excellent agreement where drop sizes could be calculated. For other injectors, drop sizes were deduced that showed an increase in drop size with injector orifice diameter for various injector types.

LEWIS RESEARCH CENTER
NATIONAL AERONAUTICS AND SPACE ADMINISTRATION
CLEVELAND, OHIO, *September 25, 1959*

APPENDIX

PHYSICAL PROPERTIES

HEPTANE WITH GASEOUS OXYGEN

Density of liquid,

$$\rho_l = 3.1662\times10^{-2} - 9.5355\times10^{-6}T_l - 6.945\times10^{-9}\,T_l^2, \text{ lb/cu in.}$$

Heat of vaporization,

$$\lambda = 139.9 + 0.181T_l - 2.7875\times10^{-4}T_l^2, \text{ Btu/lb}$$

Specific heat of liquid,

$$c_{p,l} = 0.231 + 5.62\times10^{-4}T_l, \text{ Btu/(lb)(°F)}$$

Specific heat of heptane vapor,

$$c_{p,a} = 0.5755 + 1.805\times10^{-4}\overline{T}, \text{ Btu/(lb)(°F)}$$

Specific heat of combustion products,

$$c_{p,b} = 0.2898 + 4.07\times10^{-5}\overline{T}, \text{ Btu/(lb)(°F)}$$

Thermal conductivity of heptane vapor,

$$k_a = 2.914\times10^{-8} + 5.847\times10^{-11}\overline{T}, \text{ Btu/(in.)(sec)(°F)}$$

Thermal conductivity of combustion products,

$$k_b = 1.3349\times10^{-7} + 3.4111\times10^{-10}\overline{T}, \text{ Btu/(in.)(sec)(°F)}$$

Vapor pressure,

$$\ln p_{a,s} = 11.94763 - \frac{5255.89687}{T_l - 101.58}, \text{ lb/sq in.}$$

Viscosity of heptane vapor,

$$\mu_a = 2.106\times10^{-7} + 7.690\times10^{-10}\overline{T}, \text{ lb/(in.)(sec)}$$

Viscosity of combustion products,

$$\mu_b = 5.5615\times10^{-7} + 1.4214\times10^{-9}\overline{T}, \text{ lb/(in.)(sec)}$$

Diffusion coefficient of vapor mixture,

$$D_{mx} = [-9.815\times10^{-4} + 1.973\times10^{-6}\overline{T} + 1.1319\times10^{-9}(\overline{T})^2]\frac{300}{P}, \text{ sq in./sec}$$

Molecular weight of combustion products,

$$\mathcal{M}_b = 31, \text{ lb/mole}$$

OXYGEN WITH GASEOUS HEPTANE

Density of liquid,

$$\rho_l = 0.023079 + 2.7359\times10^{-4}T_l - 9.9465\times10^{-7}T_l^2, \text{ lb/cu in.}$$

Heat of vaporization,

$$\lambda = 61.332 + 0.5916T_l - 2.48\times10^{-3}T_l^2, \text{ Btu/lb}$$

Specific heat of liquid,

$$c_{p,l} = 0.3726 + 2.0482\times10^{-4}T_l, \text{ Btu/(lb)(°F)}$$

Specific heat of oxygen vapor,

$$c_{p,a} = 0.21333 + 2.2111\times10^{-5}\overline{T}, \text{ Btu/(lb)(°F)}$$

Specific heat of combustion products,

$$c_{p,b} = 0.2898 + 4.07\times10^{-5}\overline{T}, \text{ Btu/(lb)(°F)}$$

Thermal conductivity of oxygen vapor,

$$k_a = 2.6611\times10^{-7}\times3.4057\times10^{-10}\overline{T}, \text{ Btu/(in.)(sec)(°F)}$$

Thermal conductivity of combustion products,

$$k_b = 1.3349\times10^{-7} + 3.4111\times10^{-10}\overline{T}, \text{ Btu/(in.)(sec)(°F)}$$

Vapor pressure,

$$\ln p_{a,s} = 11.9584 - \frac{1476.4912}{T_l - 3.5680}, \text{ lb/sq in.}$$

Viscosity of oxygen vapor,

$$\mu_a = 2.2500\times10^{-7} + 1.1702\times10^{-9}\overline{T}, \text{ lb/(in.)(sec)}$$

Viscosity of combustion products,

$$\mu_b = 5.5615\times10^{-7} + 1.4214\times10^{-9}\overline{T}, \text{ lb/(in.)(sec)}$$

Diffusion coefficient of vapor mixture,

$$D_{mx} = [-2.36396\times10^{-3} + 5.7897\times10^{-6}\overline{T} + 2.87685\times10^{-9}(\overline{T})^2]\frac{300}{P}, \text{ sq in./sec}$$

Molecular weight of combustion products,

$$\mathcal{M}_b = 31, \text{ lb/mole}$$

AMMONIA WITH GASEOUS OXYGEN

Density of liquid,

$$\rho_l = 3.13955\times10^{-2} - 6.0219\times10^{-6}T_l - 2.23169\times10^{-8}T_l^2, \text{ lb/cu in.}$$

Heat of vaporization,

$$\lambda = 676.362 + 0.32247T_l - 1.210\times10^{-3}T_l^2, \text{ Btu/lb}$$

Specific heat of liquid,

$$c_{p,l} = 0.8314 + 5.7993\times10^{-4}T_l, \text{ Btu/(lb)(°F)}$$

Specific heat of ammonia vapor,

$$c_{p,a} = 0.60931 + 8.31361\times10^{-5}\overline{T}, \text{ Btu/(lb)(°F)}$$

Specific heat of combustion products,

$$c_{p,b} = 0.403578 + 6.996\times10^{-6}\overline{T}, \text{ Btu/(lb)(°F)}$$

Thermal conductivity of ammonia vapor,

$$k_a = 4.6853\times10^{-7} + 3.551\times10^{-10}\overline{T}, \text{ Btu/(in.)(sec)(°F)}$$

Thermal conductivity of combustion products,

$$k_b = 5.10692\times10^{-8} + 7.616145\times10^{-10}\overline{T}, \text{ Btu/(in.)(sec)(°F)}$$

Vapor pressure,

$$\ln p_{a,s} = 13.1485 - \frac{3899.209}{T_l - 58.2354}, \text{ lb/sq in.}$$

Viscosity of ammonia vapor,

$$\mu_a = 1.07097\times10^{-6} + 8.11607\times10^{-10}\overline{T}, \text{ lb/(in.)(sec)}$$

Viscosity of combustion products,

$$\mu_b = 1.64352\times10^{-7} + 2.45252\times10^{-9}\overline{T}, \text{ lb/(in.)(sec)}$$

Diffusion coefficient of vapor mixture,

$$D_{mx} = [-4.87304\times10^{-2} + 4.01198\times10^{-5}\overline{T} - 8.358\times10^{-10}(\overline{T})^2]\frac{300}{P}, \text{ sq in./sec}$$

Molecular weight of combustion products,

$$\mathcal{M}_b = 24, \text{ lb/mole}$$

HYDRAZINE WITH GASEOUS OXYGEN

Density of liquid,

$$\rho_l = 3.062318\times10^{-2} + 4.028897\times10^{-5}T_l - 5.54321\times10^{-8}T_l^2, \text{ lb/cu in.}$$

Heat of vaporization,

$$\lambda = 730.747 - 0.3591305T_l + 1.214\times10^{-4}T_l^2, \text{ Btu/lb}$$

Specific heat of liquid,

$$c_{p,l} = 0.589125 + 2.80708\times10^{-4}T_l, \text{ Btu/(lb)(°F)}$$

Specific heat of hydrazine vapor,

$$c_{p,a} = 0.3360 + 1.804\times10^{-4}\overline{T}, \text{ Btu/(lb)(°F)}$$

Specific heat of combustion products,

$$c_{p,b} = 0.403578 + 6.996\times10^{-6}\overline{T}, \text{ Btu/(lb)(°F)}$$

Thermal conductivity of hydrazine vapor,

$$k_a = 1.23753\times10^{-8} + 2.230358\times10^{-10}\overline{T}, \text{ Btu/(in.)(sec)(°F)}$$

Thermal conductivity of combustion products,

$$k_b = 5.10692\times10^{-8} + 7.616145\times10^{-10}\overline{T}, \text{ Btu/(in.)(sec)(°F)}$$

Vapor pressure,

$$\ln p_{a,s} = 14.328787 - \frac{7363.22}{T_l - 63.1713}, \text{ lb/sq in.}$$

Viscosity of hydrazine vapor,

$$\mu_a = 4.19981\times10^{-8} + 9.581164\times10^{-10}\overline{T}, \text{ lb/(in.)(sec)}$$

Viscosity of combustion products,

$$\mu_b = 1.64352\times10^{-7} + 2.45252\times10^{-9}\overline{T}, \text{ lb/(in.)(sec)}$$

Diffusion coefficient of vapor mixture,

$$D_{mx} = [-5.3537\times10^{-4} + 3.13874\times10^{-6}\overline{T} + 3.37045\times10^{-9}(\overline{T})^2]\frac{300}{P}, \text{ sq in./sec}$$

Molecular weight of combustion products,

$$\mathcal{M}_b = 24, \text{ lb/mole}$$

FLUORINE WITH GASEOUS HYDROGEN

Density of liquid,

$$\rho_l = 6.846 \times 10^{-2} - 3.036 \times 10^{-5} T_l - 3.9308 \times 10^{-7} T_l^2, \text{ lb/cu in.}$$

Heat of vaporization,

$$\lambda = 48.8196 + 0.4993 T_l - 2.2932 \times 10^{-3} T_l^2, \text{ Btu/lb}$$

Specific heat of liquid,

$$c_{p,l} = 0.349 + 1.212 \times 10^{-4} T_l, \text{ Btu/(lb)(°F)}$$

Specific heat of fluorine vapor,

$$c_{p,a} = 0.223994 + 1.667 \times 10^{-6} \overline{T}, \text{ Btu/(lb)(°F)}$$

Specific heat of combustion products,

$$c_{p,b} = 0.32332 + 2.068 \times 10^{-5} \overline{T}, \text{ Btu/(lb)(°F)}$$

Thermal conductivity of fluorine vapor,

$$k_a = 2.7606 \times 10^{-7} + 3.47122 \times 10^{-10} \overline{T}, \text{ Btu/(in.)(sec)(°F)}$$

Thermal conductivity of combustion products,

$$k_b = 1.0765 \times 10^{-7} + 4.31280 \times 10^{-10} \overline{T}, \text{ Btu/(in.)(sec)(°F)}$$

Vapor pressure,

$$\ln p_{a,s} = 12.3171 - \frac{1482.9545}{T_l - 2.5645}, \text{ lb/sq in.}$$

Viscosity of fluorine vapor,

$$\mu_a = 1.2591 \times 10^{-6} + 1.584 \times 10^{-9} \overline{T}, \text{ lb/(in.)(sec)}$$

Viscosity of combustion products,

$$\mu_b = 2.60098 \times 10^{-7} + 1.04178 \times 10^{-9} \overline{T}, \text{ lb/(in.)(sec)}$$

Diffusion coefficient of vapor mixture,

$$D_{mz} = \left[-4.5732 \times 10^{-3} + 1.078 \times 10^{-5} \overline{T} + 5.421 \times 10^{-9} (\overline{T})^2\right] \frac{300}{P}, \text{ sq in./sec}$$

Molecular weight of combustion products,

$$\mathcal{M}_b = 20, \text{ lb/mole}$$

REFERENCES

1. Crocco, L.: Considerations on the Problem of Scaling Rocket Motors. AGARD Selected Combustion Problems, II, Butterworths Sci. Pub., 1956, pp. 457–468.
2. Penner, S. S.: Rational Scaling Procedures for Liquid-Fuel Rocket Engines. Jet Prop., vol. 27, no. 2, pt. 1, Feb. 1957, pp. 156–161.
3. Ross, Chandler C.: Scaling of Liquid Fuel Rocket Combustion Chambers. AGARD Selected Combustion Problems, II, Butterworths Sci. Pub., 1956, pp. 444–456.
4. Penner, S. S., and Datner, P. P.: Combustion in Liquid-Fuel Rocket Engines. Fifth Symposium (International) on Combustion, Reinhold Pub. Corp., 1955, pp. 11–29.
5. Bittker, David A.: An Analytical Study of Turbulent and Molecular Mixing in Rocket Combustion. NACA TN 4321, 1958.
6. Heidmann, Marcus F., Priem, Richard J., and Humphrey, Jack C.: A Study of Sprays Formed by Two Impinging Jets. NACA TN 3835, 1957.
7. Bittker, David A., and Brokaw, Richard S.: An Estimate of Chemical Space Heating Rates in Gas-Phase Combustion with Applications to Rocket Propellants. Paper No. 824–59, Am. Rocket Soc., 1959.
8. Hougen, Olaf A., and Watson, Kenneth M.: Chemical Process Principles. John Wiley & Sons, Inc., 1943.
9. Sherwood, Thomas K., and Pigford, Robert L.: Absorption and Extraction. Second ed., McGraw-Hill Book Co., Inc., 1952.
10. Ranz, W. E., and Marshall, W. R., Jr.: Evaporation from Drops, pt. I. Eng. Prog., vol. 48, no. 3, Mar. 1952, pp. 141–146. (See also pt. II, vol. 48, no. 4, Apr. 1952, pp. 173–180.)
11. Priem, R. J., Borman, G. L., El Wakil, M. M., Uyehara, O. A., and Myers, P. S.: Experimental and Calculated Histories of Vaporizing Fuel Drops. NACA TN 3988, 1957.
12. El Wakil, M. M., Priem, R. J., Brikowski, H. J., Myers, P. S., and Uyehara, O. A.: Experimental and Calculated Temperature and Mass Histories of Vaporizing Fuel Drops. NACA TN 3490, 1956.
13. Prandtl, L., and Tietjens, O. G.: Applied Hydro- and Aero-mechanics. McGraw-Hill Book Co., Inc., 1934.
14. Ingebo, Robert D.: Vaporization Rates and Drag Coefficients for Isooctane Sprays in Turbulent Air Streams. NACA TN 3265, 1954.
15. Ames Research Staff: Equations, Tables, and Charts for Compressible Flow. NACA Rep. 1135, 1953. (Supersedes NACA TN 1428.)
16. Sutton, George P.: Rocket Propulsion Elements. Second ed., John Wiley & Sons, Inc., 1956.
17. Bevans, Rowland S.: Mathematical Expressions for Drop Size Distribution in Sprays. Conf. on Fuel Sprays, Univ. of Mich., Mar. 30–31, 1949.
18. Godsave, G. A. E.: Studies of the Combustion of Drops in a Fuel Spray—The Burning of Single Drops of Fuel. Fourth Symposium (International) on Combustion, The Williams & Wilkins Co., 1953, pp. 818–830.
19. Mayer, E.: On Vaporization Rate Limited Combustion in Bipropellant Rocket Chambers. Paper presented at Am. Rocket Soc. Meeting (N.Y.), Nov. 17–21, 1958.
20. Spalding, D. B.: A One-Dimensional Theory of Liquid-Fuel Rocket Combustion. Rep. 20, 175, British ARC, May 19, 1958.

21. Gordon, Sanford, and Huff, Vearl N.: Theoretical Performance of Liquid Hydrogen and Liquid Fluorine as a Rocket Propellant. NACA RM E52L11, 1953.
22. Gordon, Sanford, and Huff, Vearl N.: Theoretical Performance of Liquid Ammonia and Liquid Fluorine as a Rocket Propellant. NACA RM E53A26, 1953.
23. Huff, Vearl N., Fortini, Anthony, and Gordon, Sanford: Theoretical Performance of JP-4 Fuel and Liquid Oxygen as a Rocket Propellant. II—Equilibrium Composition. NACA RM E56D23, 1956.
24. Heidmann, M. F., and Auble, C. M.: Injection Principles from Combustion Studies in a 200-Pound Thrust Rocket Engine Using Liquid Oxygen and Heptane. NACA RM E55C22, 1955.
25. Ingebo, Robert D.: Drop-Size Distributions for Impinging-Jet Breakup in Airstreams Simulating the Velocity Conditions in Rocket Combustors. NACA TN 4222, 1958.
26. Heidmann, Marcus F.: Injection Principles for Liquid Oxygen and Heptane Using Two-Element Injectors. NACA RM E56D04, 1956.
27. Neu, Richard F.: Injection Principles for Liquid Oxygen and Heptane Using Nine-Element Injectors in an 1800-Pound-Thrust Rocket Engine. NACA RM E57E13, 1957.
28. Heidmann, M. F.: Propellant Vaporization as a Criterion for Rocket-Engine Design; Experimental Effect of Fuel Temperature on Liquid-Oxygen—Heptane Performance. NACA RM E57E03, 1957.
29. Priem, Richard J., and Hersch, Martin: Effect of Fuel-Orifice Diameter on Performance of Heptane-Oxygen Rocket Engines. NACA RM E57I26, 1958.
30. Clark, Bruce J., Hersch, Martin, and Priem, Richard J.: Propellant Vaporization as a Criterion for Rocket-Engine Design; Experimental Performance, Vaporization and Heat-Transfer Rates with Various Propellant Combinations. NASA MEMO 12-29-58E, 1959.
31. Clark, Charles C.: Hydrazine. Mathieson Chem. Corp., Baltimore (Md.), 1953.
32. Heidmann, Marcus F.: Propellant Vaporization as a Criterion for Rocket Engine Design; Experimental Effect of Chamber Diameter on Liquid Oxygen—Heptane Performance. NASA TN D-65, 1959.
33. Ingebo, Robert D., and Foster, Hampton H.: Drop-Size Distribution for Crosscurrent Breakup of Liquid Jets in Airstreams. NACA TN 4087, 1957.
34. Rossmann, Theodor G.: Program of Exploratory Research on Rocket Engine Combustion. Rep. 02-982-026, Final Rep., Third Contract Year, Sept. 15, 1956 to Sept. 14, 1957, Bell Aircraft Corp., Oct. 15, 1957. (Contract AF18(600)-1156.)
35. Wieber, Paul, and Mickelsen, William R.: Effect of Transverse Acoustic Oscillations on the Vaporization of a Liquid-Fuel Droplet. NASA TN D-287, 1960.

U.S. GOVERNMENT PRINTING OFFICE: 1961